A STUDY
OF CONDITIONS
IN THE UPPER ATMOSPHERE
AND THEIR DEDUCTION
FROM
RADIO MEASUREMENTS.

Being a Thesis for the degree of
Doctor of Philosophy of the University of South Africa
submitted jointly by

J. A. GLEDHILL, M.Sc. (S.A.),
Lecturer in Chemistry, R. U. C.

and

M. E. SZENDREI, M.Sc. (S.A.),
Lecturer in Physics, R. U. C.

Physics Department,
Rhodes University College,
Grahamstown.
June 1947.

CONTENTS.

Part 3.

Acknowledgements.

In a research of this kind, in which it has been necessary to build the required equipment from commercial, and sometimes home-made, components, completeness would demand that a large number of persons be thanked. For lack of space we shall mention by name only those without whose help this research would not have been carried out.

To Professor R.W. Varder, M.A., who directed this work and put at our disposal the resources, both financial and material, of this Physics department, the authors wish to tender their appreciation and gratitude.

Thanks are due to the National Research Council and Board for a grant of £ 100 towards the cost of apparatus.

The authors wish to thank Professor A. Ogg, M.A., Ph.D. D.Sc., F.Inst.P., late director of the Hermanus Magnetic Observatory, for his kindness in supplying very promptly the magnetic data used in the correlation.

Thanks are also due to:

Messrs. P.R.K. Ponsonby, B.Sc., U.E.D.; A.R. Morris, M.Sc.; C.K. Hill, M.Sc.; P.K. Faure, B.Sc.; and A.N. Stroh, B.Sc. for help in taking the photographic records.

Mr. A.R. Scanlan for constructing the camera used for recording purposes.

and to:

Messrs. F.H. Flanter, of United Africa Electric, and G.F.G. Knipe, B.Sc., A.Inst.P., of Kodak (S.A.), Ltd., for supplying electrical and photographic equipment when wartime conditions made such equipment practically impossible to obtain.

PART 1

comprising

Part 1 (a)

Experimental Methods

and

the Reduction and Presentation of Observations,

and

Part 1 (b)

Theory of the Production of an Ionised Layer

in a Non-Isothermal Atmosphere

and

its Application to Experimental Results.

by

J.A. Gledhill and M.E. Szendrei.

Summary.

In part 1 (a), after a brief historical outline of methods of ionospheric investigation and their development, the construction in this laboratory of manually operated equipment for sounding the ionosphere is described. Photographic records of good definition were taken at regular intervals over a period of four months during the summer of 1945-6. These were fully scaled for critical frequencies, true heights and thicknesses of all the layers present, and mean monthly values of these quantities for each hour are tabulated. An extensive correlation with magnetic data from Hermanus indicated good correlation between magnetic activity and disturbed ionospheric conditions. On these grounds some disturbed days were rejected, and others were eliminated on ionospheric grounds. Smoothed mean values are tabulated and graphs drawn. These are presented in concise form on "electron density maps", which are graphs showing lines of constant electron density plotted as functions of time and height.

In part 1 (b), a new theory of layer-formation is developed, in which the temperature is assumed to vary linearly with height. The equations are compared at each step with those obtained by Chapman in his theory of layer-formation in an isothermal atmosphere. The equations for the maximum of electron density and its height are also given. The effect of the parameters on the shape of the layer is shown in graphical form.

The equations are somewhat complex in form, but an ingenious graphical method has been devised suitable for the/

the application of the theory to results given in the form of those in section 1 (a). From this application values are obtained for the temperature gradient, the temperature at 200 km. and its variation over the middle part of the day. The results obtained are in accordance with previous estimates, and offer numerical confirmation of the theory that the atmosphere expands bodily upwards during the middle part of a summer day.

Part 1 (a).

Experimental Methods

and

the Reduction and Presentation

of Observations.

Experimental Methods.

Introduction.

It is a well-known fact that wireless signals can be detected on parts of the globe remote from those of their origin, although being electro-magnetic waves they should be propagated along straight lines in the atmosphere. Calculations made in the first 15 years of this century (1:1),(1:2),(1:3) showed that diffraction cannot account adequately for the strength of the received signals. The alternative theory of the existence of a conducting layer in the upper atmosphere, suggested independently by Kennelly and Heaviside in 1902, was proved to be true by the experiments of Appleton and Barnett (1:4) and Breit and Tuve (1:5).

Appleton and Barnett varied linearly the frequency of a transmitter by a small amount; interference fringes were produced at a receiving station some distance away and could only be attributed to interference between a "ground ray" coming direct from the transmitter and a "sky wave" reflected from the conducting layer (fig. 1.1). By counting the fringes they were able to calculate the apparent path difference and hence the virtual height of the layer.

More direct evidence came from the experiments of Breit and Tuve (1:5), who modulated a commercial transmitter with a series of pulses of 500 microseconds duration. An oscillograph coupled to the receiver showed that there were two received pulses, again one direct by the ground wave, the other received a little later by the sky path. By

measuring/

measuring the time interval between the two received pulses the virtual height could be calculated.

A third method was devised by Appleton and Ratcliffe in 1927 (1:6) using a directional receiving antenna system to measure the angle of incidence, i (fig. 1.1) of the downcoming sky wave.

The method of Breit and Tuve has proved to be preferable to the others in further investigation and has been improved and developed: with modern radio technique the receiver may be brought into the same room as the transmitter and the frequency of the signals may be varied over a useful range. Completely automatic apparatus has been devised by Berkner, Wells and Seaton (1:7) and others and at a number of stations including Huancayo (Peru), Watheroo (Western Australia) and College (Alaska) the Carnegie Institute maintains such apparatus in continuous operation for recording conditions in the upper atmosphere.

Work over the last 20 years has shown that there is more than one reflecting layer:

(i) A layer at a height just above 100 km., called the Kennelly-Heaviside or E layer;

(ii) A layer at a height of approximately 300 km., called the Appleton or F_2 layer;

(iii) A layer at a height of approximately 200 km., called the F_1 layer; this layer differs from the other two in being present only during the daytime in summer;

(iv) Occasional intense reflections from a height of about 100 km. are found - these cannot be attributed to the normal E layer and have received the name of "sporadic/

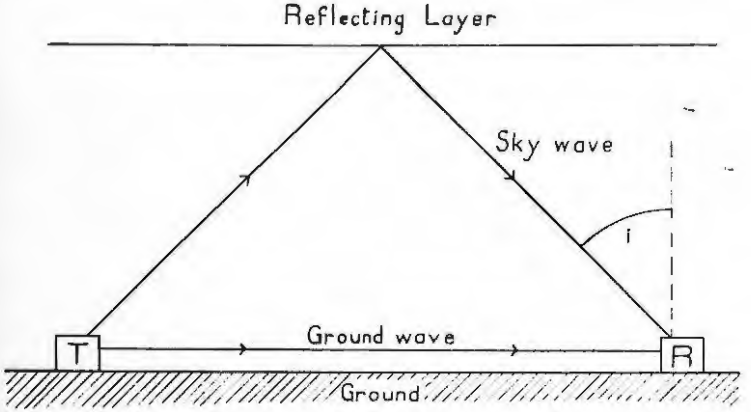

FIG. 1·1
GROUND AND SKY WAVES.

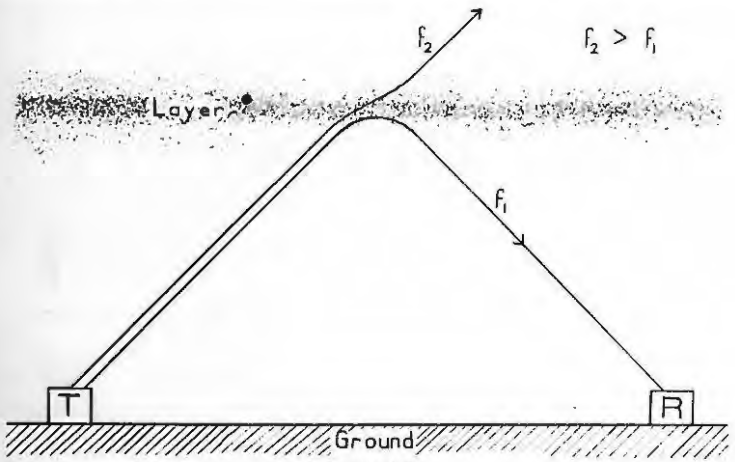

FIG. 1·3
PENETRATION OF LAYER.

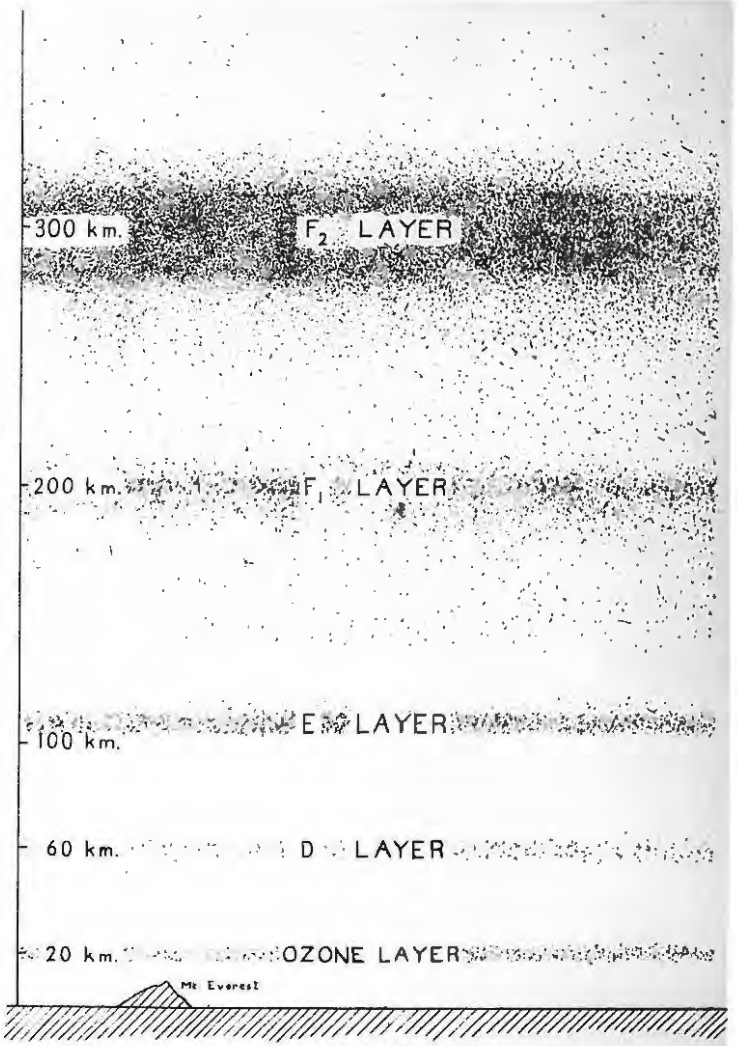

FIG. 1·2
STRUCTURE OF THE ATMOSPHERE.

"sporadic E".

The whole region from 70 to 400 km. is now called the ionosphere.(fig. 1.2).

The diurnal and seasonal variations of the first three layers indicate the sun as their chief agent in their production and it is generally agreed that the layers consist of ionised molecules and free electrons, produced by radiation from the sun. A theory of formation of these layers has been worked out by Chapman (1:8) and others; this will be considered in more detail in parts 1 (b) and 2.

The theory of propagation and reflection of e.m. waves in an ionised layer has been worked out by Appleton (1:9) and has been extended into the magneto-ionic theory. The theory shows that reflection of an e.m. wave will take place provided the electron density is sufficiently high. A wave of higher frequency requires a higher electron density for reflection; if the electron density is insufficient, no reflection occurs and the wave passes right through the layer (fig. 1.3). In the developed Breit and Tuve method of investigation the transmitter frequency is continuously increased and the value at which penetration of the layer occurs, called the critical frequency for that layer, is noted.

The presence of free ions and electrons has the effect of reducing the refractive index of the medium, and hence the group velocity, i.e. the velocity with which the energy is propagated. In calculating the apparent height of the layer from time delay measurements, it is assumed that the energy is everywhere propagated with the velocity of light; thus the apparent height is always

greater/

greater than the true height by an amount depending on the density of ionisation at all points along the path.

Another result of the theory is that, owing to its being propagated in the earth's magnetic field the wave is split into two components elliptically polarised with opposite rotation. Each of the polarised components has its own critical frequency; for the ordinary wave this critical frequency, f^o, is related to the maximum electron density, N, by the formula:

$$N = \frac{\pi m}{e^2} (f^o)^2 \quad . \quad . \quad . \quad . \quad . \quad . \quad . \quad (1.1)$$

where m and e are the electronic mass and charge in e.s.u. Substituting the numerical value for $e = 4.80 \times 10^{-10}$ e.s.u. and $e/m = 5.27 \times 10^{17}$ e.s.u., and expressing f^o in Mc/sec., this becomes:

$$N = 1.24 \times 10^4 (f^o)^2 \quad . \quad . \quad . \quad . \quad . \quad (1.2)$$

The critical frequency, f^x, for the extraordinary wave is found to differ from f^o by an amount which depends on the strength and direction of the magnetic field, and, since at a given place these are practically constant, the separation between the two critical frequencies is also constant.

During the past 15 years considerable discussion has taken place on the advisability of applying Lorentz's theory of electrons to the magneto-ionic theory (1:10), (1:11), (1:12), (1:13), (1:14). If this is done, the general results of Appleton's theory are not altered, but the numerical values obtained are changed by as much as 50% in some cases. In the present work, the Lorentz term has not been included, in view of the uncertainty still prevailing.

Investigation/

Investigation of ionospheric conditions at the relatively few places where such work is carried on has shown not only that the critical frequencies and virtual heights of the layers vary with time of day, season, etc., but also that the way in which this variation takes place differs in different parts of the globe. It has been repeatedly advocated by well known physicists engaged in this kind of work that "ionospheric readings should be taken in a large number of locations on the surface of the earth, in order to get as complete a picture as possible"(1:15).

In South Africa very little ionospheric work has been done. Halliday has reported some work on the accurate measurements of virtual heights (1:16); in 1940, three groups of workers took observations over a short period centering over the solar eclipse of 1st October: A.J. Higgs (1:17), G.D. Walker (1:18) and J.A. Pierce, whose work has not yet been published. The writers accompanied the last expedition and gained some valuable experience in ionospher research.

During the war no indication was given of the opening of any station of this sort, and in 1943 the writers approached Prof. R.W. Varder with the object of building a small research station with which some data at least might be obtained. Permission and financial assistance were readily given and work was started at once. As no research on modern telecommunication had been carried out here before, it was necessary as a preliminary step to build a considerable amount of test equipment; this, accompanied by the difficulty of obtaining supplies of radio components, etc., under wartime conditions, did not accelerate the proceedings. However, by the end of 1944

all/

all the equipment, with the exception of the photographic recorder, was in working order; it was severely tested over a short period, including another solar eclipse, whic occurred over Grahamstown in January 1945 (1:19). With the addition of a photographic recorder and a few modifications, this apparatus was used in the work reported here. It is gratifying to note that since the middle of 1946, the Council for Scientific and Industrial Research has begun taking a series of regular records of ionospheric conditions over Johannesburg, under the direction of Mr. F.J. Hewitt.

Design of Transmitting and Receiving Apparatus.

As previously stated the method consists of sending out short pulses of suitable length, varying the frequency of the transmitter and receiving both ground wave and reflected echo on a special receiver, its output being coupled to a recording device. There are various methods of doing this, of which the most satisfactory is probably the completely automatic multifrequency apparatus used by the Carnegie Institute (1:7). As equipment of this kind would have cost more than £1500, it was decided to build the less ambitious apparatus shown in the form of a block diagram in fig. 1.4.

The various sections of the apparatus will now be considered.

Transmitter.

The power output of the transmitter over the whole range of frequencies should be sufficient to secure a reflection even under the most adverse conditions: a power output of 100 watts or more is found to be

satisfactory/

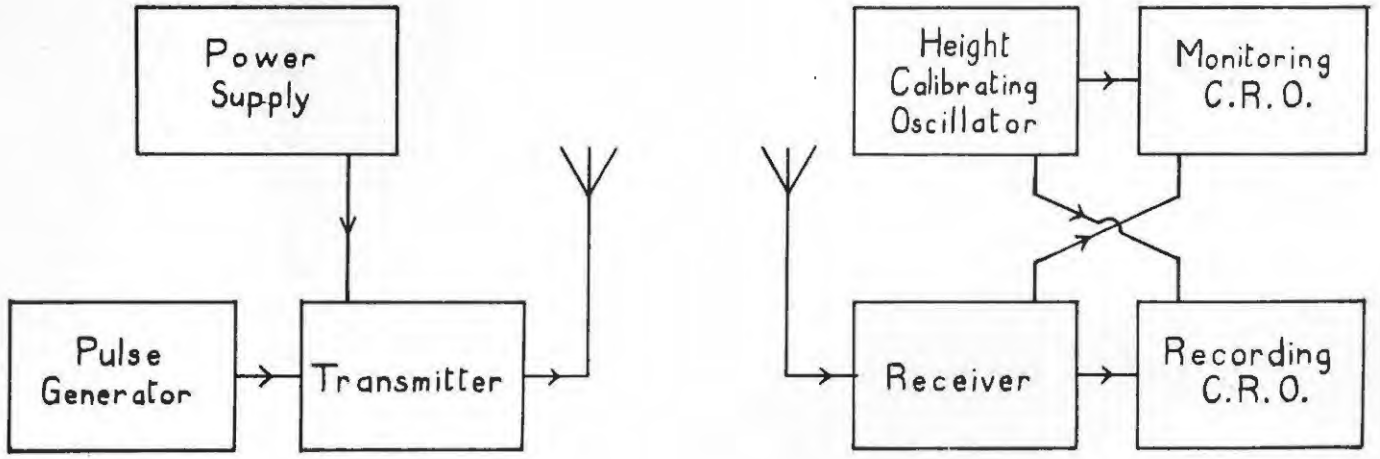

FIG. 1·4

BLOCK DIAGRAM OF IONOSPHERIC APPARATUS.

satisfactory. It must also be modulated so that it is completely off the air except during pulses; otherwise it would paralyse the receiver and render it very insensitive. The only kind of tube available to satisfy these requirements even approximately was the triode 811. Two of these were arranged in a shunt-fed push-pull oscillator of the Hartley type (fig. 1.5), the plate voltage of 1500 Volts being supplied by a rectifier of conventional design through B+.

The transmitter is first adjusted to work as a class C power oscillator with the tap X brought to the grounded end of R_2. The grid resistors R_3 and R_4 are wire-wound and also act as chokes to prevent bypass of the R.F. to ground. For pulse operation the tap X on R_2 is adjusted to bias the transmitter, so that it remains completely cut off. By injecting a pulse of suitable amplitude and polarity at AB the transmitter is brought into action for the durati of the pulse.

The highest frequencies reflected by the F_2 layer do not normally exceed 15 Mc/sec. nor do they drop below 2 Mc/sec. In order to investigate this layer the transmitter must cover a continuous range between these limits. It is then also suitable for a study of the F_1 layer and the daytime variation of the E layer. With ordinary variable transmitting condensers, this can only be done in 4 bands; these were arranged to give a suitable amount of overlap and the coils were chosen to work between the limits shown in table 1:1. A special band switch was built to stand an R.F. potential of 3000 volts peak.

The antenna system must be designed to radiate as efficiently as possible in a vertical direction over the range of frequencies used. This is accomplished

by/

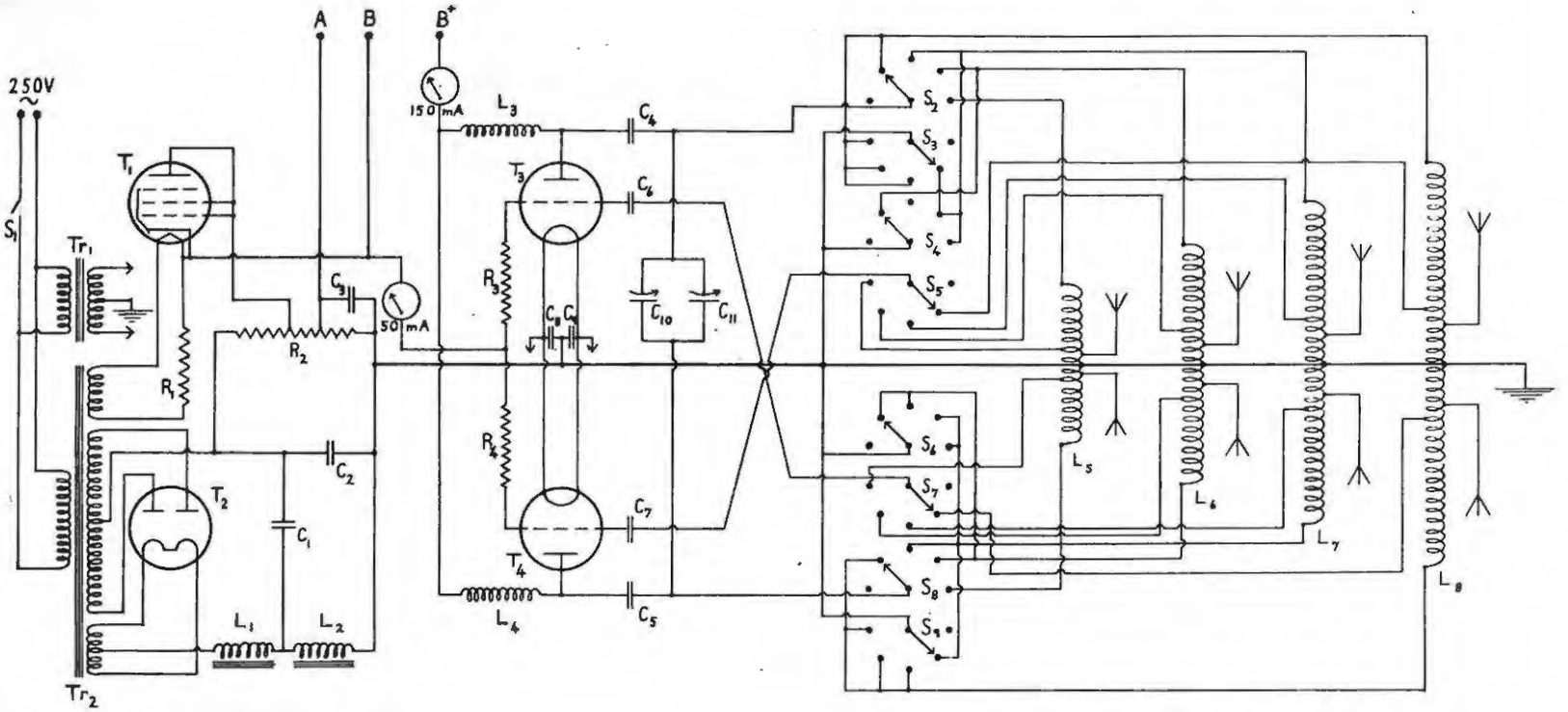

R_1	=	2	Ohms	1	Watt
R_2	=	10,000	"	100	"
R_3, R_4	=	2,500	"	10	"
T_1	=	6F6			
T_2	=	80			
T_3, T_4	=	811			
S_1	=	Main Switch			
$S_2 - S_9$	=	Ganged Waveband Switch			

C_1	=	8 μFd.	450 V.W.	Electrolytic
C_2, C_3	=	16 "	"	"
C_4, C_5	=	0·001 "	2000 "	Mica
C_6, C_7	=	75 $\mu\mu$Fd		"
C_8, C_9	=	0·005 μFd		"
$C_{10}+C_{11}$	=	Hammarlund TCD 100A Tuning Condenser		

L_1, L_2	=	20 H
L_3, L_4	=	2·5 mH
L_5	=	5 μH
L_6	=	9 μH
L_7	=	16 μH
L_8	=	28 μH

Tr_1	=	Filament Transformer, 6·3V, 10A.
Tr_2	=	Mains Transformer

FIG. 15

CIRCUIT OF TRANSMITTER AND BIAS SUPPLY.

by having a separate dipole antenna for each coil; the length of each dipole is 0.475 of the mean wavelength radiated by that coil and is placed in a horizontal direction at a height of approximately ¼ of this wavelength above the ground. To this purpose poles were erected on the roofs of the Physics and Chemistry Departments at R.U.C.. The feeders are of the parallel wire type spaced by 6 ins. spreaders at 3 ft. from each other. (fig. 1.6).

Band	Lowest Frequency (Mc/sec.)	Highest Frequency (Mc/sec.)
1	1.83	3.2
2	3.1	5.0
3	4.8	8.0
4	8.0	13.9

Table 1:1 - Transmitter Bands.

The coupling of the antennae to the coils caused considerable difficulty, as the load presented by the feeder-antenna system to the transmitter was very uneven; a compromise was reached by tapping down until a reasonable amount of power was radiated all over the scale: even so two short skips on the transmitted frequencies could not be eliminated:

on Band 1, from 1.95 to 2.17 Mc/sec.;
" " 2, " 9.30 "10.00 " .

Although these short skips did not present any difficulty in the interpretation of the records, an improvements could have been obtained by feeding from a master oscillator into a separate power amplifier, in this way preventing reaction of the antenna system on the

oscillator/

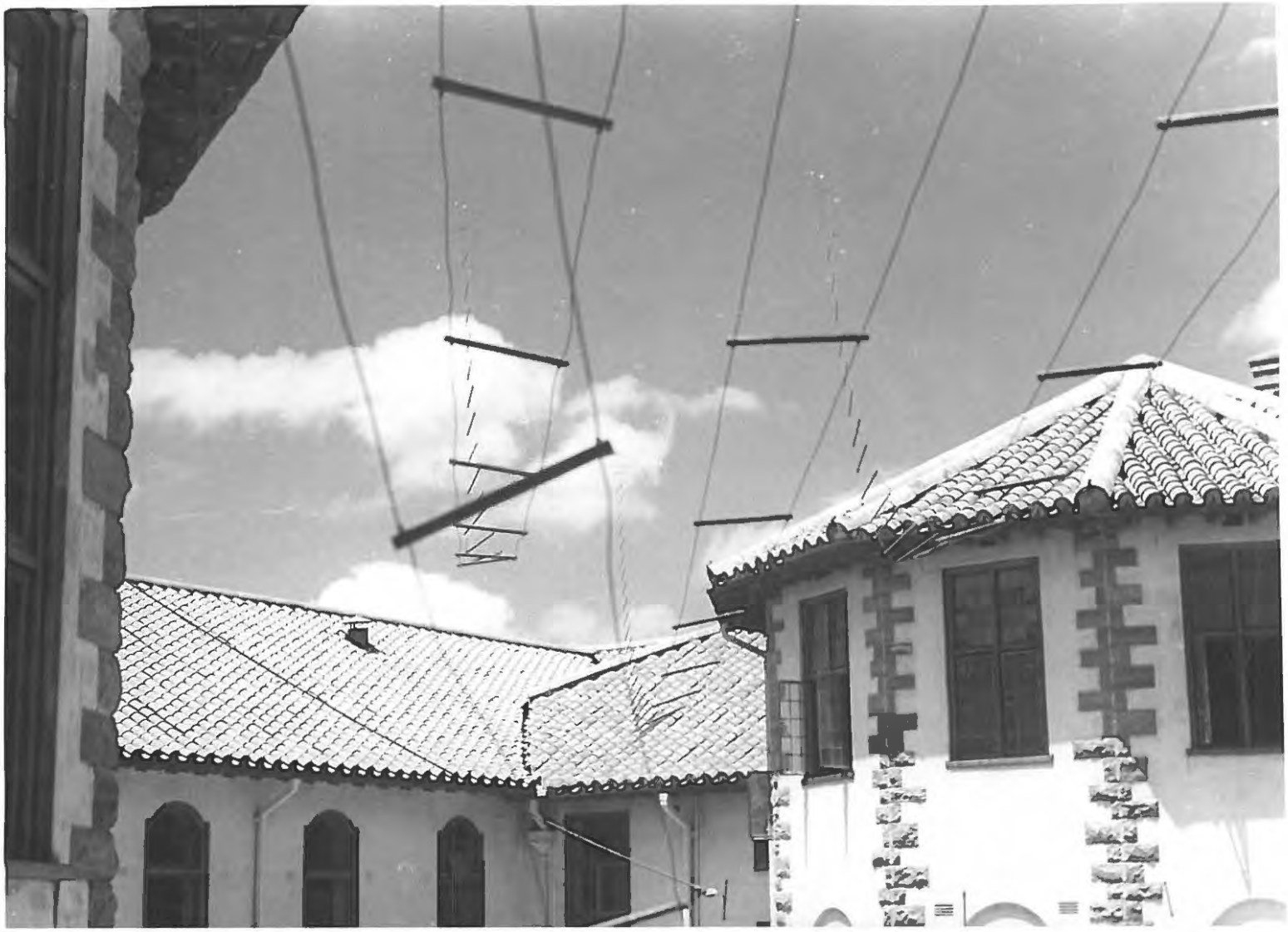

FIG. 1·6

Antenna System.

oscillator frequency. The complete apparatus is shown in fig. 1.7.

Pulse Generator and Modulator.

The duration of the pulse must be sufficiently short not to overlap the leading edge of the reflection from the lowest layer. Taking the height of the E layer as 100 km., the length of the forward and return path at vertical incidence is 200 km. Neglecting retardation, the signal travels with the speed of light i.e. 3×10^5 km/sec., so that

$$\text{time delay of echo} = \frac{200}{3 \times 10^5} = 6.67 \times 10^{-4} \text{sec.}$$

$$= 667 \, \mu\text{sec.}$$

The pulse should not be very short, because a large number of harmonics will be included in the sidebands, resulting in unnecessary interference with other stations and poor definition of critical frequencies. This is because the higher sidebands will penetrate the layer while the lower ones are still being reflected. In addition the amount of energy which may be radiated with a given transmitter decreases as the pulses are shortened. Practically a pulse length of 100 microseconds is found to be suitable.

The interval between pulses must be large compared with the time delay of an echo from the highest layer. Considering that near the critical frequencies of the F_2 layer, virtual heights of 1000 km. are not uncommon, this delay, by a similar calculation to that above, may be seen to be about 7000 microseconds; therefore the pulse rate should not exceed 150 per second.

The/

FIG. 1·7

Transmitter.

The persistence of the glow on the C.R.O. screen sets a lower limit for the pulse rate. In a town supplied with A.C. mains, it is very convenient to control the pulse rate from the mains, the usual rate in South Africa being 50 per second. This method offers the advantage that other apparatus may be synchronised easily with the pulse rate and will not go out of synchronisation even if the mains frequency fluctuates somewhat.

Many methods have been suggested for the generation of such pulses (1:20), (1:21), (1:22), (1:23). The thyratron offers a simple method of generating pulses, and a simple thyratron circuit was first employed (figs. 1.8 and 1.9). The tap E on R_1 is adjusted so that when C_4 is fully charged through R_2 its potential is not sufficient to strike the thyratron with the steady grid bias applied. A small A.C. voltage injected from TR_2 is sufficient to bring the grid up to striking potential near the peak of each cycle. On closing S_2, C_4 discharges through T_2, R_3 and R_4 when this point on the cycle is reached; the plate potential of T_2 therefore falls rapidly and it extinguishes, the time of conduction depending on the value of the product $C_4(R_3 + R_4)$, R_6 being large compared to $(R_3 + R_4)$. This produces a voltage pulse across R_6, which is applied to the grids of the parallel power amplifier tubes T_3 and T_4. The length of this pulse may be varied by the aid of R_4. During the remainder of the cycle C_4 recharges through R_2, the time constant of C_4R_2 being adjusted so that it is ready to strike again on the following cycle.

The pulse is ~~applied~~ amplified through T_3 and T_4 and fed/

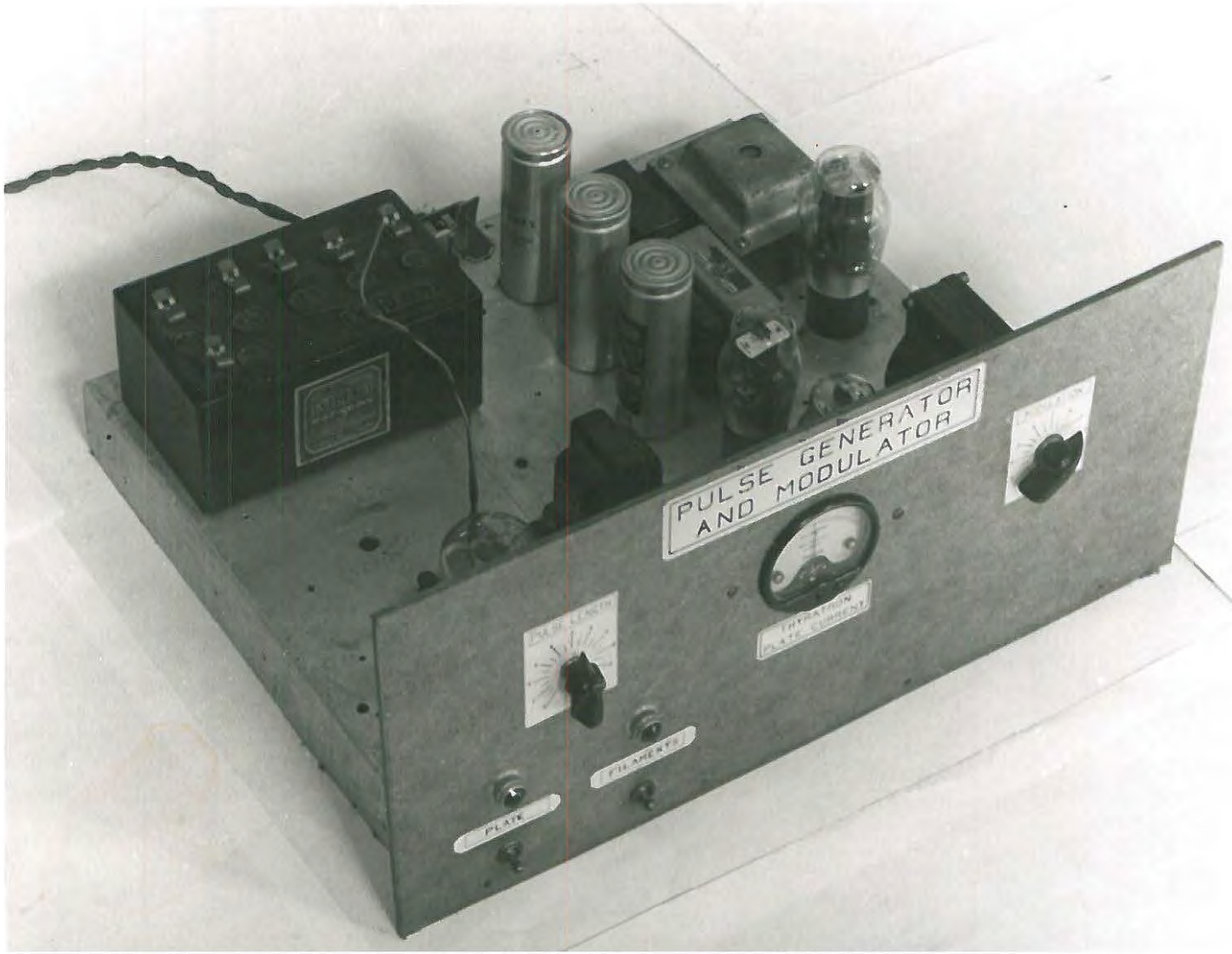

FIG. 1·8

Thyratron Pulse Generator.

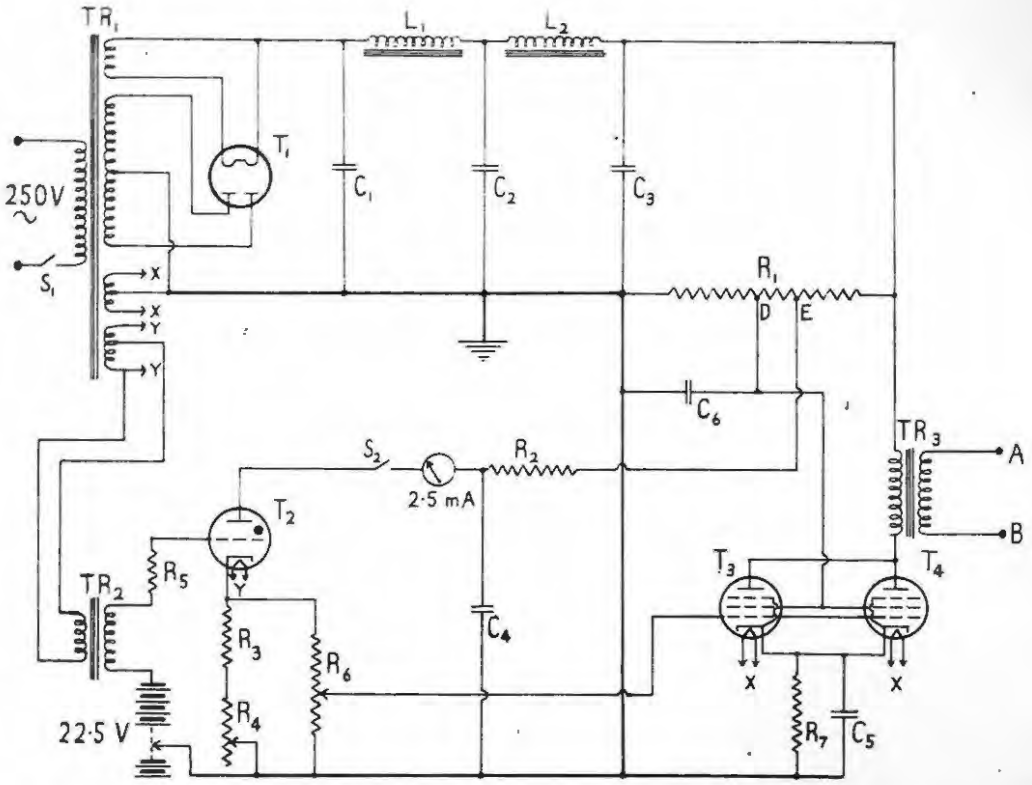

R_1	= 50,000 Ohms	25 Watt	C_1, C_2, C_3	=	8μFd. 600 V.W. Electrolytic
R_2	= 0·25 Megohm		C_4	=	0·03 μFd.
R_3	= 400 Ohms		C_5, C_6	=	0·5 "
R_4	= 200 "				
R_5	= 1,500 "		L_1, L_2	=	20 H
R_6	= 0·1 Megohm				
R_7	= 1,000 Ohms		TR_1	=	Mains Transformer
			TR_2	=	Synchronising Transformer
T_1	= 5Z3		TR_3	=	Output Transformer (1:1)
T_2	= GT1C (Osram)				
T_3, T_4	= 2A5		S_1	=	Power Switch
			S_2	=	Pulse H.T. Switch

FIG. 1·9

CIRCUIT OF THYRATRON PULSE GENERATOR.

fed through the audio transformer TR_3 into the grid circuit of the transmitter. This transformer differentiat the waveform of the pulse thus sharpening it; it was found, however, that the sudden large change in voltage produced a damped oscillation in the output. The second positive peak gave a second pulse in the transmitter; this effect was eliminated by the introduction of T_1 (fig. 1.5), a power pentode connected as diode - this clipped off the first negative peak and thus prevented the first oscillation from taking place.

This pulse unit was quite satisfactory, but unfortunat no replacements for the thyratron could be obtained. Recourse was therefore had to a hard valve pulse generator (fig. 1.10). This circuit is derived from Puckle's time base (1:24); the pentode T_3 has a high load resistanc R_7 and therefore its plate potential is low. T_2 does not conduct because its grid is connected to this plate and is therefore many volts negative with respect to its cathode, tapped at 160 V. on the bleeder R_1. As $(C_4 + C_5)$ charge through R_3, the cathode of T_2 drops in potential until the valve conducts; this causes a negative impulse on the grid of T_3, its plate rises and so does the grid of T_2, thus making T_2 conduct more. A pulse of current is thus built up. $(C_4 + C_5)$ quickly discharge through R_5 and T_2, however, and this results in a fall of current through T_2, T_3 becomes more conducting and the circuit falls back into the starting condition.

Synchronisation with the main frequency was attained by adjusting the return of the cathode of T_2 to the bleeder until the circuit did not strike at all. A comparatively large A.C. voltage was then applied to the

suppressor/

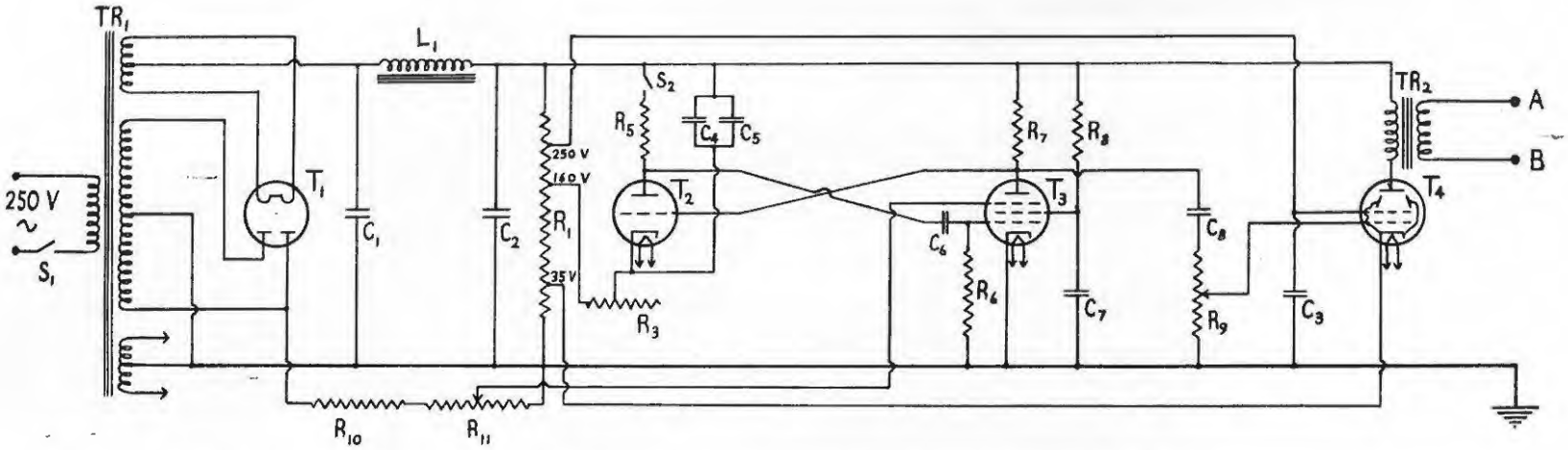

R_1	= 25,000 Ohms 100 Watt	C_1, C_2, C_3	= 10μFd 450 V.W. Electrolytic	L_1	= 20 H
R_3	= 0·75 Megohm	C_4	= 0·01 " Mica		
R_5	= 2,500 Ohms	C_5	= 0·005" "	TR_1	= Mains Transformer
R_6	= 10,000 "	C_6	= 0·02 "	TR_2	= Output Transformer
R_7	= 0·1 Megohm	C_7	= 0·05 "		
R_8	= 0·5 "	C_8	= 0·005"	T_1	= 5Y3 G
R_9	= 75,000 Ohms			T_2	= 6C5 GT/G
R_{10}	= 0·1 Megohm	S_1	= Power Switch	T_3	= 6J7 G
R_{11}	= 50,000 Ohms	S_2	= Pulse H.T. Switch	T_4	= 6L6 GA

FIG. 1·10

CIRCUIT OF VACUUM-TUBE PULSE GENERATOR.

suppressor grid of T_3 from the potential divider $R_{10}R_{11}$; this brought the circuit into operation once every cycle. By suitable arrangement of R_{11} and R_3 the pulse phase may be shifted by as much as 90°. This circuit was used in the latter part of the work and proved more successful than the thyratron.

It should be pointed out that a method not requiring an injected voltage for synchronisation has been developed in connection with radar, but this circuit was still on the secret list at the time of building the above two generators.

Receiver.

The more important pre-requisites of the receiver are

(i) It must recover quickly from the strong ground pulse and be back at full sensitivity by the time the first echo arrives.

(ii) Its normal sensitivity must be sufficient to receive even the weakest reflected signals.

It was hoped at first that a good quality domestic receiver would satisfy these requirements with only slight alterations. To this end an H.M.V. model 473 was purchased, but by the time modification was completed little was left of it save the chassis and tuning unit. The final circuit is shown in fig. 1.11 and the apparatus itself in figs. 1.12 and 1.13. The following departures from conventional design should be noted: the time constants of all the circuits in the R.F. section are as small as possible, most of them being below 100 microseconds. As the usual type of A.V.C. has a time

constant/

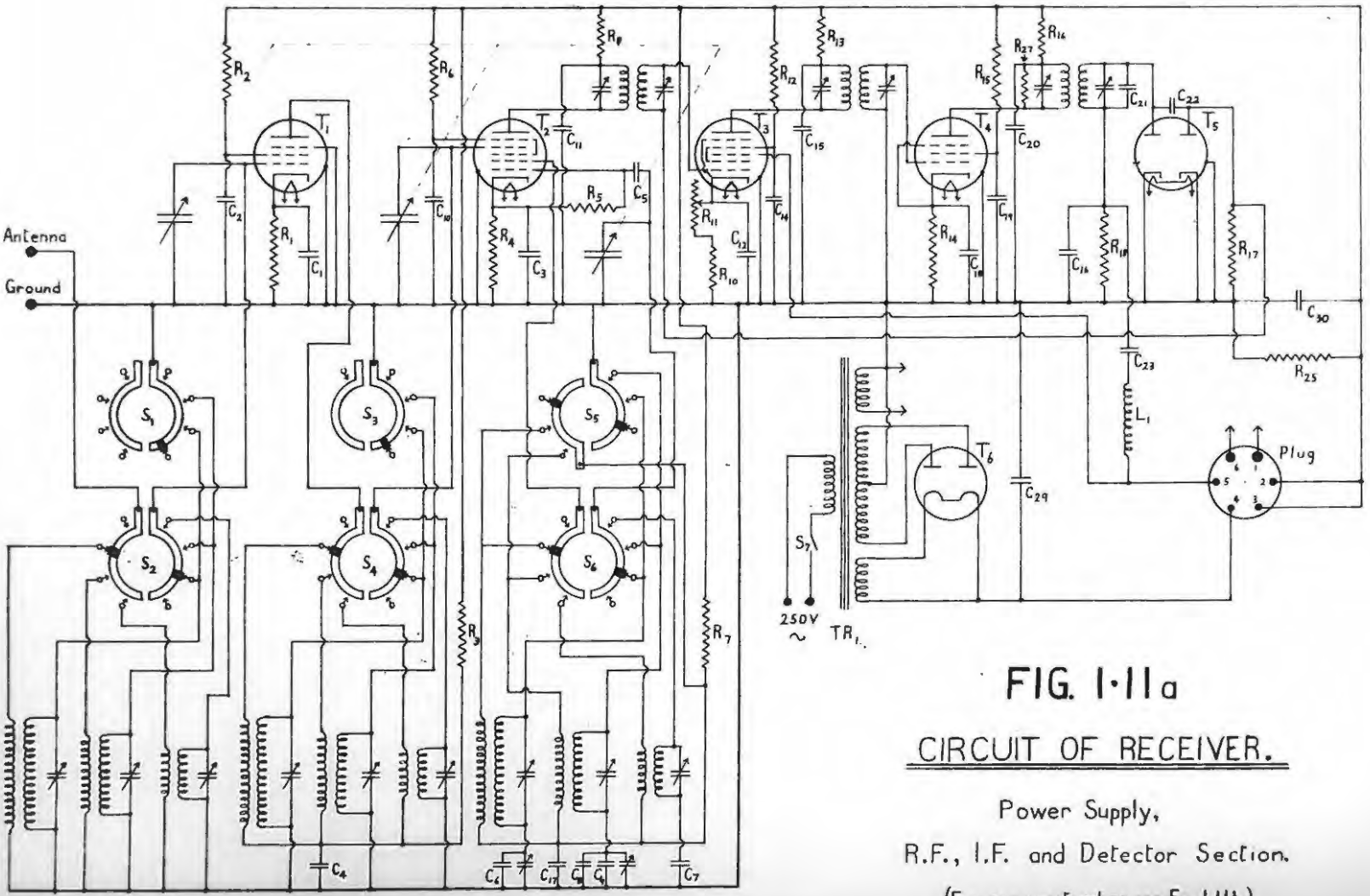

FIG. 1·11a

CIRCUIT OF RECEIVER.

Power Supply,

R.F., I.F. and Detector Section.

(For component values see Fig. 1·11b.)

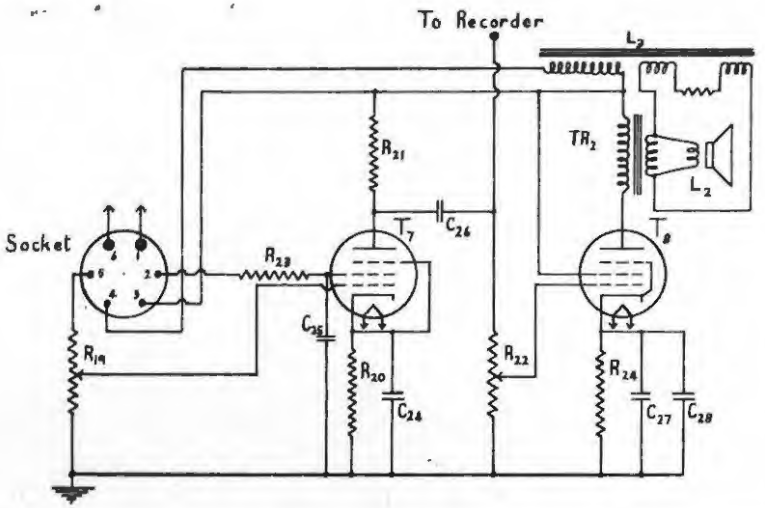

T_1	= 6SK7	S_1–S_6	= Waveband Switch
T_2	= 6A8	S_7	= Power Switch
T_3	= 6L7		
T_4	= 6D6	TR_1	= Mains Transformer
T_5	= 6H6G	TR_2	= Speaker Output Transformer
T_6	= 80		
T_7	= 6C6	The plug of Fig 1·11a fits the socket of	
T_8	= 42	Fig. 1·11b in the position indicated.	

L_1	= 30 mH
L_2	= Voice Coil
L_3	= Speaker Field Coil

R_1	= 300 Ohms		
R_2	= 80,000 Ohms		
R_3	= 5,000 "		
R_4	= 300 "		
R_5	= 50,000 "		
R_6	= 75,000 "		
R_7	= 25,000 "		
R_8	= 15,000 "		
R_9	= 2·0 Megohms		
R_{10}	= 500 Ohms		
R_{11}	= 10,000 "	(R.F. Gain)	
R_{12}	= 0·125 Megohm		
R_{13}	= 8,000 Ohms		
R_{14}	= 500 "		
R_{15}	= 0·1 Megohm		
R_{16}	= 6,000 Ohms		
R_{17}	= 0·2 Megohm		
R_{18}	= 0·25 "		
R_{19}	= 0·5 "	(A.F. Gain)	
R_{20}	= 1,000 Ohms		
R_{21}	= 75,000 "		
R_{22}	= 75,000 "	(P.A. Gain)	
R_{23}	= 0·45 Megohm		
R_{24}	= 500 Ohms		
R_{25}	= 50,000 "	25 Watt	
R_{27}	= 0·15 Megohm		

C_1	= 0·1	μFd	
C_2	= 0·001	"	
C_3	= 0·1	"	
C_4	= 0·01	"	
C_5	= 40	$\mu\mu$Fd	
C_6	= 300	"	
C_7	= 2,300	"	
C_8	= 400	"	
C_9	= 0·001	μFd	
C_{10}	= 0·001	"	
C_{11}	= 0·005	"	
C_{12}	= 0·05	"	
C_{13}	= 0·01	"	
C_{14}	= 0·01	"	
C_{15}	= 0·01	"	
C_{16}	= 100	$\mu\mu$Fd	
C_{17}	= 0·005	μFd	
C_{18}	= 0·1	"	
C_{19}	= 0·001	"	
C_{20}	= 0·003	"	
C_{21}	= 300	$\mu\mu$Fd	
C_{22}	= 100	"	
C_{23}	= 0·05	μFd	
C_{24}	= 25	"	25 V.W. Electrolytic.
C_{25}	= 1	"	
C_{26}	= 0·1	"	
C_{27}	= 16	"	450 V.W. "
C_{28}	= 16	"	450 V.W. "
C_{29}	= 8	"	450 V.W. "
C_{30}	= 16	"	450 V.W. "

FIG. 1·11b

CIRCUIT OF RECEIVER.

A.F. Section and Legend.

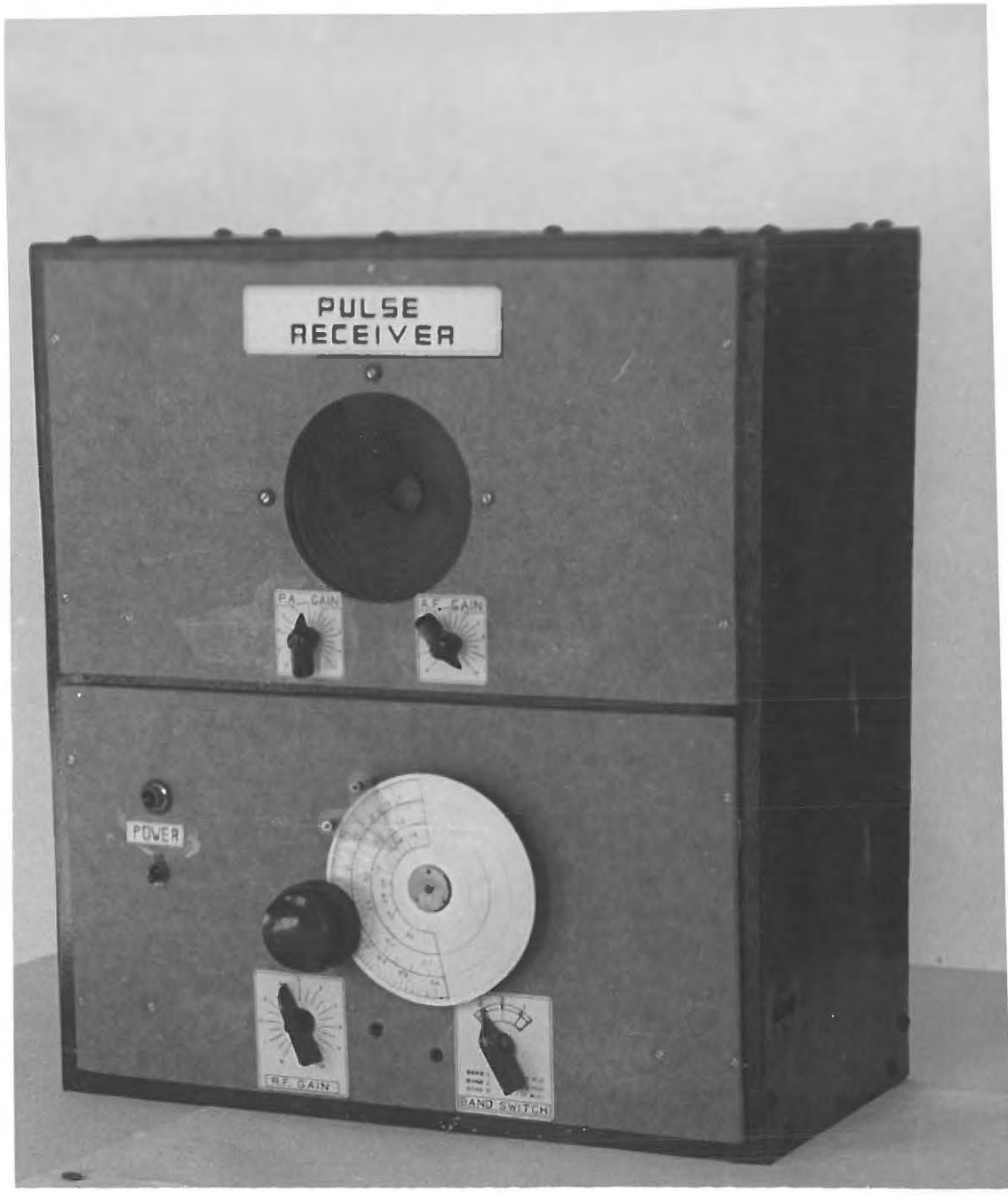

FIG. 1·12

FIG. 1·13

Receiver.

(R.F., I.F. and Detector Section.)

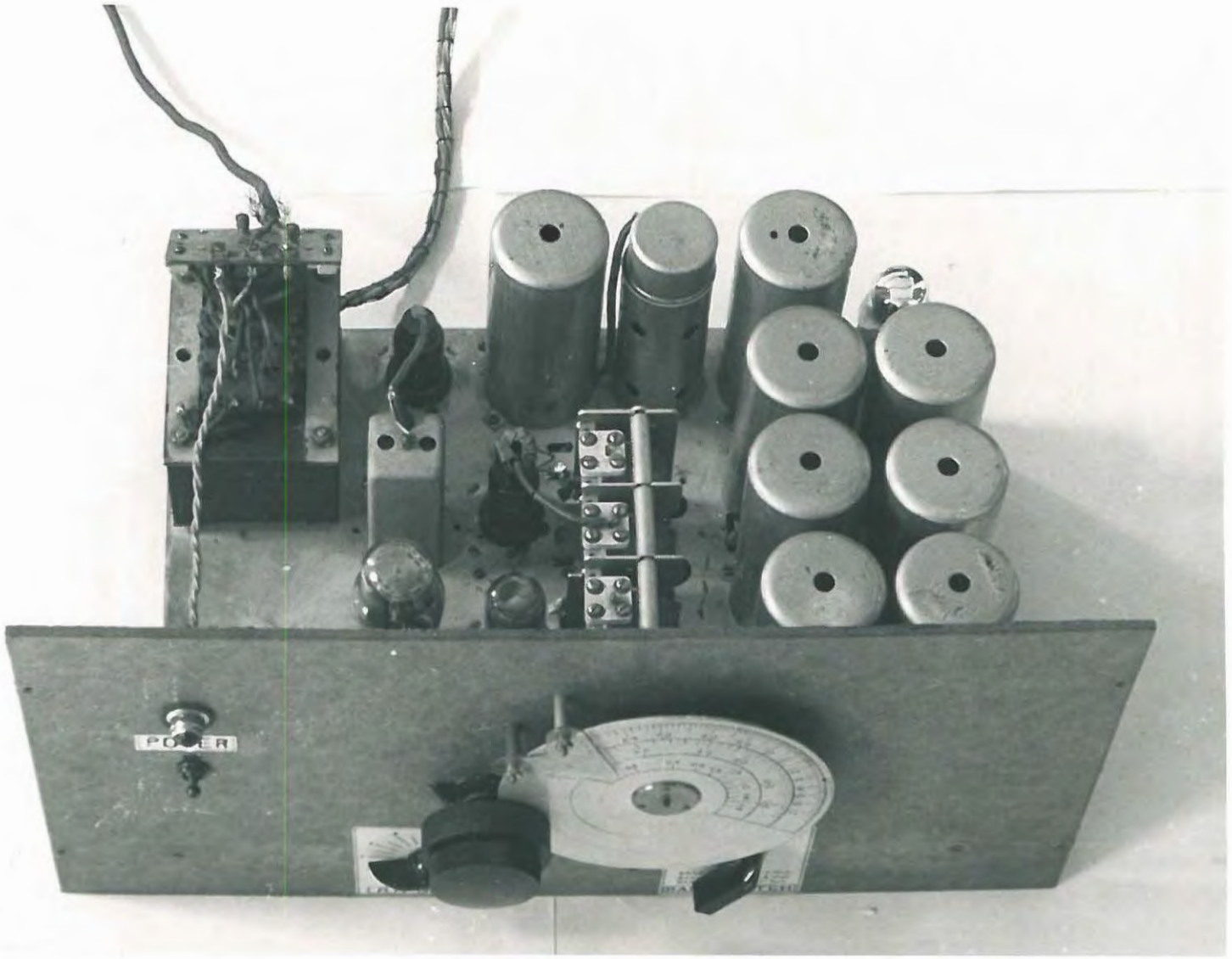

constant of the order of a few seconds, it cannot be used in a receiver of this type; however, some kind of A.V.C. is necessary to prevent oscillations: two such circuits are included, one an integrating circuit consisting of R_{17}, R_9 and C_{13} to reduce the gain under disturbed conditions; the other, by the application of the output pulse from the detector to the third grid of T_3 reduces the gain momentarily after any strong pulse.

The audio section is designed with very long time constants, so that all the harmonics of the pulse may be amplified and its duration not lengthened.

The useful range of the receiver is covered in two bands and only one change is necessary at 5.4 Mc/sec.

Frequency Calibration.

Since the frequency plays a very important part in ionospheric measurements, being one of the few quantites which can be measured accurately, both the transmitter and the receiver must be carefully calibrated and the calibration must be checked at regular intervals.

The most reliable secondary standard of frequency is provided by a crystal controlled oscillator, usually working at a frequency of 100 kc/sec., giving a waveform rich in harmonics. A rectangular waveform is particularly suitable, and it is not uncommon to detect harmonics as high as the 200th in the output of such an oscillator. An instrument of this kind provides therefore a series of signals of standard frequency from 100 kc/sec. to about 10 or 20 Mc/sec., and provides the most suitable standard for the calibration of ionospheric equipment.

Owing/

Owing to war conditions it was impossible to obtain a crystal resonating at this frequency and attempts to cut a quartz crystal to the required dimensions proved unsuccessful. Resort was therefore made to a less ambitious frequency standard by buiding a conventional form of oscillator and achieving frequency stability in the following ways:

(i) A screen grid tube was operated as an oscillator of the electron-coupled type. In this type of circuit, where the screen grid acts as oscillator plate, it is possible, by a suitable choice of the screen grid potential, to make the frequency practically independent of the plate supply potential (1:38).

(ii) Battery operated tubes with 2 volt filaments were used throughout with low potentials to avoid frequency drift due to heating.

(iii) Hard-drawn 14 gauge copper wire was used in all circuits connected with the tuning elements, to avoid changes of frequency due to displacement of wires.

(iv) The output was taken through a buffer amplifier tube.

(v) The oscillator tube and circuits were carefully shielded.

Fig. 1.14 shows the circuit used. T_1 is the oscillator tetrode. R_1 and R_2 form a potential divider to supply the screen with the required fraction of the plate voltage. The frequency stability was tested by changing the supply voltage from 180 to 45 volts without altering the frequency by more than 10 c/sec.

In/

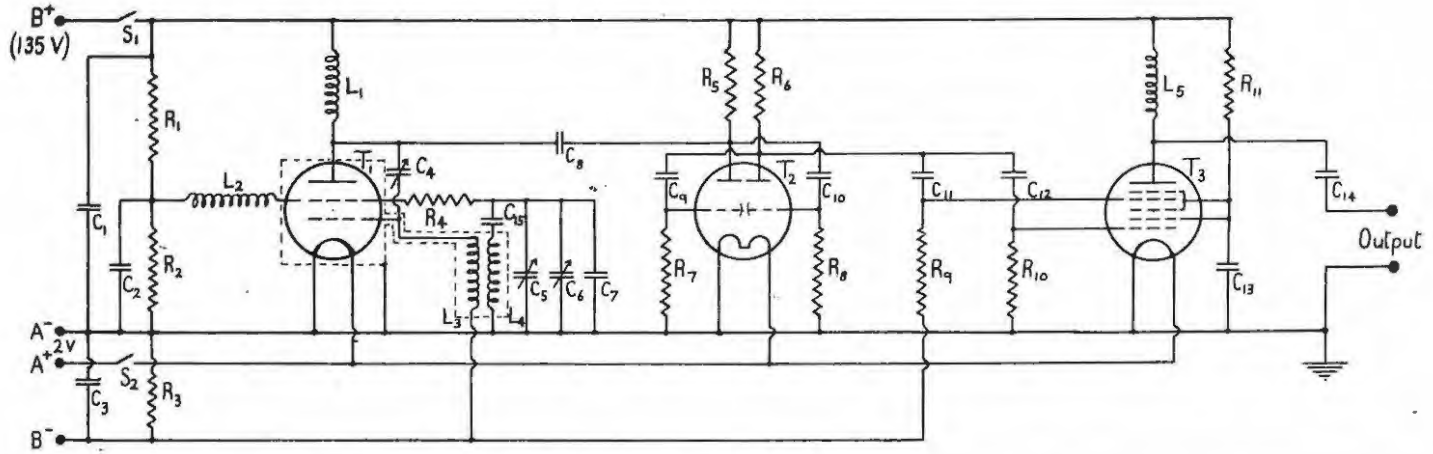

R_1	=	56,000	Ohms	C_1, C_2, C_3	=	0·1	μFd.	L_1, L_2 = R.F. Choke
R_2	=	44,000	"	C_4, C_5	=	20	μμFd Trimmer	L_3, L_4 = Oscillator coils
R_3	=	200	"	C_6	=	100	" "	L_5 = 0·25 mH R.F. Choke
R_4	=	75,000	"	C_7, C_9	=	400	" Mica	
R_5, R_6	=	50,000	"	C_8, C_{10}	=	100	" "	T_1 = 32
R_7, R_8	=	25,000	"	C_{11}	=	50	" "	T_2 = 19
R_9	=	0·125	Megohm	C_{12}	=	40	" "	T_3 = 1C6
R_{10}	=	0·25	"	C_{13}	=	0·25	μFd	
				C_{14}	=	75	μμFd	$S_1 + S_2$ = D.P.S.T. Switch.
				C_{15}	=	0·1	μFd.	

FIG. 1·14

CIRCUIT OF 100 KC./S. FREQUENCY STANDARD.

In addition to being electron-coupled the load of the oscillator was reduced to a minimum by using only a small capacity C_8 to control the frequency of the conventional multivibrator T_2. The rectangular waveform from the multivibrator was injected into the buffer amplifi T_3 through C_{11} and C_{12}. Although T_3 is actually a pentagrid converter, it seems to isolate effectively the output from the input on account of its many grids.

The output was compared with the 10 Mc/sec. signal of station WWV maintained by the American Bureau of Standards, the carrier frequency of which is guaranteed to be accurate to one part in ten million. By adjustment of the trimmer condensers C_5 and C_6 the 100th harmonic was brought into zero beat with the WWV carrier. Long and repeated tests have failed to show a beat note of frequency greater than 20 cycles, showing that the fundamen is constant to within 0.2 of a cycle or 2 parts in a million.

Both transmitter and receiver were calibrated against the harmonics of this oscillator, and the calibrations were checked at regular intervals.

Operational Technique.

In taking a reading, the frequency of both transmitter and receiver are increased simultaneously manually (fig. 1.15); to keep the receiver in tune some sort of monitoring device is necessary: the loudspeaker of the receiver forms a useful adjunct to the 3 ins. R.C.A. oscillograph, model TMV 122B, used as a visual monitor, since the reflection makes its presence heard by a change in note.

When both receiver and transmitter are tuned to the same f-requency, and the output of the receiver is connected

to/

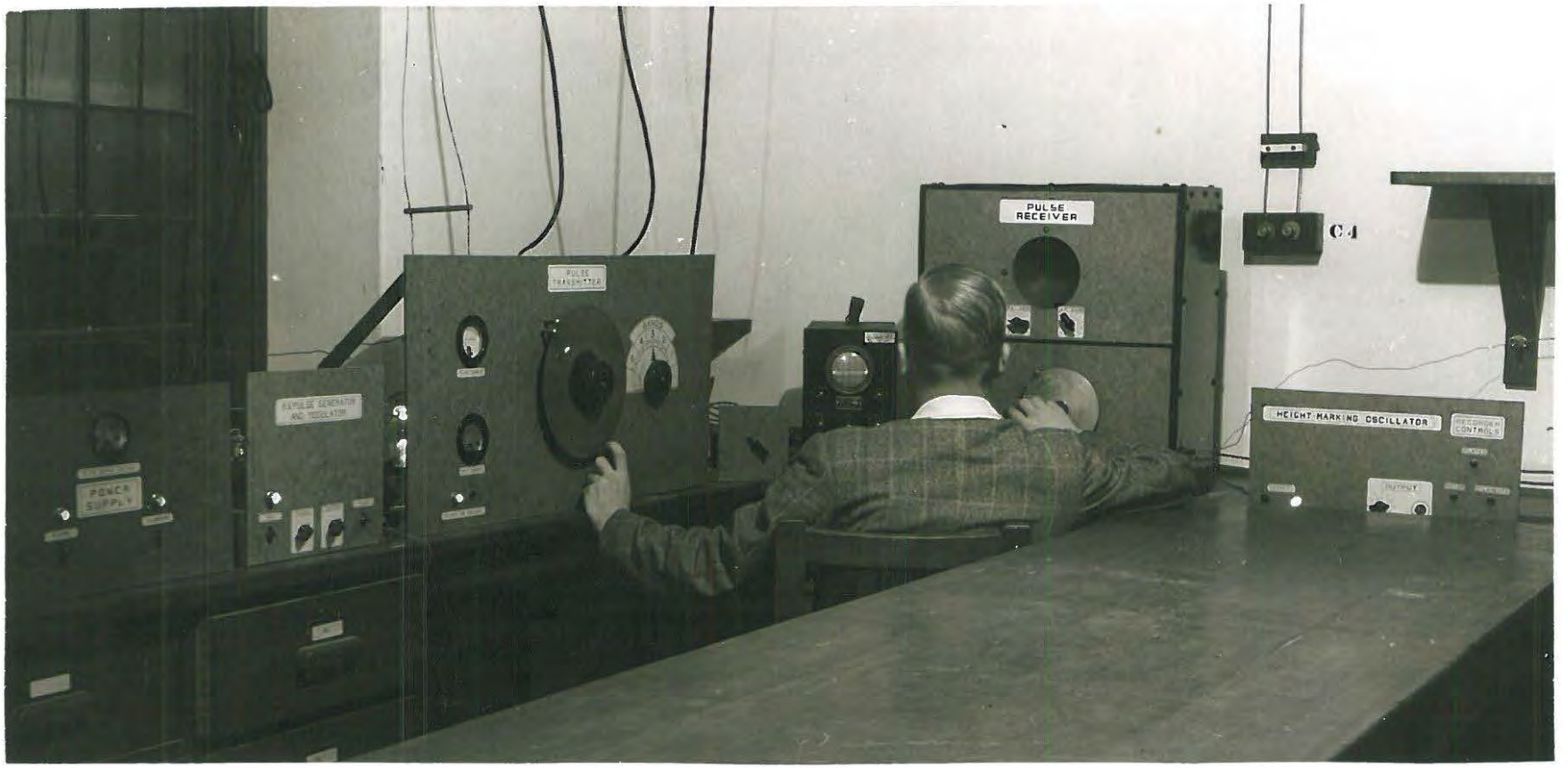

FIG. 1·15

Sweep in Progress.

to the vertical deflecting plates of the monitoring C.R.O., a linear or sinusoidal time-base being applied to its horizontal plates, and synchronised to the A.C. mains, a pattern as shown in fig. 1.16(a) results. As will be

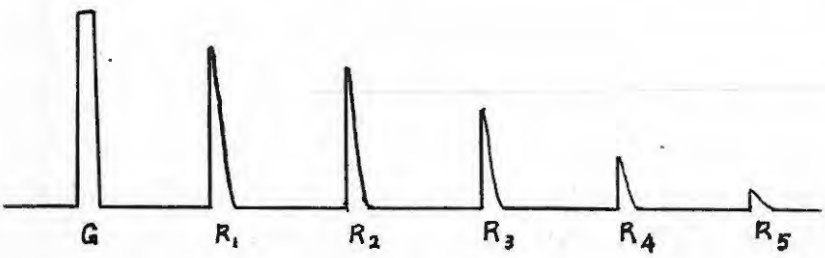

Fig. 1.16(a) - Appearance of C.R.O. screen.

seen, the pattern consists of one strong vertical deflection G which saturates the receiver: it represents the ground pulse. This first deflection is followed by a number of similar deflections, varying in number according to conditions and decreasing in strength towards the right. They represent reflections from one of the layers of the ionosphere. The first one, R_1, is due to a pulse which has travelled to the layer concerned and back. This particular pulse may be reflected at the surface of the earth and repeat the return journey, giving rise to the second reflection R_2. This process may be repeated any number of times; at each reflection, however, a certain amount of absorption occurs, the signal is weakened and hence the number of reflections R_1, R_2, R_3, R_4, etc., which can be seen on the oscillograph screen varies with

the/

the conditions prevailing along the path of the signal.

This explanation may be checked if the C.R.O. has a truly linear time base, in which case the various reflections are equally spaced.

The usual procedure with manually operated transmitter and receivers is to start at the low frequency end of the scale. The frequency of the transmitter is then increased at a constant rate and the receiver is kept tuned to the transmitter by keeping the strength of the reflected signal at maximum with the aid of the two monitoring devices. As the frequency is increased, the critical frequencies of the E region and F_1 region are passed. These are noted by the sudden increases in the separation between the ground pulse and the reflection.

Owing to the greater thickness of the F_2 layer, the approach to its critical frequency is accompanied by an increase in the retardation of the reflection, as it penetrates further and further into the layer. Under good conditions it is not unusual to follow the reflection to the extreme right of the horizontal sweep, i.e., a virtual height of 3000 km. The above process will, throughout this work, be referred to as a "sweep".

From such a sweep it should be possible theoretically to measure two types of data:

(a) The critical frequencies for the ordinary and extraordinary rays (i.e., the frequencies at which complete penetration occurs for each ~~layer~~ ray).

(b) The virtual or apparent height at any required frequency along the sweep.

However, measurements of this kind made directly on

a/

a C.R.O. screen would be both long and inaccurate; it has been estimated that even an expert operator could not take all the desired measurements on a complete sweep, including all three layers, in less than two hours.

This would be practically useless, because ionospheric layers are in a state of continuous and sudden change, which includes variations in height, thickness and electron density. Modern measurements are therefore always derived from some kind of photographic records, and to produce these a recording device must be added to the equipment already described.

Photographic Recorder.

The photographic recorder used consisted of a Cossor cathode ray tube, type 3237-J, with a blue short-persistence screen suitable for photographic purposes. The correct voltages for the electrodes were supplied by the rectifier T_1, while the time-base, amplifiers, etc., were supplied by T_2. These are all shown in fig. 1.17.

The time-base was produced by the gas-filled triode, T_6, the condenser C_{11} being charged linearly through the pentode T_7. After passing through the amplifier, T_5, with long time constants, the time-base signal was applied to the horizontal deflecting plates of the cathode ray tube. The time-base was synchronised with the mains through the transformer TR_1 in the thyratron grid circuit, and a certain amount of phase shift could be obtained by the use of R_9.

The output of the receiver was amplified by T_4 and, after/

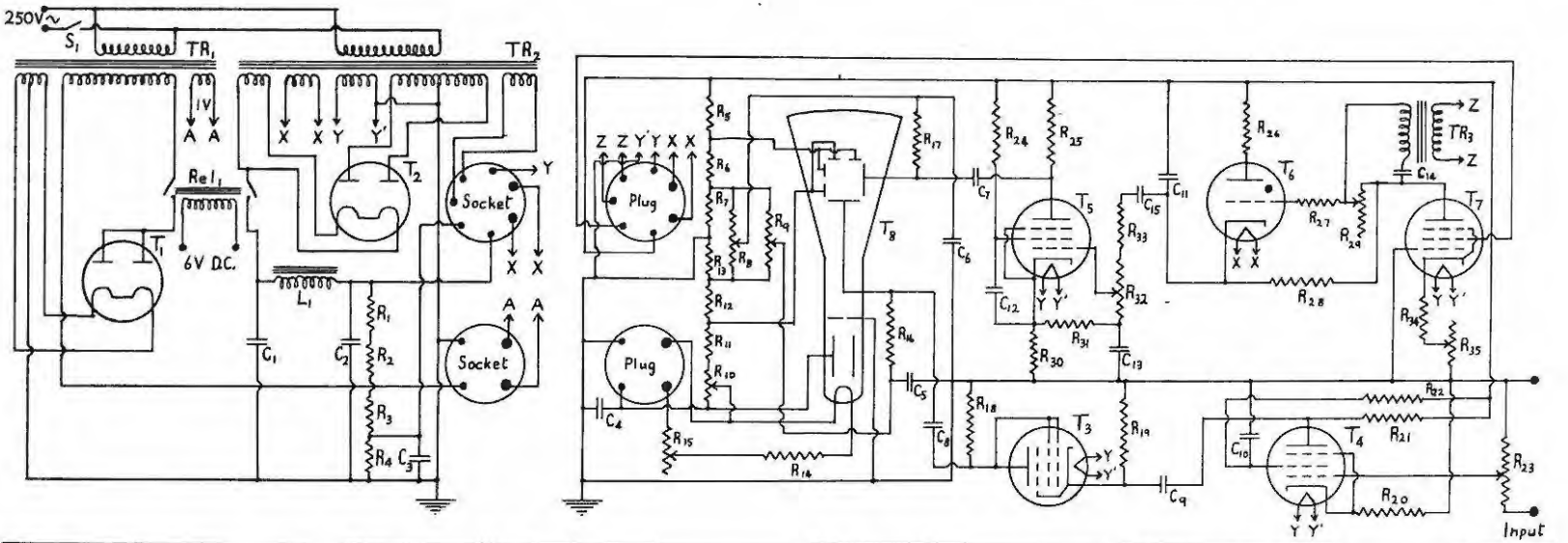

R_1, R_2	=	75,000	Ohms	R_{14}	=	0·15	Ohm	R_{27}	=	20,000	Ohms
R_3	=	40,000	"	R_{15}	=	0·3	" Intensity	R_{28}	=	7,000	"
R_4	=	50,000	"	R_{16}, R_{17}	=	5·0	Megohm	R_{29}	=	60,000	" Hor. Synch.
R_5	=	1·0	Megohm	R_{18}	=	0·5	"	R_{30}	=	5,000	"
R_6	=	0·2	"	R_{19}	=	1·0	"	R_{31}	=	0·125	Megohm
R_7	=	0·8	"	R_{20}	=	500	Ohms	R_{32}	=	2·0	" Hor. Gain
R_8	=	1·0	" Hor. Position	R_{21}	=	0·125	Megohm	R_{33}	=	0·5	"
R_9	=	1·0	" Vert. Position	R_{22}	=	0·5	"	R_{34}	=	5,000	Ohms
R_{10}	=	0·25	" . Focus	R_{23}	=	2·0	" Vert. Gain	R_{35}	=	10,000	" Hor. Sweep Frequency
R_{11}	=	2·0	"	R_{24}	=	0·2	"				
R_{12}	=	0·2	"	R_{25}	=	40,000	Ohms	L_1	=	20 H	
R_{13}	=	1·0	"	R_{26}	=	500	"	Rel_1	=	H.T. Remote Control Relay	

C_1, C_2	=	10	µFd	450 V.W. Electrolytic
C_3	=	16	"	450 V.W. "
C_4	=	2	"	800 V.W.
C_5, C_6	=	0·5	"	
C_7	=	0·1	"	
C_8, C_9	=	0·25	"	
C_{10}	=	0·1	"	
C_{11}, C_{12}	=	0·25	"	
C_{13}	=	0·5	"	
C_{14}	=	0·05	"	
C_{15}	=	0·5	"	

T_1	=	DW 15 (Mullard)
T_2	=	5Y3G
T_3	=	6F6
T_4, T_5	=	6SJ7
T_6	=	GT1A (Osram)
T_7	=	39/44
T_8	=	3237 J (Cossor)
TR_1	=	C.A.T. Supply Transformer
TR_2	=	Amplifier Supply Transformer
TR_3	=	1:1 Synch. Transformer

FIG. 1·17

CIRCUIT OF PHOTOGRAPHIC RECORDER.

after passing the D.C. restoring diode T_3, the purpose of which is to eliminate the "tail" following the pulses, the signal was applied to the vertical deflecting plates of the C.R. tube. A pattern, photographed in fig. 1.16(b), thus resulted.

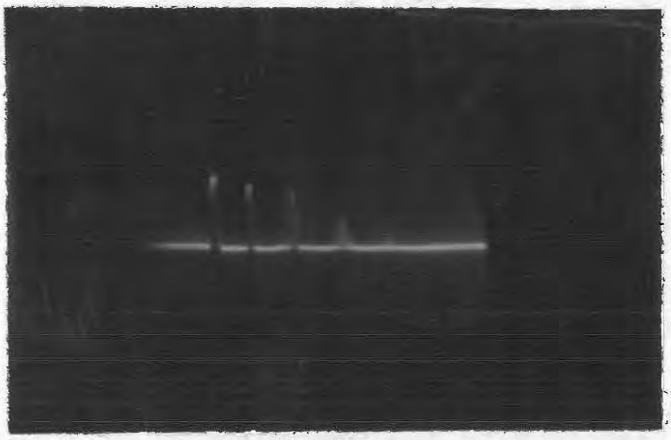

Fig. 1.16(b) - Appearance of C.R.O. screen.

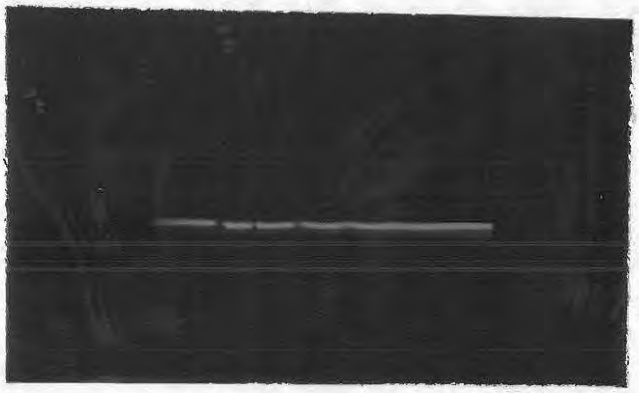

Fig. 1.20 - Effect of placing a lead sheet with slit in front of C.R.O. screen.

The photographic records were made on 35 mm. film, for/

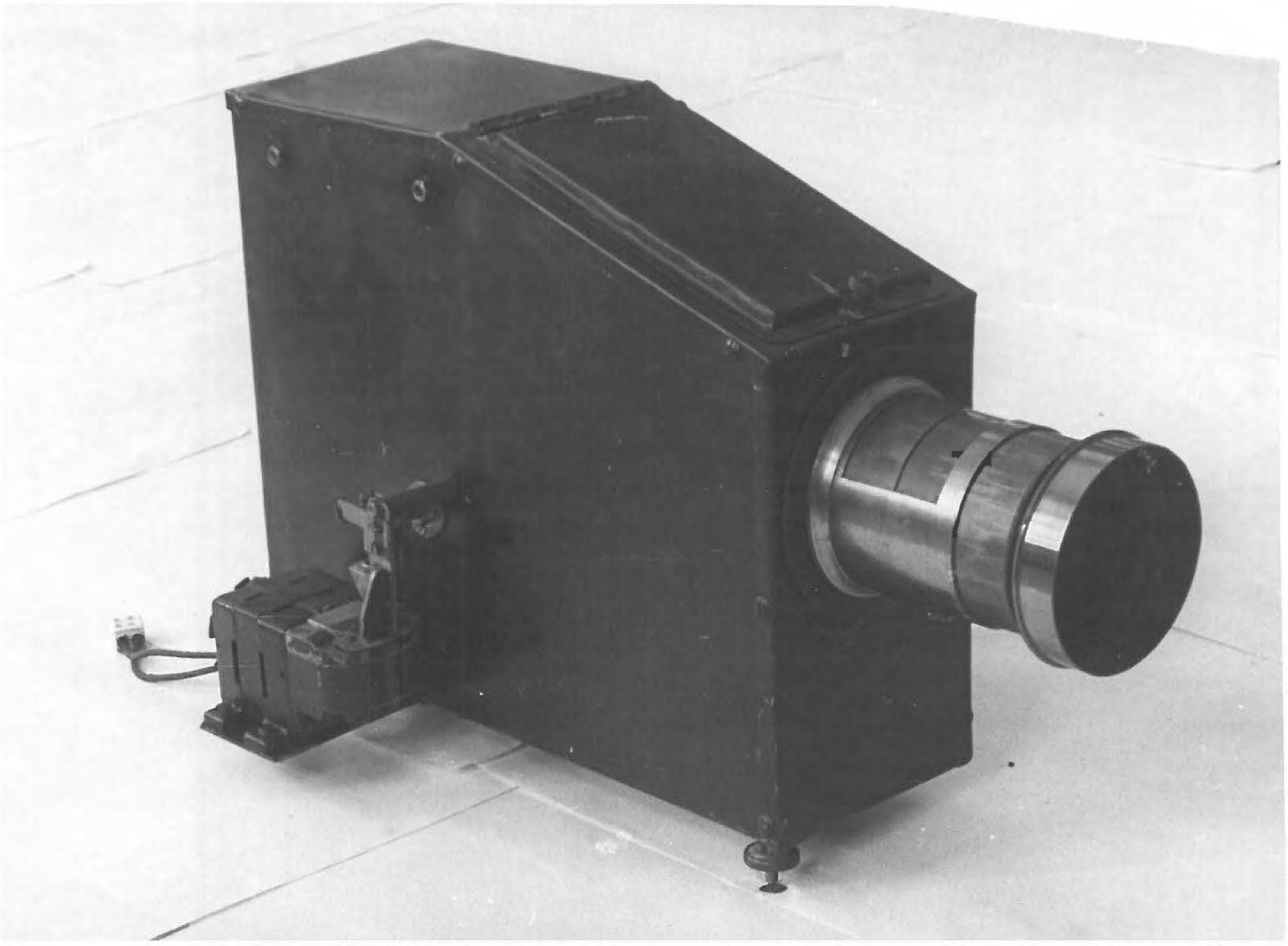

FIG. 1·18

Recording Camera.

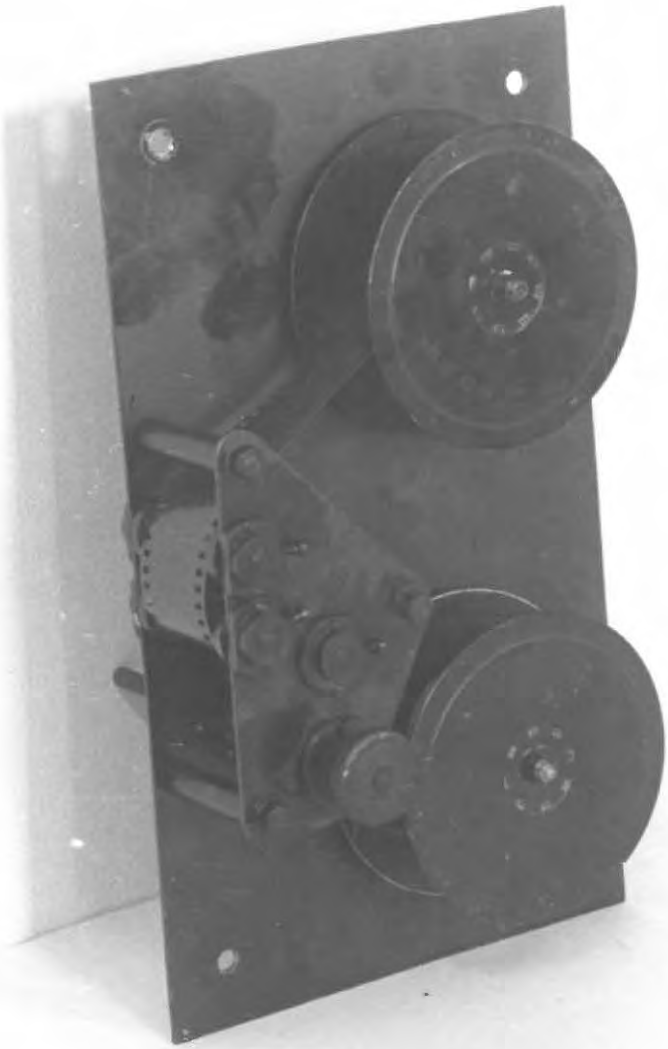

FIG. 1·19

Camera Mechanism.

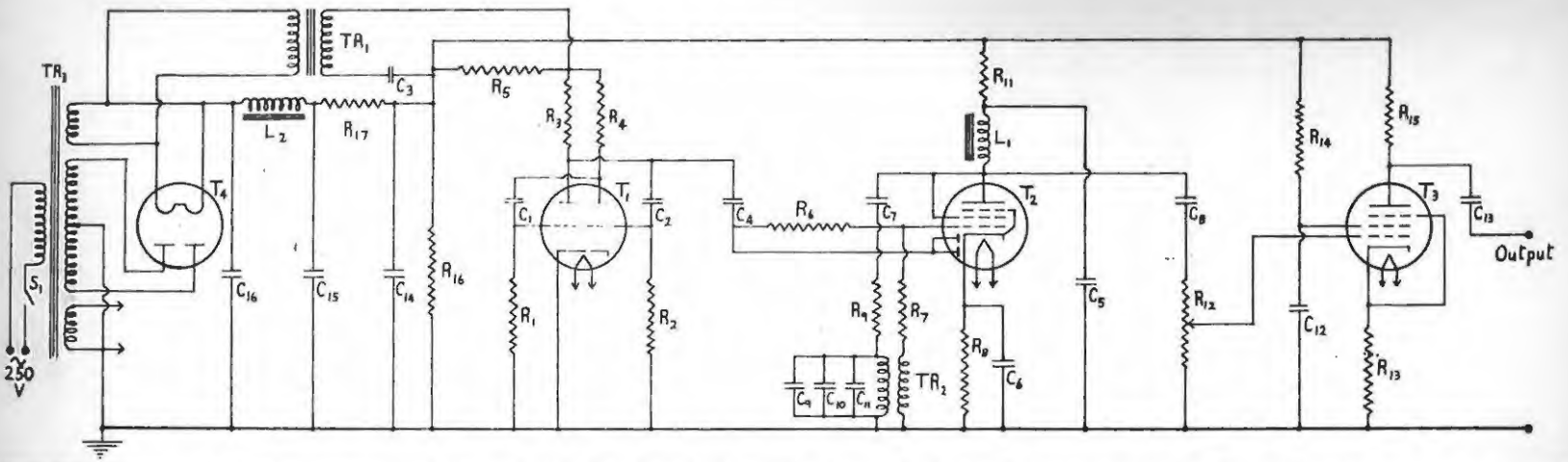

R_1	= 1·0	Megohm	R_{17}	= 10,000	Ohms 10 Watt	C_1	= 0·03	μFd
R_2	= 0·25	"	S_1	= Power Switch		C_2	= 0·001	"
R_3	= 0·1	"	L_1	= 50 H		C_3	= 0·1	
R_4	= 0·5	"	L_2	= 20 H		C_4	= 100	μμFd
R_5	= 75,000	Ohms				C_5	= 0·05	μFd
R_6	= 0·25	Megohm	TR_1	= Synch. Transformer		C_6	= 4	" Electrolytic
R_7	= 0·1	"	TR_2	= General Radio Co. Type 271 M.F. Transformer		C_7	= 0·5	"
R_8	= 300	Ohms	TR_3	= Mains Transformer		C_8	= 0·01	"
R_9	= 50,000	"				C_9	= 0·07	"
R_{11}	= 75,000	"	T_1	= 53		C_{10}	= 0·003	"
R_{12}	= 0·25	Megohm Output Control	T_2	= 287		C_{11}	= 0·002	"
R_{13}	= 5,000	Ohms	T_3	= 59		C_{12}	= 4	" 450 V.W. Electrolytic
R_{14}	= 0·5	Megohm	T_4	= 5Y3G		C_{13}	= 0·05	"
R_{15}	= 75,000	Ohms				C_{14}	= 8	" 450 V.W. "
R_{16}	= 0·2	Megohm				C_{15}, C_{16}	= 10	" 450 V.W. "

FIG. 1·21

CIRCUIT OF HEIGHT-CALIBRATING OSCILLATOR.

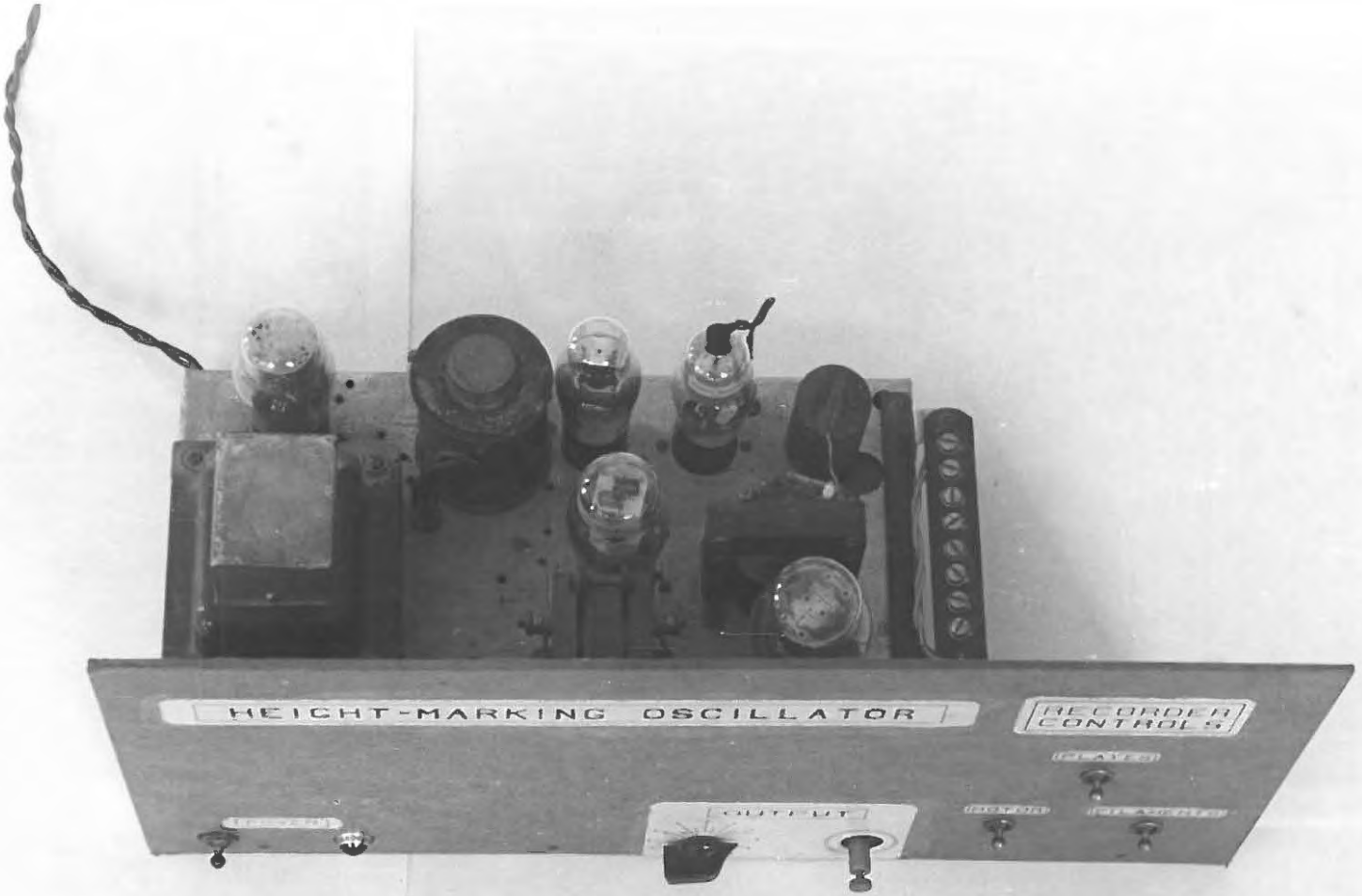

FIG. 1·22

of the mains. This was done by applying the output of the unsymmetrical multivibrator T_1, detected by the diode section of T_2, to the oscillator control grid. The output was fed to the buffer amplifier T_3, and, when desired, applied by means of a two-way foot switch, to the recorder, instead of the receiver ouput.

Reduction and Presentation of Observations.

Photographic Records and their Interpretation.

Two typical examples of records made with the apparatus described are shown in figs. 1.23 and 1.24.

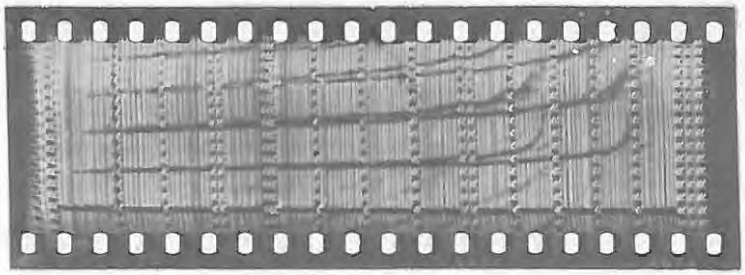

Fig. 1.23 - Sweep for December 6th, 1945, 2 hours.

The sweep illustrated in fig. 1.23 is typical of nighttime conditions. The height-calibrating oscillator marks are at intervals of 0.2 Mc/sec., starting at 2.4 and ending at 5.0, with double marks at every whole number of megacycles. The long mark at 3.2 covers a band change of the transmitter. The duration of the sweep was three minutes, the film speed being just less than 3 cm. per minute. The ground pulse shows as the straight line, running parallel to the lower edge of the

film/

film and the reflections are visible from only one layer, the F layer. At the beginning (left) of the sweep, two strong lines and two weak ones may be seen; the lowest of these is the first reflection for the F region and the others are higher order multiples (fig. 1.20). As the frequency is increqsed, the apparent height of reflecti represented by the distance between the reflection and the base line, slowly increases - this may be seen more clearly on the higher order reflections. At 3.9 Mc/sec. the first reflection splits into two, one of which, identified with the ordinary ray, rapidly increases in virtual height and finally penetrates the layer at 4.35 Mc/sec.: this then represents the ordinary critical frequency, f^{o}. The lower reflection, which is the extraordinary, follows a similar course, but does not penetrate until 4.80 Mc/sec.

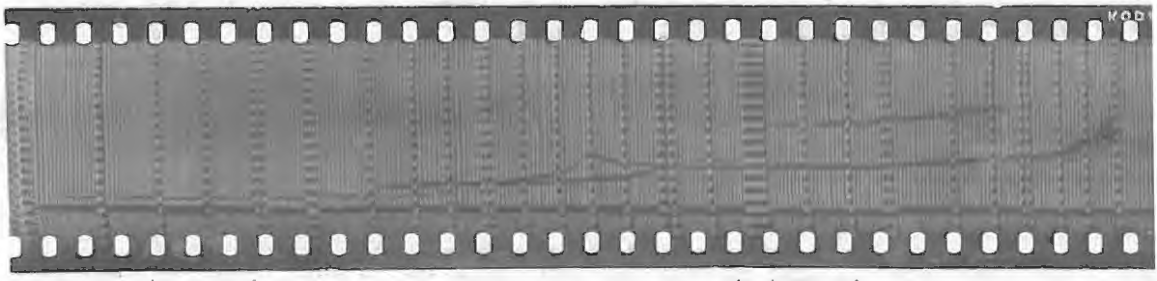

Fig. 1.24 - Sweep for December 28th, 1945, 9 hours.

In fig. 1.24, a daytime sweep, ranging between 2.2 and 8.0 Mc/sec. and taken over 6 minutes, the structure of the ionosphere is obviously more complex than that of fig. 1.23. From 2.2 to 6.0 the frequency marks are every 0.2 Mc/sec., the next mark is 6.5 and from 6.8 on marking is resumed at 0.2 Mc/sec. intervals. Long marks at 3.2 and 5.4 are due to band changes of transmitter

and/

and receiver respectively. At the low frequency end of this record a single reflection at a height of approximately 100 km. is due to the E layer. Just over 3.2 Mc/sec, penetration of the ordinary ray occurs and the ordinary reflection is then returned from a virtual height of about 130 km. At 3.35 Mc/sec. penetration occurs to the F_1 layer, for which the ordinary ray critical frequency is 4.60 Mc/sec. From here onwards the ray is returned from the F_2 layer, which it finally penetrates with some broadening at 7.6 Mc/sec. The downward slope of the trace immediately after the E and F_1 critical frequencies is accounted for by the fact that at these points the frequency of the wave is only slightly greater than the critical frequency of the layer which has just been penetrated and hence it suffers much retardation in passing through that layer; this has the effect of increasing the virtual height. The extraordinary ray will be seen to follow a course similar to that of the ordinary ray, but displaced towards the higher frequencies by about 0.5 Mc/sec.; it is, however, somewhat more absorbed and in places altogether missing, e.g., F_2 critical frequency.

The reflection returned from an apparent height of 130 km. between 3.2 and 3.35 Mc/sec. has been interpreted by some workers as due to the presence of sporadic E ionisation above the normal E layer; during the observations of the present work, this type of reflection was encountered practically every day and it is here suggested that something more regular than sporadic ionisation is involved; the presence of two E layers has already been suggested by Halliday (1:16)

and/

and others (1:25), but more recent American workers still seem to attribute such regular reflections to sporadic E (1:26).

Evaluation of true heights.

The heights which may be scaled from ionosphere records, such as those illustrated in figs. 1.23 and 1.24, are virtual heights and these records are indeed nothing more than graphs in which the virtual height of the layer is plotted as ordinate and the frequency as abscissa. The problem of deducing the true height of maximum electron density from such graphs was attacked by Appleton (1:27), (1:28) and Murray and Hoag (1:29); but their results lacked ease of application.

A reasonably simple method was published by Booker and Seaton in 1940 (1:30), depending on the following argument:

If a parabolic distribution of electron density with height is assumed (this being the simplest function which will give a maximum) then Appleton has shown (1:28) that

$$\frac{h' - h_m}{h_M - h_m} = \frac{f}{2f^o} \log_e \frac{f^o + f}{f^o - f} \quad . \quad . \quad . \quad . \quad (1.3)$$

where h' is the virtual height of reflection of a signal of frequency f, h_m is the true height at which on the parabolic distribution the electron density becomes zero (i.e., the minimum height of the layer), h_M is the true height of maximum electron density and f^o is the ordinary critical frequency. The meaning of these symbols will be perhaps made clearer from fig. 1.25.

Defining/

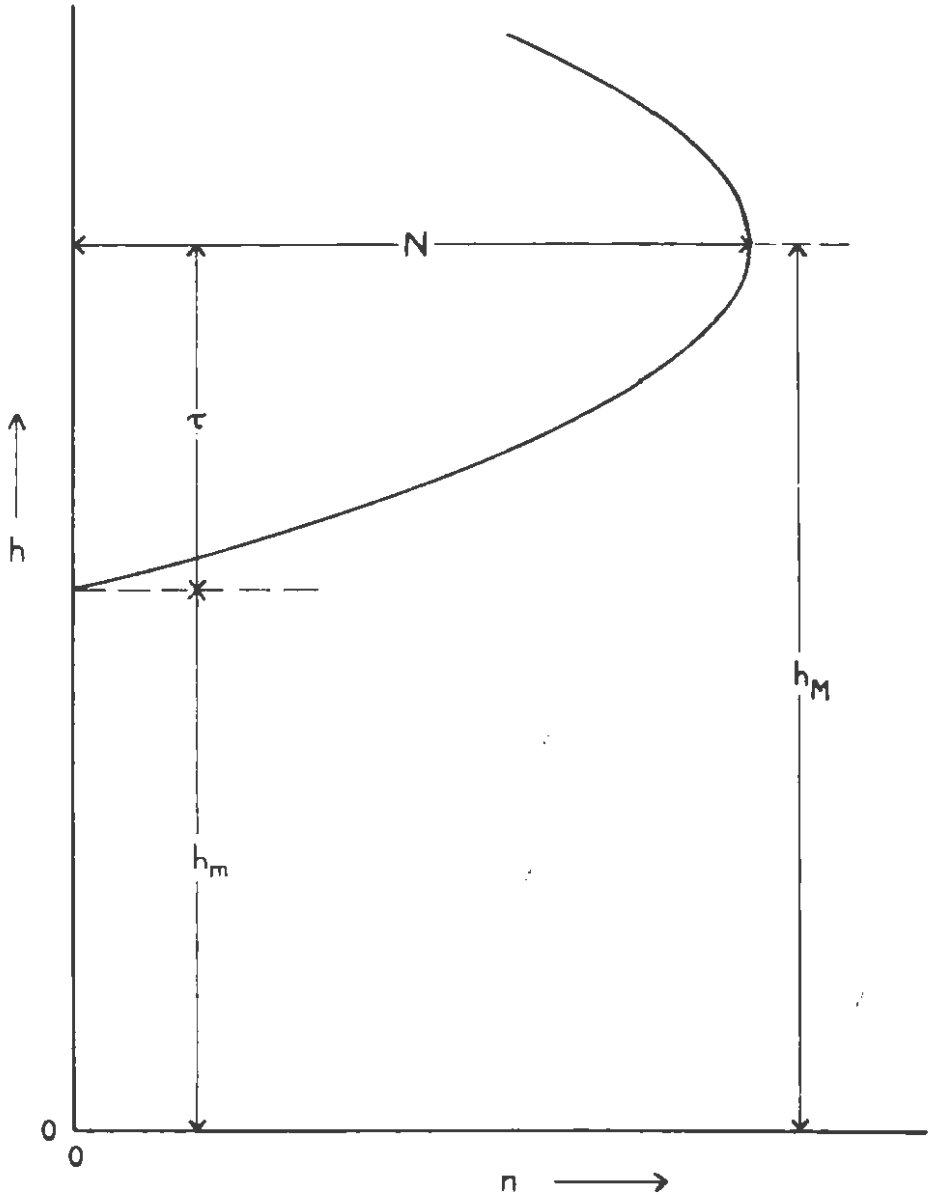

FIG. 1·25

PARABOLIC LAYER.

Defining a function $\phi(x)$ by the equation

$$\phi(x) = \frac{x}{2} \log_e \left|\frac{1+x}{1-x}\right| - 1 \quad . \quad . \quad . \quad . \quad (1.4)$$

and writing $\tau = h_M - h_m$ = semithickness of the layer, eqn. (1.3) may be written:

$$h' = h_M + \tau\phi\left(\frac{f}{f^o}\right) \quad . \quad . \quad . \quad . \quad . \quad (1.5)$$

Values of $\phi(x)$ have been tabulated and shown graphically by Booker and Seaton (1:30). Hence from the graph of h' vs. f, i.e., the ionosphere record, h_M and τ may be estimated as follows:

(i) Measure the values of h' corresponding to any two values of $\frac{f}{f^o}$ lying between 0 and 1.

(ii) From the tabulated function find the values of ϕ corresponding to these two values of $\frac{f}{f^o}$.

(iii) Substitute the two pairs of corresponding values of h' and ϕ into eqn. (1.5) and solve for τ and h_M.

In practice it is convenient to choose the values of $\frac{f}{f^o}$ so that ϕ takes on specially simple numerical values, such as those shown in table 1:2.

$\frac{f}{f^o}$	0.648	0.725	0.757	0.834	0.887	0.901	0.925	0.969
ϕ	$-\frac{1}{2}$	$-\frac{1}{3}$	$-\frac{1}{4}$	0	$+\frac{1}{4}$	$+\frac{1}{3}$	$+\frac{1}{2}$	+1

Table 1:2 - Frequency ratios for simple values of ϕ.

In spite of its comparative simplicity, Booker and Seaton's/

Seaton's method does not seem to have been used to any great extent. Even recent investigators (1:31) have used the virtual height in the discussion of problems for which the true height was obviously required.

In the present work a routine method for the application of Booker and Seaton's analysis to the records has been developed. For purposes of measurement the records were enlarged 10 times in a microfilm reader. On the base of this was drawn a scale of heights to fit the height-calibrating oscillator marks on an average record. Owing to slight variations in the time base of the recording oscillograph, the actual scale rarely fitted this prepared scale accurately and a correction was always applied for this by reading the difference at the nearest 100 km. mark. With this apparatus it was found that the heights obtained could be reproduced to 2 km. Where multiple reflections were available, their heights were also read and divided by the proper integer; the final result was taken as the mean of all such estimates.

In fig. 1.26 is shown an enlargement of fig. 1.23, by approximately the same amount. It will be seen that the definition particularly at the beginning of the ground pulse and reflections is good enough to allow such accuracy.

First f^o and f^x for a layer were estimated by inspection to two decimal places of a megacycle; fractions $\frac{f}{f^o}$, having the values shown in table 1:2, were then calculated and the height at each of these frequencies,

where/

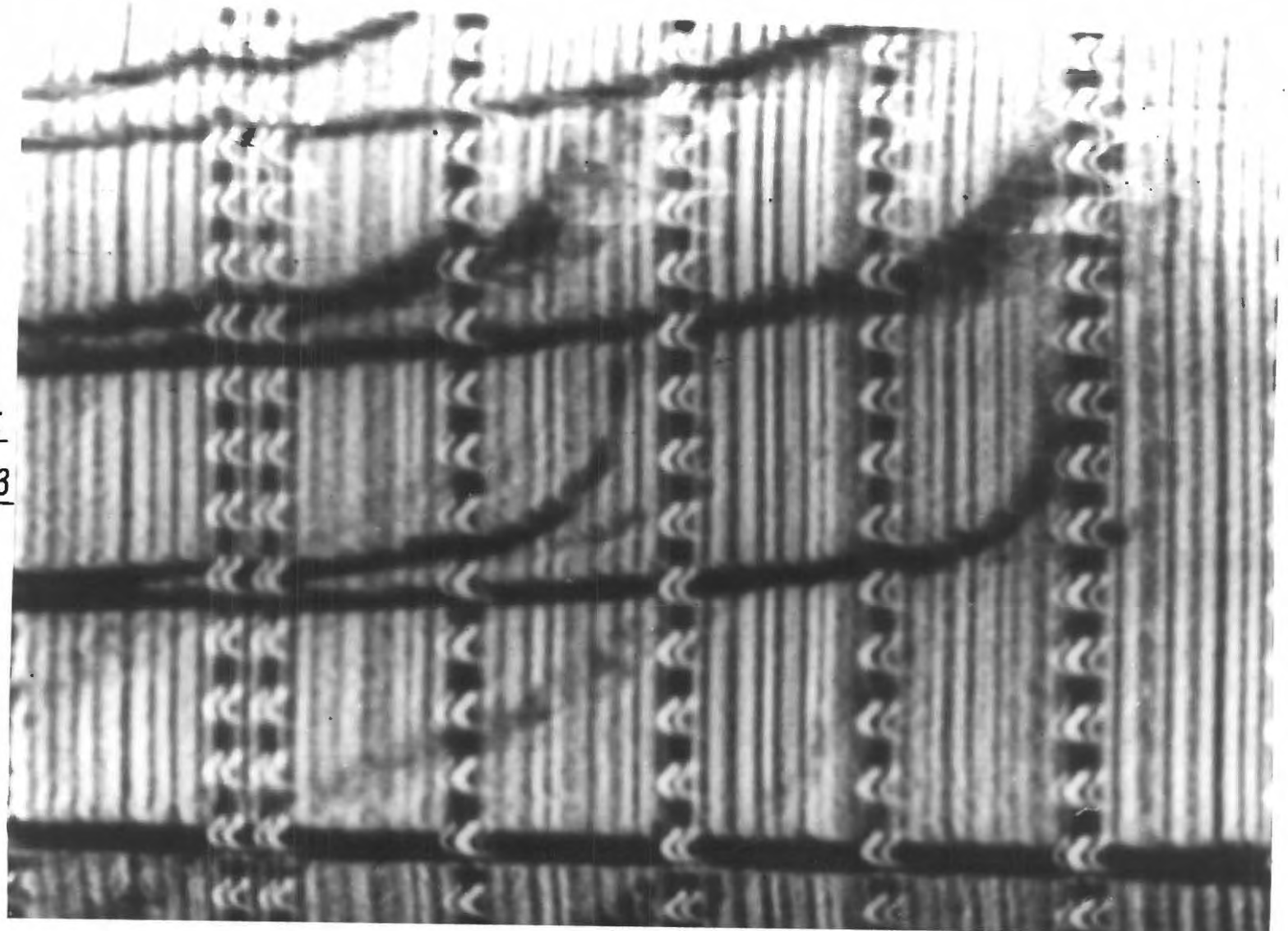

FIG. 1·26

Enlargement
From Fig. 1·23

where available, was read. These were then paired off and h_M and τ calculated for each pair, using equation (1.5)

Let h'_{648} be the value of h' for $\frac{f}{f^0} = 0.648$,

" h'_{925} " " " " " " " " $= 0.925$, etc.

By equation (1.5)

$$h'_{648} = h_M - \tfrac{1}{2}\tau$$

and $$h'_{925} = h_M + \tfrac{1}{2}\tau$$

Hence $$h_M = \tfrac{1}{2}(h'_{648} + h'_{925})$$

and $$\tau = h'_{925} - h'_{648}$$

By a similar process the relations shown in table 1:3 may be obtained. Wherever possible the first

h_M	τ
$\frac{1}{2}(h'_{648} + h'_{925})$	$h'_{925} - h'_{648}$
$\frac{1}{2}(h'_{725} + h'_{901})$	$\frac{3}{2}(h'_{901} - h'_{725})$
$\frac{1}{2}(h'_{757} + h'_{887})$	$2(h'_{887} - h'_{757})$
h'_{834}	$h'_{969} - h'_{834}$
$2h'_{887} - h'_{925}$	$4(h'_{925} - h'_{887})$
$3h'_{901} - 2h'_{925}$	$6(h'_{925} - h'_{901})$
$\frac{1}{2}(3h'_{901} - h'_{969})$	$\frac{3}{2}(h'_{969} - h'_{901})$
$2h'_{925} - h'_{969}$	$2(h'_{969} - h'_{925})$
$\frac{1}{3}(4h'_{887} - h'_{969})$	$\frac{4}{3}(h'_{969} - h'_{887})$
$\frac{1}{5}(2h'_{925} + 3h'_{725})$	$\frac{6}{5}(h'_{925} - h'_{725})$

Table 1:3 - Formulae for h_M and τ.

four of these were used, but when some values could not be obtained, the remaining relations and other similar ones were used; the same value of h' was never considered in more than one pair. The resulting values of h_M and τ were then averaged to obtain representative values for that record.

A complication is introduced by the presence of other layers below the one being measured, since these produce some r-etardation of the reflection. If it is assumed that these layers are parabolic, a correction for this effect may easily be introduced by a further application of eqn. (1.3), as pointed out by Booker and Seaton (1:30). The retardation produced by the passage through a parabolic layer of a wave of frequency f, greater than the critical frequency f^o of that layer, is $\tau\phi(\frac{f}{f^o})$, where τ is the semithickness. Since the reflection traverses the layer twice, an amount $2\tau\phi(\frac{f}{f^o})$ must be subtracted from the uncorrected virtual height, where τ and f^o refer to the lower retarding layer.

On application of this method, it is found that, while it is perfectly satisfactory for the E layer, the upper half of the F_1 layer is usually completely within the F_2 layer and the correction for the presence of the F_1 layer is therefore halved.

The retardation falls off rapidly as f is increased above f^o and thus the effect produced by the E layer on the virtual heights of the F_2 layer is practically always negligible.

All data pertaining to a given record are conveniently recorded/

recorded and reduced on a sheet of the type shown in fig. 1.27, which refers to the record illustrated in fig. 1.24.

In cases where f^o was not directly observable (generally due to extended scattering), the extraordinary reflection was used for scaling purposes.

Regular Observations.

In pursuance of the original object of this research, it was decided to take a series of photographic records, one each hour on alternate days, over a period of 4 months. This choice of intervals and duration of observations was dictated by the shortage of observing staff available: the observations had to be taken during the college vacation, because the academic duties of the observers were not compatible with the continuous running of an ionospheric station. The observations were actually made between 1st November 1945 and 28th February 1946 and the scaling of records was laboriously accomplished during the writers' spare time between then and the end of June.

The records show the usual wide variations, particularly of the F_2 layer.

(i) Particularly at night, the reflection became at times very broad and scattered. In extreme cases the magnetic splitting could not be observed at all, as, e.g., in fig. 1.28. It will be noted that not only is the f^o impossible to determine, but that the reflection persists in a broken and irregular form for some time even after what would

normally/

SCALING OF RECORDS.

Record No. 722. Date: 28/12/45. Mean time: 8 h. 57 m.

General Characteristics:

Sporadic E. f^o = 3·32 Mc/sec. f^x = — Mc/sec. Time: 8 h. 55 m.
E region f^o = 3·22 Mc/sec. f^x = 3·70 Mc/sec. Time: 8 h. 55 m.

f/f°	f	Virtual height, h' (km.) 1st	2nd	3rd	4th	Mean h'
0.648	—	—	—	—	—	—
0.725	2·34	108	—	—	—	108
0.757	2·44	116	—	—	—	116
0.834	2·68	120	—	—	—	120
0.887	2·86	120	—	—	—	120
0.901	2·90	122	—	—	—	122
0.925	2·98	126	—	—	—	126
0.969	3·12	130	—	—	—	130

h_1'	h_2'	$h_1' + h_2'$	h_M	$h_2' - h_1'$	τ
h'_{648} = —	h'_{925} = 126	—	—	—	—
h'_{725} = 108	h'_{901} = 122	230	115	14	21
h'_{757} = 116	h'_{887} = 120	236	118	4	8
h'_{834} = 120	h'_{969} = 130	—	120	10	10

Mean h_M = 118
" τ = 13
h_m = 105

F1 region f^o = 4·60 Mc/sec. f^x = 5·10 Mc/sec. Time: 8 h. 57 m.

f/f°	f	Virtual heights, h' (km.) 1st	2nd	3rd	4th	Mean h'	f/f^M_E	$2\tau\psi(f/f^o_E)$	Corr.h'
0.648	—	—	—	—	—	—	—	—	—
0.725	—	—	—	—	—	—	—	—	—
0.757	3·48	208	—	—	—	208	1·08	20	188
0.834	3·84	226	225	—	—	225	1·19	12	213
0.887	4·08	234	—	—	—	234	1·27	9	225
0.901	4·15	242	248	—	—	245	1·29	9	236
0.925	4·25	266	—	—	—	266	1·32	8	258
0.969	4·45	336	350	—	—	343	1·38	7	336

h_1'	h_2'	$h_1'+h_2'$	h_M	$h_2'-h_1'$	τ
h'_{648} = —	h'_{925} = 258		192		132
h'_{725} = —	h'_{901} = 236				
h'_{757} = 188	h'_{887} = 225	413	206	37	74
h'_{834} = 213	h'_{969} = 336	—	213	123	123

Mean h_M = 204
" τ = 110
h_m = 94

F2 (or F) region. f^o = 7·63 Mc/sec. f^x = abs Mc/sec. Time: 9 h. 00 m.

f/f°	f	Virtual Height, h' (km) 1st	2nd	3rd	4th	Mean h'	$f/f^o_{F_1}$	$\tau\psi(f/f^o_{F_1})$	Corr.h'
0.648	4·94	384	385	—	—	384	1·07	89	295
0.725	5·53	376	369	—	—	372	1·20	48	324
0.757	5·78	374	370	—	—	372	1·24	40	332
0.834	6·36	392	395	—	—	393	1·38	29	364
0.887	6·70	418	415	—	—	416	1·46	25	391
0.901	6·88	440	436	—	—	438	1·50	23	415
0.925	7·05	470	—	—	—	470	1·53	22	448
0.969	7·39	534	—	—	—	534	1·61	19	515

h_1'	h_2'	$h_1'+h_2'$	h_M	$h_2'-h_1'$	τ
h'_{648} = 295	h'_{925} = 448	743	371	153	153
h'_{725} = 324	h'_{901} = 415	739	369	91	136
h'_{757} = 332	h'_{887} = 391	723	361	59	118
h'_{834} = 364	h'_{969} = 515	—	364	151	151

Mean h_M = 366
" τ = 139
h_m = 227

FIG. 1·27

Scaling Sheet.

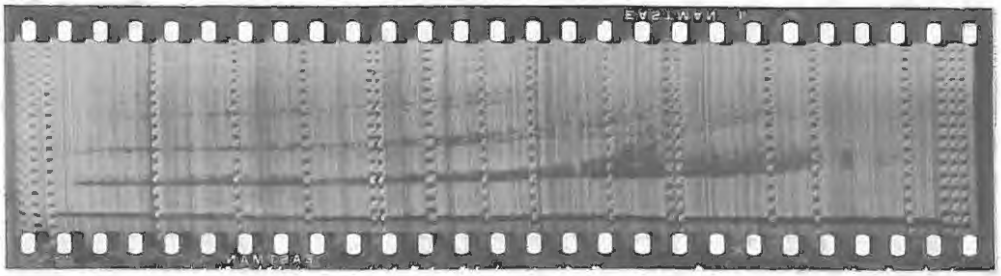

Fig. 1.28 - Sweep for November 8th, 1945. 0 hours.

normally be taken as the f^x. Such scattering has been noticed by others, and has been attributed to magnetic disturbances and also to "patchy" formations in the layer.

(ii) The F_2 layer critical frequencies and true heights were found to change tremendously between two successive days of observations. All quantities measured were tabulated and plotted, and, in the absence of more detailed information, the points were joined by straight lines. These sudden variations between successive readings and between alternate days are illustrated in figs. 1.29 and 1.30, which compare the conditions of the F_2 layer on the 8th and 10th February 1946. As will be pointed out in a later section, these disturbances seemed to be correlated in some manner with magnetic disturbances and with disturbed conditions on the sun. It will be noted that between 8 and 13 hours on the 8th no reflections could be obtained owing to a radio fade-out, or Dellinger effect.

(iii) Regular seasonal variations were observable even

over/

FIG. 1·29

F_2 Layer Electron Densities.

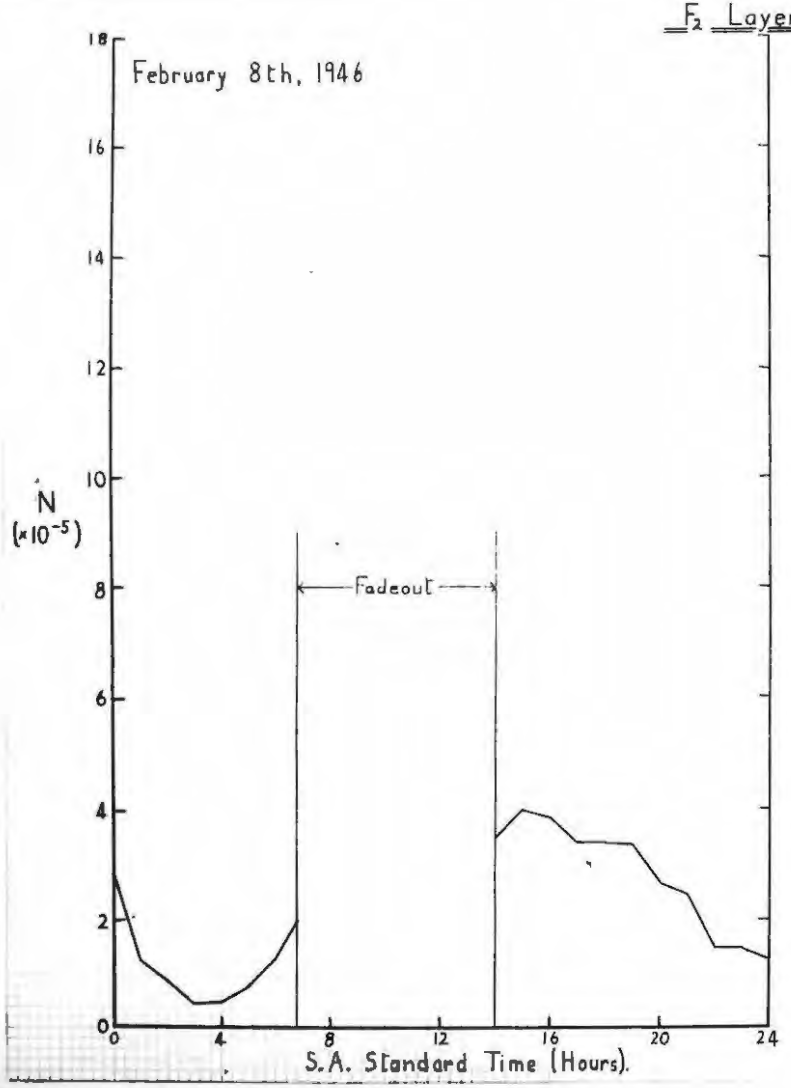

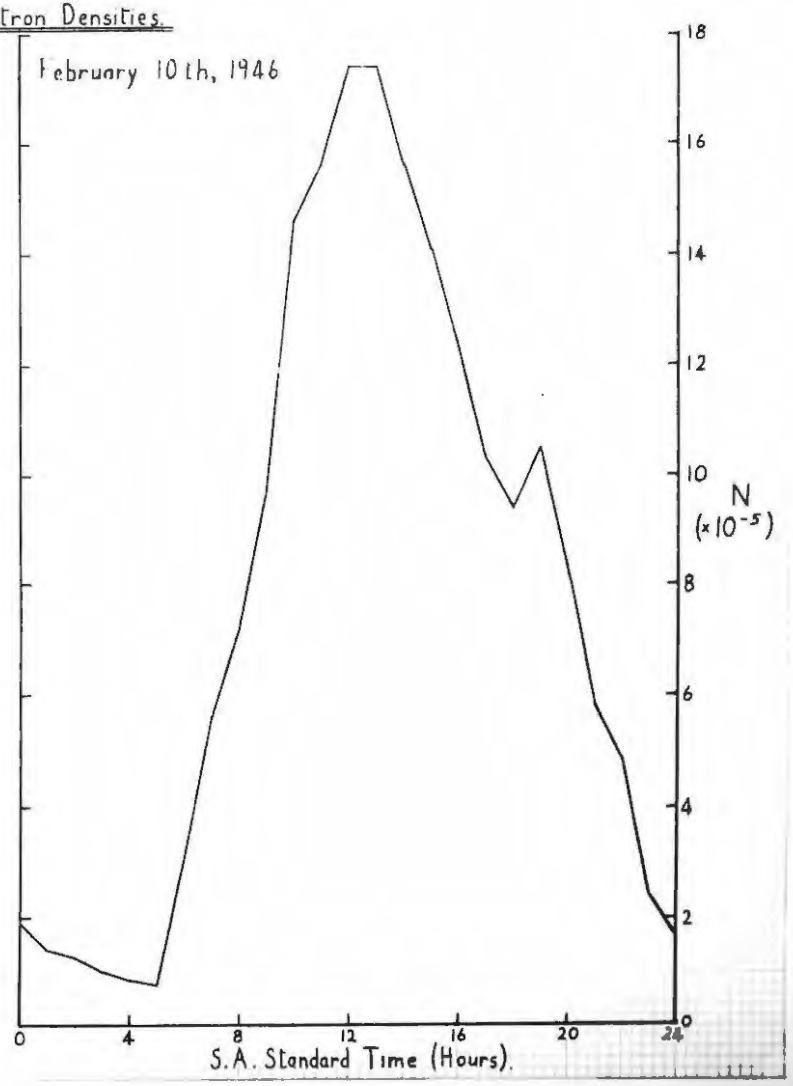

FIG. 1·30

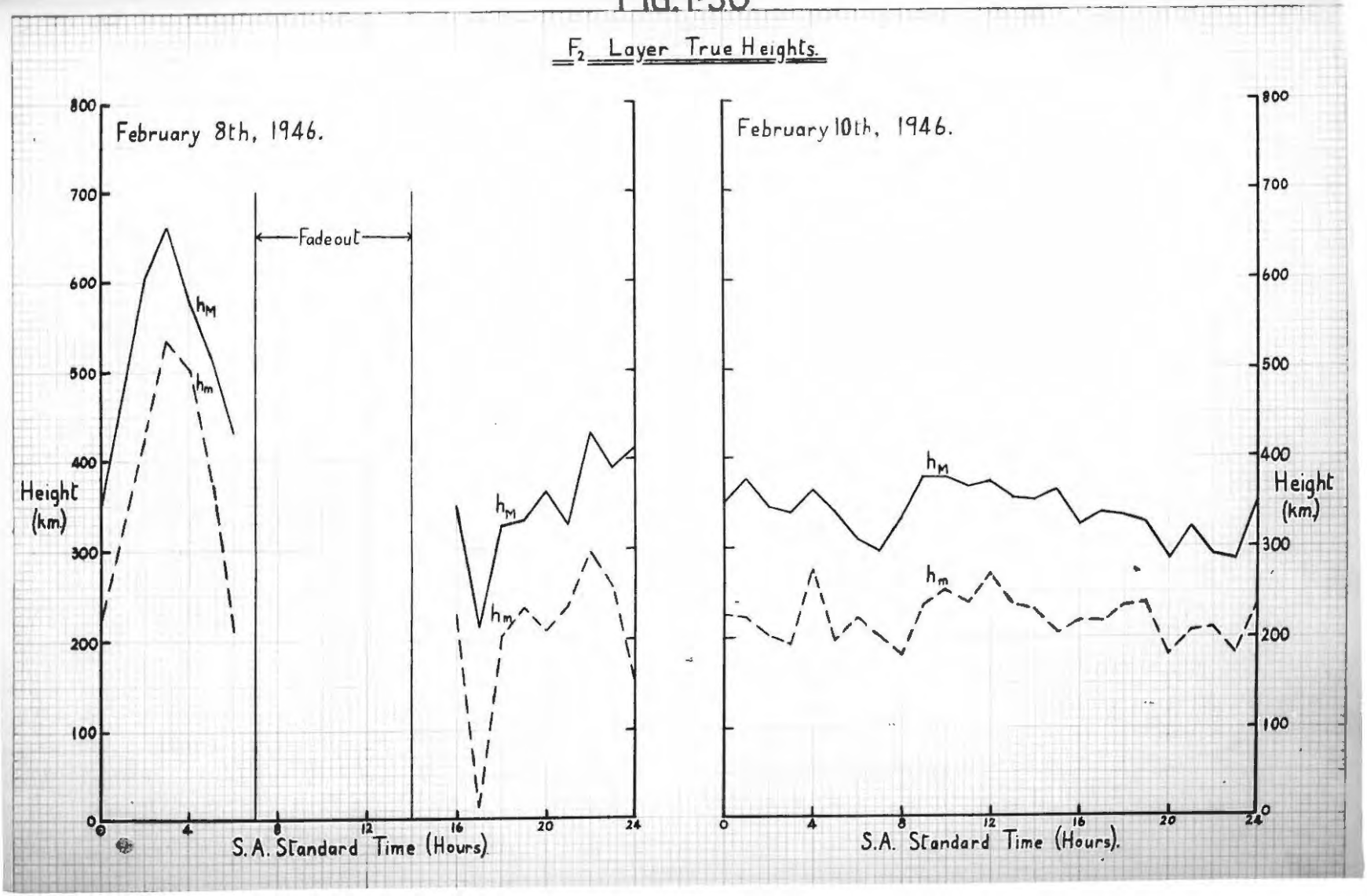
F2 Layer True Heights.
February 8th, 1946.
Fade out
hM
hm
Height (km.)
800
700
600
500
400
300
200
100
0
0
4
8
12
16
20
24
S.A. Standard Time (Hours).
February 10th, 1946.
hM
hm
Height (km.)
S.A. Standard Time (Hours).

over the short period of 4 months' investigation. Most notable among these was the appearance of the F_1 critical frequencies: while in December and January the F_1 critical frequency was very sharply and unmistakeably defined, as in fig. 1.24, during the months of November and February this layer only manifested itself for a few hours in the middle of the day as a change in gradient in the record.

Under the circumstances, in order to eliminate hourly and daily fluctuations, it was decided to calculate the mean values for each hour of all the quantities measured over monthly periods. As there were 16 days of readings for January and only 14 for February, the 31st of January was included in the February readings; throughout this work, whenever the results for February are mentioned, it is to be understood that they include this day. We thus have 4 periods of 30 days duration, each including 15 days of readings. These mean values are shown in tables 1:4, 1:5 and 1:6.

The probable deviations r were calculated by Peter's formula

$$r = 0.845 \frac{\sum d_i}{\sqrt{n(n-1)}} \quad . \quad . \quad . \quad . \quad . \quad . \quad (1.6)$$

where d_i is the deviation of the ith reading from the mean and n is the total number of readings over which the mean is taken. These probable deviations are added as an index of the scatter of the individual values about the mean.

Time (hours)	November		December		January		February	
	N	r	N	r	N	r	N	r
6	0.642	0.062	0.594	0.059	0.451	0.042	0.464	0.061
7	0.897	0.047	0.890	0.030	0.796	0.040	0.791	0.088
8	1.193	0.053	1.178	0.040	1.074	0.042	1.166	0.11
9	1.424	0.075	1.382	0.057	1.310	0.040	1.400	0.11
10	1.578	0.084	1.508	0.042	1.477	0.058	1.621	0.092
11	1.658	0.104	1.616	0.061	1.560	0.064	1.720	0.15
12	1.724	0.115	1.693	0.067	1.641	0.078	1.779	0.16
13	1.724	0.104	1.698	0.097	1.630	0.092	1.714	0.13
14	1.588	0.079	1.572	0.101	1.535	0.084	1.679	0.15
15	1.439	0.064	1.428	0.108	1.441	0.085	1.540	0.092
16	1.271	0.039	1.218	0.086	1.268	0.074	1.408	0.092
17	0.960	0.071	0.995	0.054	1.041	0.059	1.136	0.081
18	0.649	0.054	0.678	0.049	0.738	0.051	0.768	0.076
19	0.35	-	0.36	-	0.447	0.039	0.45	-

Table 1:4(a) - Mean values of N (electrons per cm^3 x 10^{-5}) for the E layer.

Time (hours)	November		December		January		February	
	N	r	N	r	N	r	N	r
5	-	-	0.80	-	-	-	-	-
6	1.7	-	1.50	0.00	1.60	-	-	-
7	2.26	0.29	2.12	0.20	2.05	0.14	2.01	0.23
8	2.58	0.15	2.44	0.15	2.38	0.11	2.36	0.18
9	2.73	0.21	2.66	0.11	2.56	0.10	2.84	0.091
10	2.93	0.23	2.73	0.12	2.69	0.10	3.00	0.15
11	3.18	0.19	2.82	0.15	2.77	0.081	3.11	0.18
12	3.17	0.12	2.81	0.11	2.80	0.10	3.25	0.22
13	3.00	0.18	2.79	0.12	2.72	0.14	3.24	0.24
14	2.88	0.18	2.67	0.16	2.77	0.085	3.16	0.16
15	2.68	0.18	2.65	0.15	2.67	0.10	2.95	0.14
16	2.43	0.13	2.43	0.13	2.51	0.12	2.78	0.10
17	1.98	0.12	2.06	0.15	2.14	0.097	2.37	0.26
18	1.70	0.17	1.62	0.14	1.64	0.076	1.89	0.061

Table 1:4(b) - Mean values of N (electrons per $cm^3 \times 10^{-5}$) for the F_1 layer.

Time (hours)	November		December		January		February	
	N	r	N	r	N	r	N	r
0	3.01	0.43	2.79	0.52	2.14	0.32	2.36	0.30
1	2.83	0.35	2.57	0.35	2.01	0.27	2.07	0.28
2	2.58	0.38	2.39	0.44	1.79	0.29	1.91	0.26
3	2.36	0.40	2.27	0.44	1.55	0.29	1.84	0.33
4	2.03	0.31	1.97	0.52	1.46	0.39	1.67	0.31
5	2.46	0.36	2.30	0.50	1.56	0.31	1.49	0.30
6	4.79	0.44	3.67	0.91	2.97	0.30	2.66	0.40
7	6.56	1.00	4.77	0.95	4.06	0.31	4.89	0.56
8	8.16	1.3	5.19	1.3	5.51	0.63	6.61	0.95
9	9.41	1.6	5.83	1.7	6.31	1.0	8.60	1.5
10	9.93	1.6	6.88	1.9	6.57	1.2	10.06	1.9
11	10.94	1.8	7.39	2.3	7.07	1.4	10.60	2.0
12	11.80	2.1	7.99	2.2	7.19	1.4	11.28	2.1
13	11.94	2.0	8.03	2.2	7.02	1.4	11.97	2.2
14	11.66	1.8	7.78	2.2	7.27	1.4	12.31	2.3
15	11.27	1.6	7.58	2.0	7.25	1.6	11.71	2.1
16	10.80	1.6	7.47	1.6	7.21	1.7	10.33	1.7
17	9.87	1.4	7.19	1.6	6.90	1.5	9.02	1.4
18	9.43	1.5	6.76	1.6	6.25	1.3	8.31	1.2
19	8.52	1.5	6.33	1.5	5.55	1.1	7.58	0.89
20	6.91	0.94	5.41	1.1	4.57	0.82	6.15	0.82
21	4.78	0.79	4.21	0.72	3.86	0.84	4.45	0.67
22	3.51	0.55	3.30	0.67	2.91	0.61	3.33	0.66
23	2.99	0.40	2.76	0.37	2.27	0.35	2.57	0.33
24	2.79	0.38	2.62	0.32	2.03	0.36	2.19	0.33

Table 1:4(c) - Mean values of N (electrons per cm^3 x 10^{-5}) for the F_2 layer.

Time (hours)	November		December		January		February	
	h_M	r	h_M	r	h_M	r	h_M	r
6	131	8.9	121	10	113	24	143	17
7	119	4.8	113	4.1	112	4.7	119	5.5
8	121	2.0	117	2.5	114	3.4	113	3.2
9	120	2.3	119	1.4	114	3.9	114	2.6
10	120	3.6	116	2.1	113	4.0	116	2.6
11	119	2.6	115	2.5	111	3.0	114	4.8
12	121	4.4	111	3.7	111	3.4	114	2.6
13	121	4.3	114	3.2	110	3.1	112	1.4
14	118	5.0	113	3.0	111	3.1	114	2.5
15	118	3.6	115	2.8	116	1.6	114	3.1
16	123	4.8	115	3.7	116	3.9	114	3.6
17	119	5.2	113	3.3	114	5.1	116	4.0
18	123	9.1	114	5.6	113	3.8	111	4.4
19	116	-	-	-	114	-	-	-

Table 1:5(a) - Mean values of h_M (km.) for the E layer.

Time (hours)	November		December		January		February	
	h_M	r	h_M	r	h_M	r	h_M	r
5	-	-	365	-	-	-	-	-
6	260	-	258	18	275	-	-	-
7	225	22	230	10	220	14	240	7.3
8	225	14	222	13	216	9.3	219	10
9	209	13	206	13	206	13	216	8.7
10	194	17	186	12	182	10	203	22
11	200	24	188	10	177	14	198	16
12	196	16	172	22	171	13	203	21
13	200	15	181	14	164	13	198	16
14	199	12	194	15	195	19	203	10
15	206	17	217	15	200	15	207	11
16	221	8.7	217	9.8	196	22	215	10
17	214	7.1	227	18	209	9.0	220	21
18	235	-	244	7.7	223	13	232	3.9

Table 1:5(b) - Mean values of h_M (km.) for the F_1 layer.

Time (hours)	November		December		January		February	
	h_M	r	h_M	r	h_M	r	h_M	r
0	357	14	356	16	334	20	342	10
1	342	14	351	25	334	15	357	27
2	325	14	361	31	321	18	359	34
3	339	14	350	42	306	14	358	38
4	339	14	340	33	319	18	350	30
5	326	12	327	22	309	12	352	32
6	295	14	317	23	284	12	315	23
7	309	18	313	24	283	11	302	20
8	331	15	339	26	305	12	319	21
9	332	12	336	19	313	16	334	22
10	333	18	334	17	318	23	336	20
11	339	19	357	35	327	16	342	24
12	339	18	319	24	334	14	341	24
13	342	14	326	18	339	24	337	14
14	340	10	335	18	326	18	332	11
15	333	13	331	14	317	26	328	13
16	323	11	327	13	304	22	321	12
17	315	12	312	16	295	15	306	15
18	310	13	315	15	293	11	306	7.1
19	304	8.7	302	9.0	294	10	299	12
20	303	12	310	9.0	311	20	297	11
21	304	9.4	319	17	315	21	302	10
22	328	11	320	18	321	20	324	22
23	347	14	345	14	340	23	328	19
24	365	15	348	13	340	20	354	23

Table 1:5(c) - Mean values of h_M (km.) for the F_2 layer.

Time (hours)	November		December		January		February	
	h_m	r	h_m	r	h_m	r	h_m	r
6	101	24	98	20	51	90	122	18
7	99	10	97	9.0	87	11	87	12
8	104	5.0	104	6.8	96	7.6	94	9.9
9	105	7.8	109	5.9	100	4.1	100	5.1
10	105	7.2	104	4.8	98	6.8	102	6.9
11	102	7.2	106	5.9	100	4.5	97	8.5
12	102	8.7	96	10.7	100	6.8	100	5.2
13	107	9.4	105	7.8	97	4.9	95	6.6
14	101	9.6	105	7.5	99	4.5	94	6.3
15	106	7.3	102	6.8	102	4.8	92	7.8
16	107	6.0	100	10	100	7.5	92	6.4
17	93	13	90	12	93	13	94	8.7
18	93	22	103	9.3	92	6.6	90	9.9
19	-	-	-	-	98	-	-	-

Table 1:6(a) - Mean values of h_m (km.) for the E layer.

Time (hours)	November		December		January		February	
	h_m	r	h_m	r	h_m	r	h_m	r
5	-	-	292	-	-	-	-	-
6	215	-	167	27	245	-	-	-
7	177	32	162	13	144	19	172	17
8	162	17	149	27	123	20	139	25
9	128	24	92	31	109	34	132	21
10	58	70	49	34	69	26	111	46
11	68	62	61	43	64	40	101	35
12	60	58	0	51	72	41	83	46
13	95	25	44	34	54	51	77	39
14	86	33	69	40	82	56	94	34
15	116	28	113	40	81	57	123	21
16	156	21	125	23	66	48	137	22
17	145	17	150	28	121	29	138	32
18	205	-	208	13	179	18	191	13

Table 1;6(b) - Mean values of h_m (km.) for the F_1 layer.

Time (hours)	November		December		January		February	
	h_m	r	h_m	r	h_m	r	h_m	r
0	257	7.3	261	16	239	18	231	16
1	241	13	249	17	243	16	245	18
2	236	17	252	13	231	17	245	28
3	239	12	249	29	221	20	246	38
4	237	14	238	20	225	24	249	37
5	231	14	224	13	235	15	245	35
6	204	13	209	29	204	15	217	12
7	202	27	192	34	152	38	201	17
8	210	23	155	46	174	29	205	17
9	211	23	198	39	177	39	208	15
10	186	43	200	26	203	48	209	18
11	209	42	223	63	203	34	210	19
12	203	53	181	53	210	31	216	32
13	239	18	198	47	218	29	212	23
14	222	26	205	33	218	29	216	14
15	230	18	203	26	211	33	215	15
16	235	17	221	21	199	24	222	14
17	233	15	212	10	199	21	202	25
18	234	12	216	12	210	12	212	10
19	216	12	204	14	207	12	212	9.4
20	210	11	212	16	203	18	201	9.9
21	206	20	216	13	211	17	205	9.6
22	225	12	225	15	222	13	223	17
23	252	14	236	18	235	19	234	18
24	265	10	252	14	242	11	245	29

Table 1:6(c) - Mean values of h_m (km.) for the F_2 layer.

Correlation with magnetic activity.

An examination of data for individual days shows at once that a large contribution to the probable deviations comes from certain days, which may be described as "ionospherically disturbed". Such a day was the 8th of February 1946, for which the graph has already been shown in figs. 1.29 and 1.30.

It is well known that high magnetic activity is generally accompanied by ionospheric disturbances (1:32) (1:33). It seemed of interest therefore to attempt a correlation between magnetic data and ionospheric conditions especially since no correlation other than with critical frequencies and virtual heights have been reported in the literature.

Unfortunately there is no magnetic observatory in Grahamstown, the nearest one being at Hermanus, C.P., approximately 500 miles away. Magnetic three-hour-range indices (1:34) and daily character figures for the four months in question were kindly supplied by Professor Ogg from this observatory.

The product-moment correlation coefficient, ρ, between two variables is defined by:

$$\rho = \frac{\sum xy}{\sqrt{\sum x^2 \sum y^2}} \quad . \quad . \quad . \quad . \quad . \quad . \quad . \quad (1.7)$$

where x and y are corresponding deviations from the mean for the two variables. Correlation coefficients were calculated by this formula for various ionospheric quantities against the magnetic three-hour range indices.

As/

As the latter are measures of the magnetic disturbance, which must be interpreted as the deviation from quiet conditions, the quantities correlated with them were not the ionospheric values themselves, but their deviations from their mean values.

F_2 layer.

Let ΔN be the deviation of the maximum electron density N from the monthly mean $\overline{N}$ at that time of day. A preliminary correlation was attempted of the three-hour range index k with the largest $|\Delta N|$ in the corresponding three-hour period, but proved to be insignificant.

A second attempt was made by correlating over complete days: the k's were added up (for the whole day), giving Σk, and all the $\left|\frac{\Delta N}{\overline{N}}\right|$ one for each hour, were summed to give $\sum\left|\frac{\Delta N}{\overline{N}}\right|$. The two sums were then correlated, with the results shown in table 1:7.

Month	November	December	January	February
ρ	0.494	0.467	0.247	0.637

Table 1:7 - Correlation coefficients of Σk with $\Sigma\left|\frac{\Delta N}{N}\right|$.

According to Fisher (1:35) all the ρ's, except that for January are significant.

The deviations of the heights of maximum electron density, Δh_M, were next correlated with the k's as

follows/

follows: since the k is determined from the maximum swing of the magnetometer over three hours, the maximum values of Δh_M over the same three-hour periods were selected and summed for each of the 15 days, $\Sigma|\Delta h_M|_{max}$. These $\Sigma|\Delta h_M|_{max}$ were correlated with Σk, as defined above, with the following results:

Month	November	December	January	February
ρ	0.340	0.769	0.749	0.390

Table 1:8 - Correlation coefficients of Σk with $\Sigma|\Delta h_M|_{max}$.

Again referring to Fisher, the correlations for December and January are very significant, but those for November and February are not so encouraging.

It was thought that a better correlation would be obtained by taking account of the signs of $(\Delta h_M)_{max}$, and the correlation was repeated using the signs.

Month	November	December	January	February
ρ	-0.222	0.789	0.826	0.496

Table 1:9 - Correlation coefficients of Σk with $\Sigma(\Delta h_M)_{max}$.

This confirms the correlation for the middle two months, improves that for February, and remains insignificant for November.

In order to approximate more nearly to a quantity which would be more analogous to the three-hour range index k, the differences between the largest and smallest values of $\overset{h_M}{\wedge}\left[(h_M)_{max} - (h_M)_{min}\right]$, over three-hour periods were/

were taken and added up for each of the 15 day periods. The values of $\Sigma\left[(h_M)_{max} - (h_M)_{min}\right]$ were again correlated with the Σk's.

Month	November	December	January	February
ρ	0.399	0.714	0.625	0.500

Table 1:10 - Correlation coefficients of Σk with $\Sigma\left[(h_M)_{max} - (h_M)_{min}\right]$.

This is more consistently good than any of the others.

Tables 1:7, 1:8, 1:9 and 1:10 establish with reasonable certainty the fact that a day with a large Σk (i.e., a magnetically disturbed day) at Hermanus is likely to be characterised by disturbed conditions in the F_2 layer over Grahamstown. In order to establish whether this correspondence extends down to individual three-hour periods, a further investigation was made.

The individual values of $\left[(h_M)_{max} - (h_M)_{min}\right]$ were plotted against those of k on a correlation diagram and the ρ's were calculated by the product-moment method (1:36).

Month	November	December	January	February	All
ρ	0.063	0.410	0.379	0.304	0.303

Table 1.11 - Correlation coefficients of k with $\left[(h_M)_{max} - (h_M)_{min}\right]$.

Although numerically these appear to be worse than the previous tables, it should be remembered that there are now 8 pairs of values for each of 15 days, i.e., 120 pairs/

pairs for each month. Reference to Fisher's table shows that in all months, except November, the correlation is definitely significant. The value 0.303, obtained by using all the 480 pairs of values shows a probability of less than 1 in 500 that the arrangement should be due to chance alone.

Corresponding with table 1:8, the three-hour period correlations of $|\Delta h_M|_{max}$ with k are shown in table 1:12.

Month	November	December	January	February
ρ	0.016	0.468	0.393	0.268

Table 1:12 - Correlation coefficients of k with $|\Delta h_M|_{max}$.

Again these are significant with the exception of November.

Finally the three-hour period equivalent of table 1:9, i.e., $(\Delta h_M)_{max}$, with correct sign, was worked out.

Month	November	December	January	February
ρ	0.075	0.313	0.321	0.432

Table 1:13 - Correlation coefficients of k with $(\Delta h_M)_{max}$.

From these tables it is evident that magnetic activity is accompanied by ionospheric disturbances, not only over whole days, but also over individual three-hour periods.

The exceptional behaviour of the month of November seems to call for comment. In table 1:14 the sums of the k indices, k_{sum}, for the four months are given, and it will be noted that that for November is lower than any

of/

Month	November	December	January	February
k_{sum}	390	488	438	506

Table 1:14 - Monthly sums of k indices.

of the others, i.e., November was magnetically the quietest month of all. In fact there was not a single day with magnetic character figure 2, and only three days with a 1.

The lack of correlation for November may then be explained by the fact that the small magnetic activity was probably localised at Hermanus and its effect could not be observed at Grahamstown, while similar local magnetic (and probably ionospheric) disturbances at Grahamstown did not extend as far as Hermanus. In December and January, on the other hand, most of the correlation comes from large disturbances which are known to be of a more general nature.

The lower correlation in February, in spite of the large magnetic disturbance, may perhaps be attributed to the influence of sunspots, solar flares, etc. for which that month was noteworthy (1:37). Shapley, in his attempt at short-term forecasting of ionospheric conditions (1:33), attributes approximately equal influences to magnetic and to solar conditions. It is suggested that these solar effects may have masked the effect of the magnetic disturbances.

F_1 layer.

Correlations of whole day sums of $\Sigma|\Delta N|$ with Σk,

and/

Month	November	December	January	February
$\rho\ (\Sigma\|\Delta N\|)$	0.001	0.373	0.304	0.576
$\rho\ (\Sigma\|\Delta h_M\|_{max})$	0.308	0.431	0.124	0.278

Table 1:15 - Correlation coefficients of Σk with $\Sigma|\Delta N|$ and $\Sigma|\Delta h_M|_{max}$.

and of $\Sigma|\Delta h_M|_{max}$ with Σk were worked out and are shown in table 1:15. There is evidently little correlation here, but what there is follows the trend of the effects noted in the F_2 region.

E layer.

Correlation was only attempted for the maximum electron density deviations $|\Delta N|$ over three-hour periods, because of the smaller percentage accuracy with which h_M may be scaled from the records and also because of the very small variations to which this height is subject. As shown in fig. 1:16, the correlation is insignificant.

Month	November	December	January	February
ρ	0.384	0.414	-0.048	0.194

Table 1:16 - Correlation coefficients of Σk with $\Sigma|\Delta N|$.

We conclude that large magnetic disturbances are mainly associated with ionospheric disturbances in the F_2 region, and bear little relation to variations in the E and F_1 regions. The effect of small magnetic disturbances, which are presumably of a local character, on the ionospheric regions, cannot be gauged when the magnetic data are supplied by a magnetic observatory as far away as 500 miles.

Smoothing of Means.

As it was intended to use the final results of this part of the work for comparison with the theory to be developed in later sections, and since such a theory makes assumptions of quiet conditions, it was deemed desirable to eliminate any large disturbances from the monthly means tabulated earlier.

The correlation with magnetic activity indicates obviously the first step to be taken in this direction. Since periods of high magnetic activity are accompanied by disturbed ionospheric conditions, they should be eliminated from the means.

Accordingly, the following criteria for rejection were adopted for all the layers:

(i) All days with magnetic character figure 2.

(ii) All three-hour periods for which the k index was greater than 4.

On this basis the following days were rejected: 14th December, 3rd January, 8th February; and the following periods: 8th November, 17-20 hours; 24th December, 11-14 hours; 17th January, 11-14 hours; 14th February, 8-11 hours; 20th February, 23-24 hours; 22nd February, 11-14 hours.

The means and probable deviations were then recalculated. It was found that some large deviations still persisted, and, after some deliberation, the more outstanding ones were removed, using the well established test that deviations larger than three times the probable deviation are unlikely to be due to chance

alone/

alone. The final, adjusted means, with their probable deviations, are tabulated in tables 1:17, 1:18 and 1:19, and are shown graphically in figs. 1.31 - 1.43.

Time (hours)	November		December		January		February	
	N	r	N	r	N	r	N	r
6	0.655	0.062	0.579	0.061	0.447	0.041	0.464	0.061
7	0.897	0.047	0.882	0.030	0.795	0.033	0.768	0.094
8	1.193	0.053	1.178	0.041	1.085	0.038	1.165	0.12
9	1.424	0.079	1.398	0.061	1.310	0.036	1.379	0.11
10	1.571	0.079	1.531	0.053	1.506	0.054	1.615	0.094
11	1.648	0.101	1.608	0.055	1.584	0.060	1.807	0.14
12	1.773	0.10	1.650	0.070	1.657	0.085	1.876	0.11
13	1.762	0.094	1.708	0.12	1.650	0.10	1.765	0.090
14	1.597	0.071	1.518	0.11	1.582	0.098	1.745	0.16
15	1.433	0.063	1.404	0.11	1.459	0.097	1.564	0.081
16	1.281	0.039	1.244	0.083	1.301	0.073	1.437	0.085
17	0.964	0.073	1.016	0.051	1.039	0.062	1.132	0.084
18	0.651	0.058	0.710	0.051	0.739	0.056	0.764	0.080

Table 1:17(a) - Adjusted mean values of N (electrons per $cm.^3$ x 10^{-5}) for the E layer.

Time (hours)	November		December		January		February	
	N	r	N	r	N	r	N	r
7	2.29	0.29	2.07	0.20	2.06	0.15	2.08	0.23
8	2.58	0.15	2.47	0.14	2.38	0.12	2.39	0.20
9	2.78	0.21	2.67	0.099	2.60	0.095	2.85	0.076
10	2.92	0.26	2.70	0.11	2.70	0.081	2.96	0.12
11	3.20	0.20	2.84	0.15	2.80	0.071	3.16	0.12
12	3.23	0.095	2.82	0.12	2.82	0.11	3.34	0.20
13	3.00	0.18	2.87	0.10	2.68	0.14	3.23	0.25
14	2.91	0.18	2.70	0.14	2.78	0.074	3.32	0.11
15	2.72	0.18	2.68	0.14	2.67	0.10	2.96	0.18
16	2.46	0.13	2.48	0.13	2.51	0.12	2.76	0.10
17	1.99	0.13	2.16	0.097	2.13	0.099	2.42	0.23
18	-	-	1.62	0.14	1.64	0.076	1.89	0.061

Table 1;17(b) - Adjusted mean values of N (electrons per $cm.^3$ x 10^{-5}) for the F_1 layer.

FIG. 1·31

Maximum Electron Densities, E and F_1 Layers

Means for November, 1945. (Adjusted.).

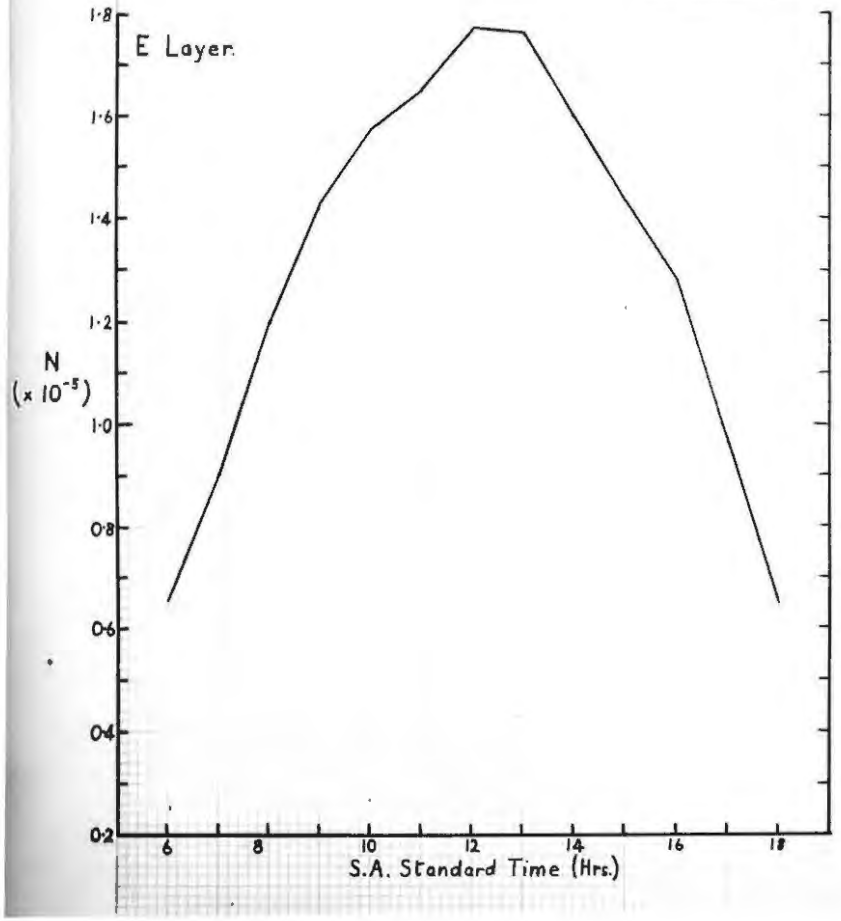

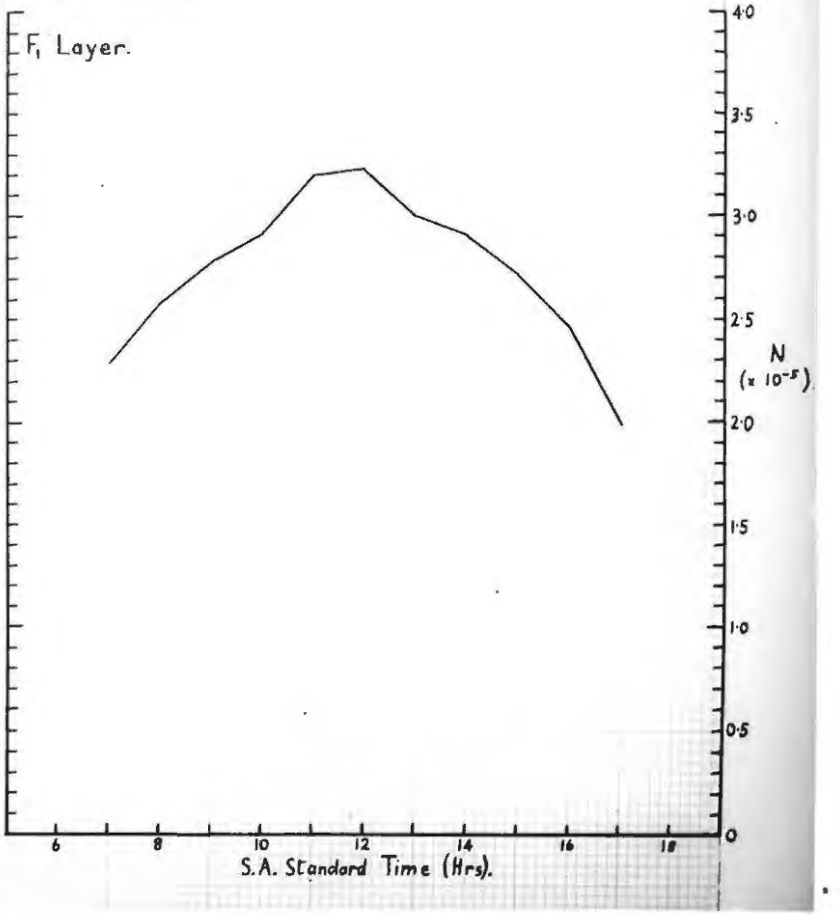

FIG. 1·32

Maximum Electron Densities, E and F_1 Layers

Means for December, 1945 (Adjusted).

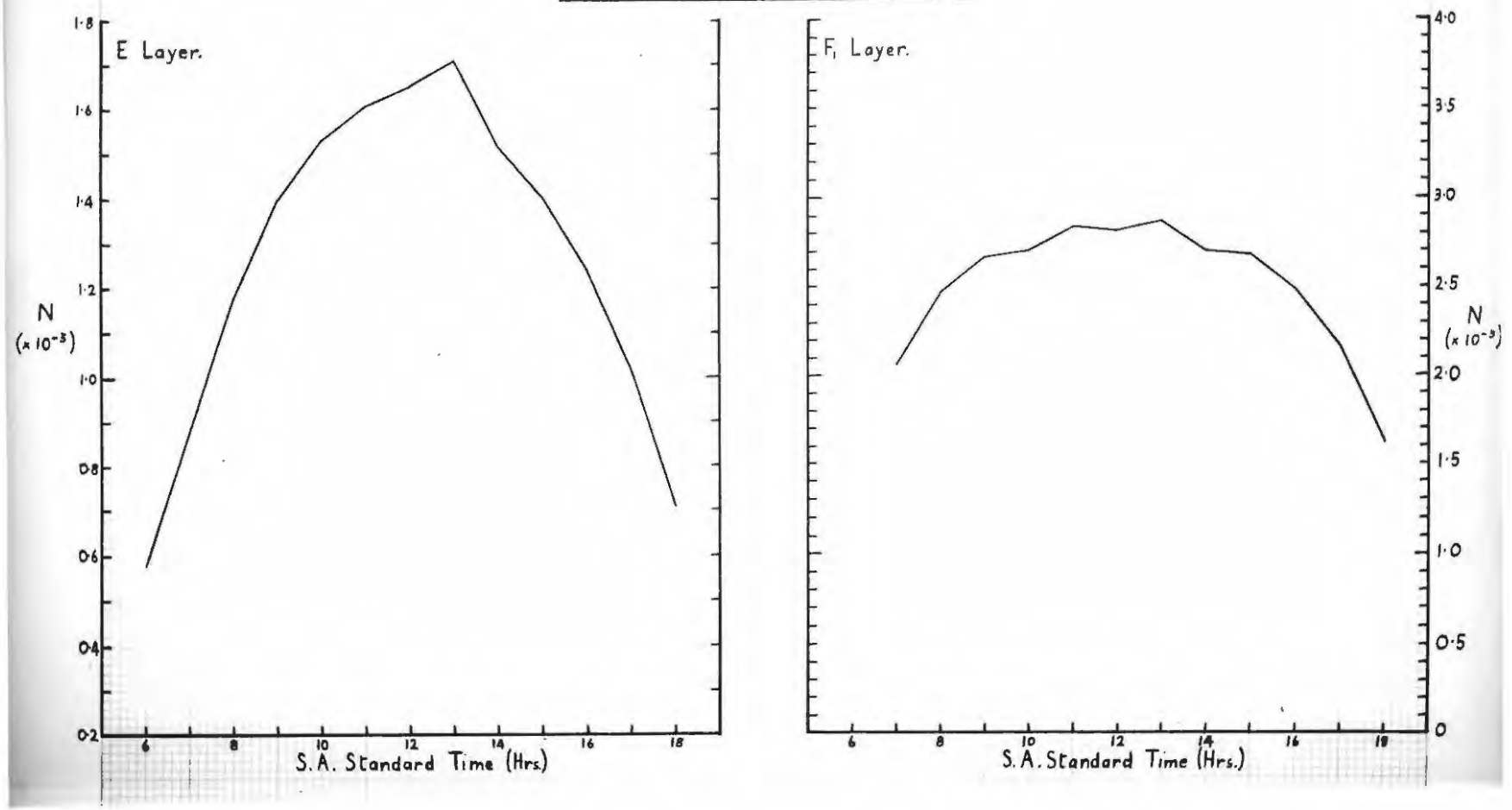

FIG. 1·33

Maximum Electron Densities, E and F_1 Layers.
Means for January, 1946 (Adjusted).

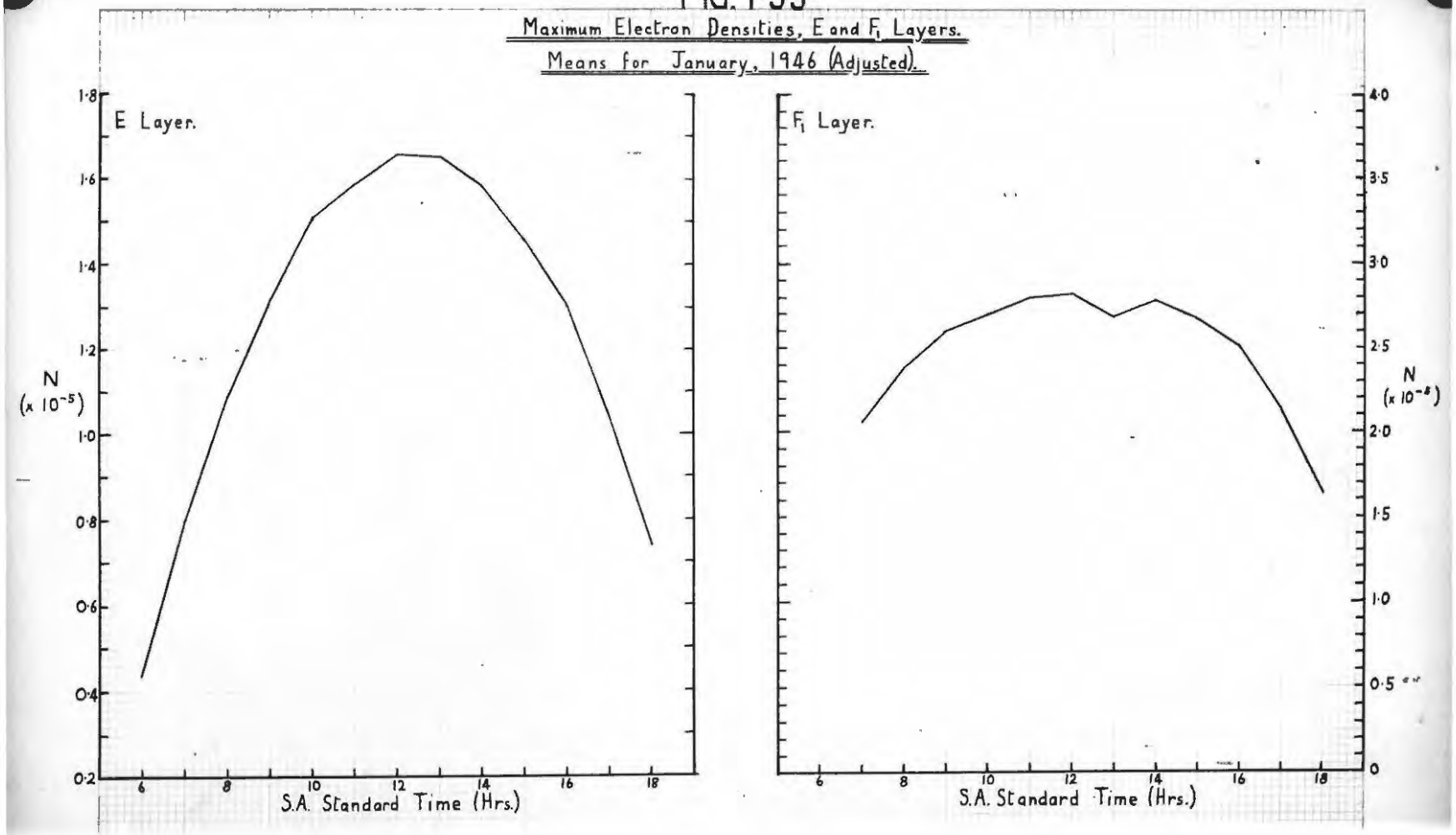

FIG. 1·34

Maximum Electron Densities, E and F_1 Layers.

Means for February, 1946 (Adjusted).

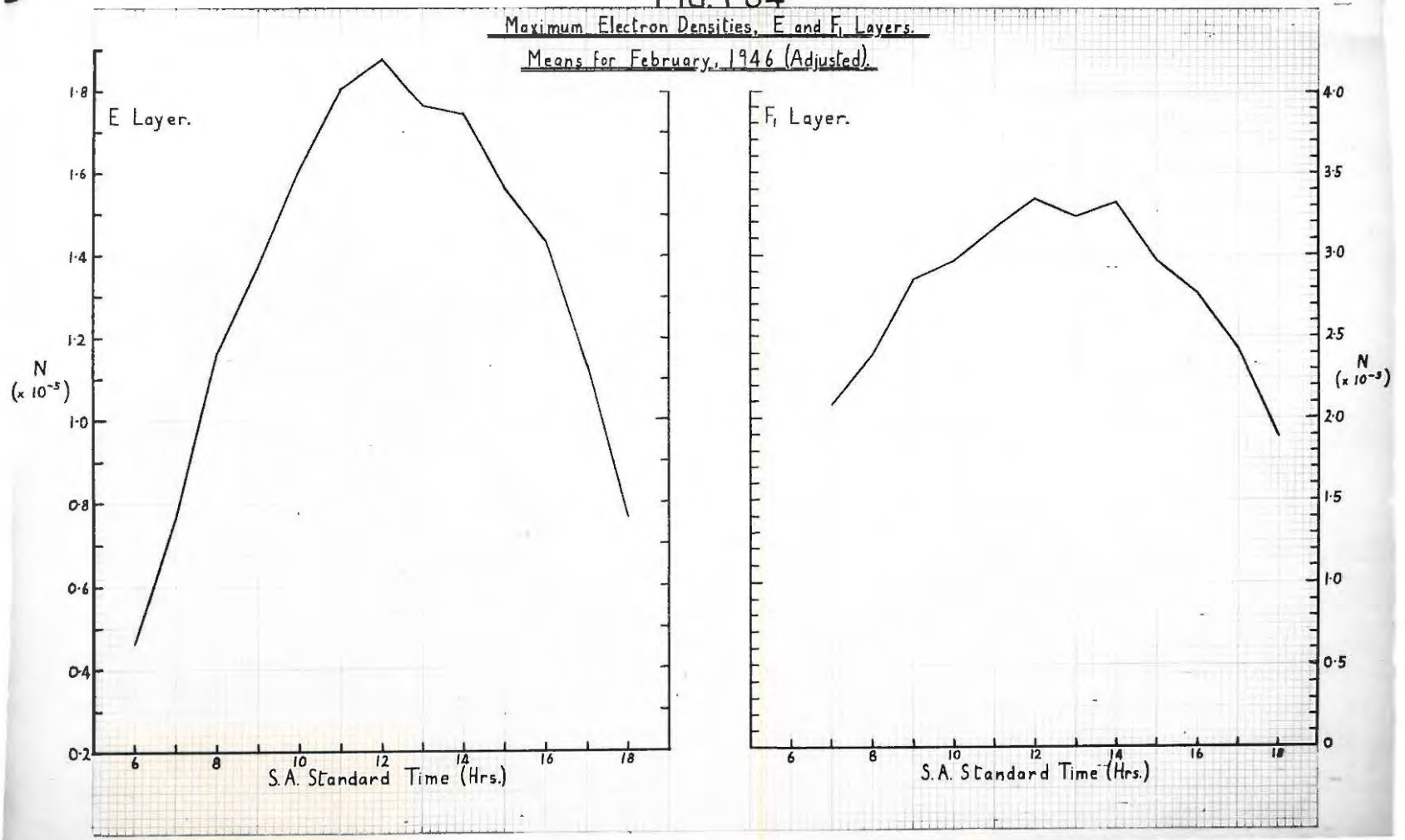

Time (hours)	November		December		January		February	
	N	r	N	r	N	r	N	r
0	2.91	0.43	2.64	0.41	2.18	0.33	2.19	0.26
1	2.83	0.35	2.46	0.28	2.05	0.27	2.12	0.24
2	2.58	0.38	2.31	0.42	1.82	0.29	1.96	0.22
3	2.36	0.40	2.26	0.46	1.56	0.30	2.02	0.25
4	1.96	0.31	1.81	0.55	1.46	0.42	1.83	0.24
5	2.46	0.36	2.36	0.50	1.54	0.31	1.60	0.28
6	4.79	0.44	3.76	0.89	2.88	0.31	2.67	0.35
7	6.56	1.00	4.91	0.90	4.17	0.34	5.02	0.36
8	8.44	1.3	5.40	1.3	5.72	0.65	6.77	0.68
9	9.08	1.6	5.97	1.7	6.58	1.0	9.22	0.96
10	10.29	1.6	7.12	1.8	6.90	1.1	10.24	1.2
11	11.85	1.8	8.02	2.1	7.34	1.5	11.09	1.6
12	13.07	2.0	8.37	2.1	7.18	1.6	12.17	1.8
13	12.37	2.0	8.60	2.1	7.04	1.5	12.40	1.7
14	12.07	1.8	8.28	2.3	7.09	1.5	12.28	1.8
15	11.69	1.6	7.86	1.9	7.09	1.6	12.54	1.5
16	11.16	1.6	7.72	1.5	6.99	1.6	11.07	1.2
17	9.89	1.5	7.33	1.4	6.44	1.1	9.42	1.0
18	9.39	1.5	7.04	1.5	5.90	1.1	8.66	0.86
19	8.56	1.5	6.25	1.4	5.35	1.1	7.87	0.63
20	6.89	0.99	5.60	0.99	4.54	0.78	6.37	0.64
21	4.58	0.79	4.30	0.70	3.48	0.72	4.72	0.58
22	3.51	0.55	3.35	0.68	2.61	0.56	3.45	0.63
23	3.08	0.40	2.67	0.39	2.35	0.37	2.57	0.29
24	2.79	0.38	2.54	0.36	2.16	0.33	2.25	0.30

Table 1:17(c) - Adjusted mean values of N (electrons per $cm.^3$ x 10^{-5}) for the F_2 layer.

FIG. 1·35

Maximum Electron Densities, F_2 Layer.

Means for November, 1945 (Adjusted).

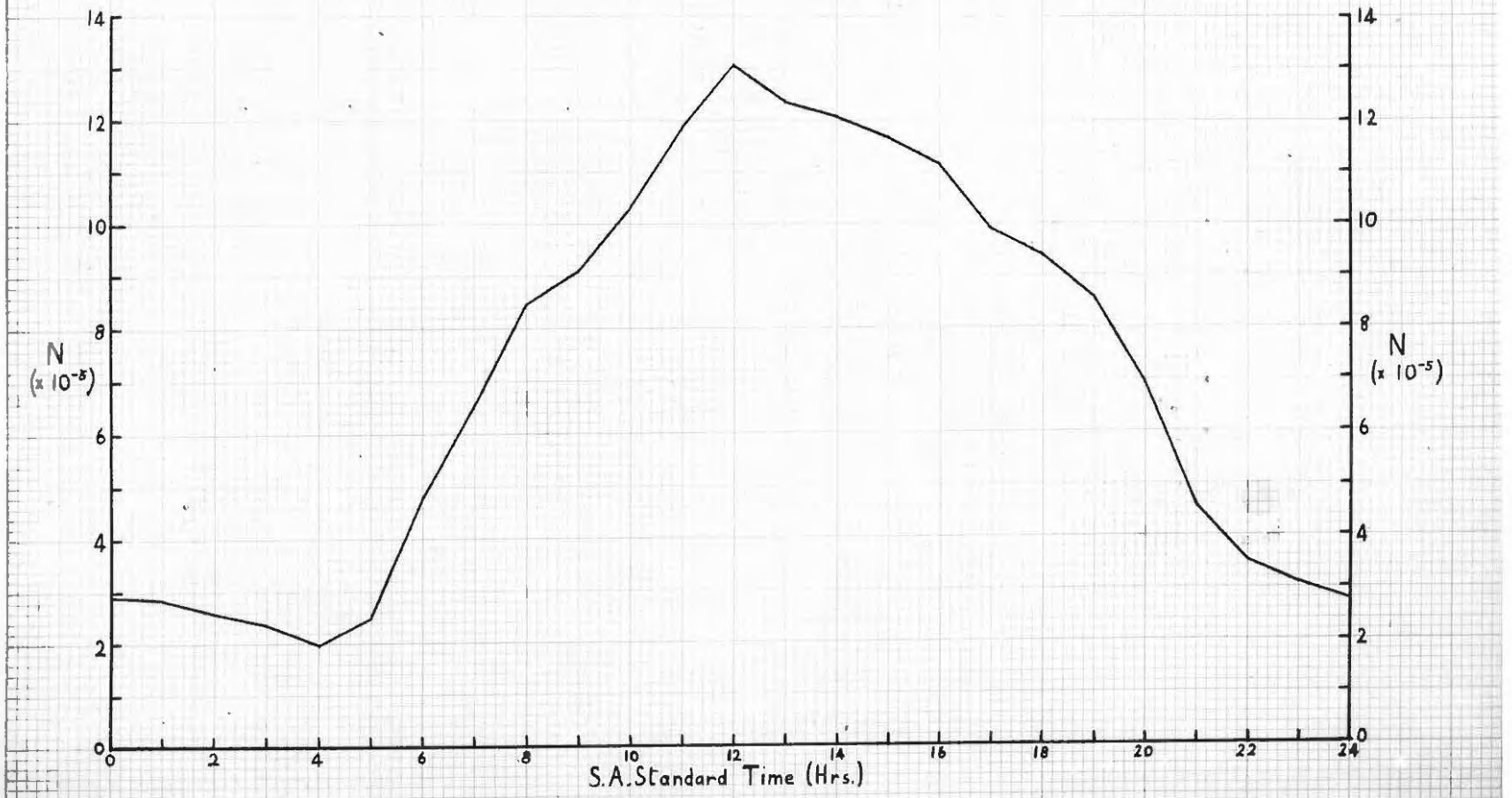

FIG. 1·36

Maximum Electron Densities, F_2 Layer.

Means for December, 1945 (Adjusted).

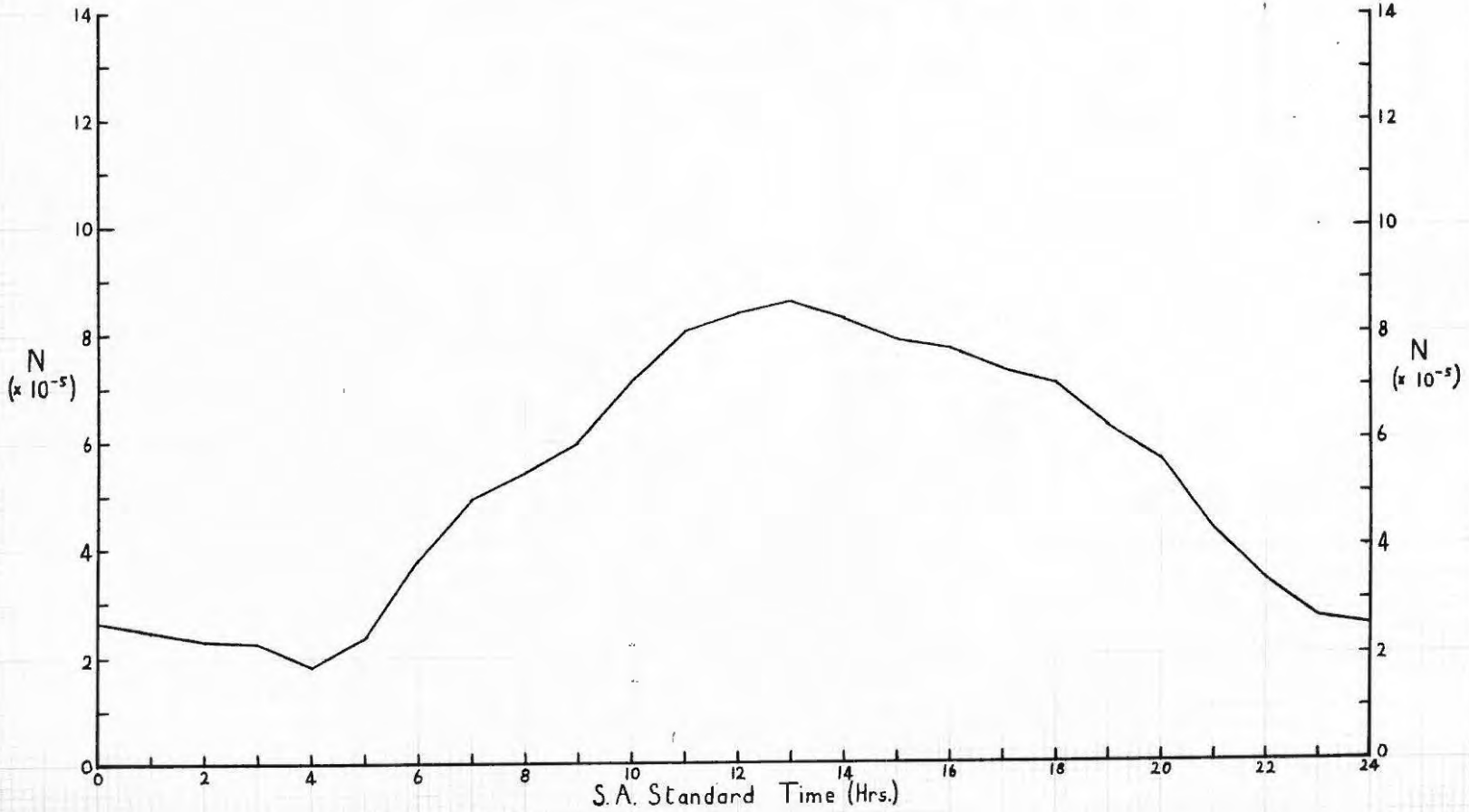

FIG. 1·37

Maximum Electron Densities, F_2 Layer.
Means for January, 1946 (Adjusted).

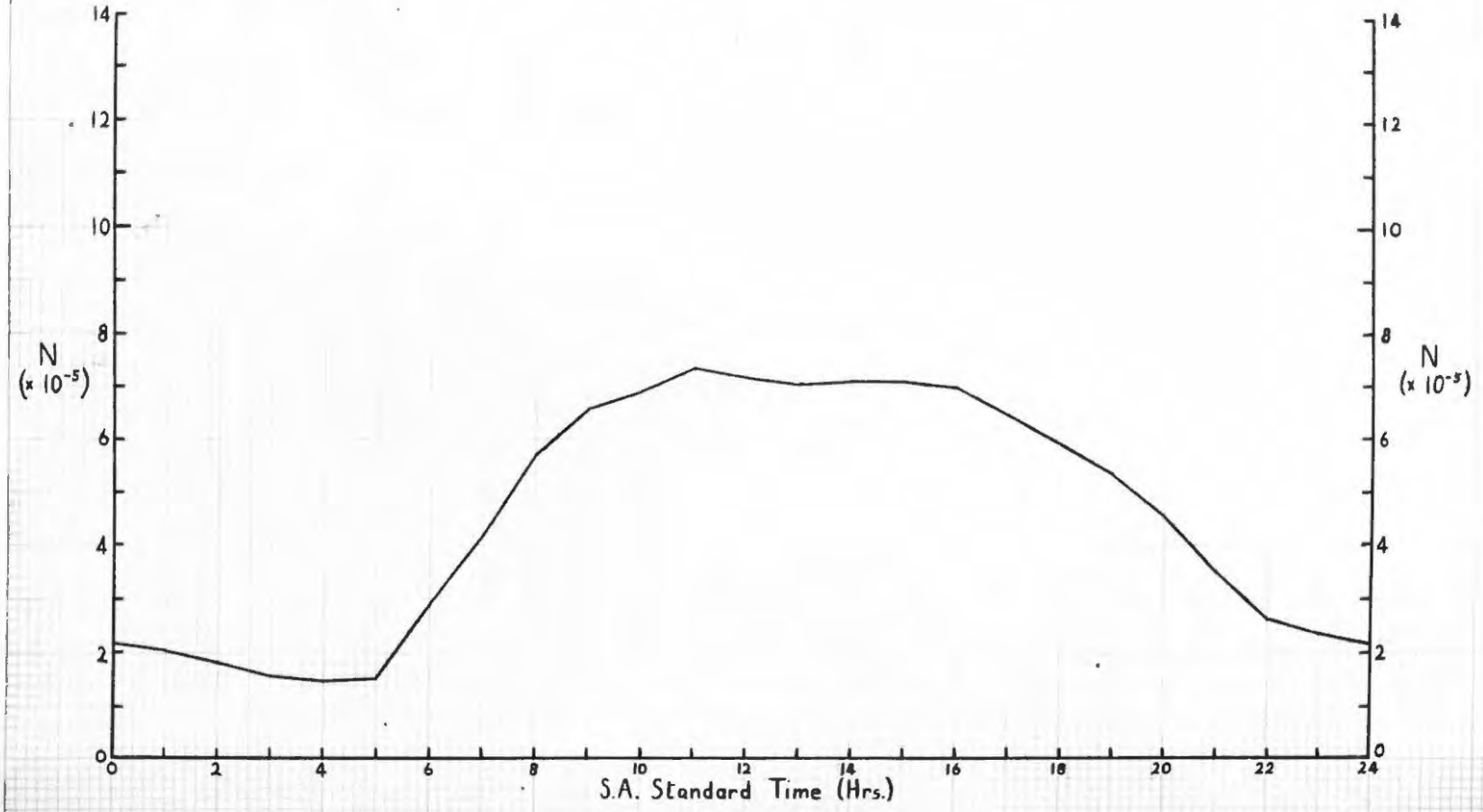

FIG. 1·38

Maximum Electron Densities, F_2 Layer.
Means for February, 1946 (Adjusted).

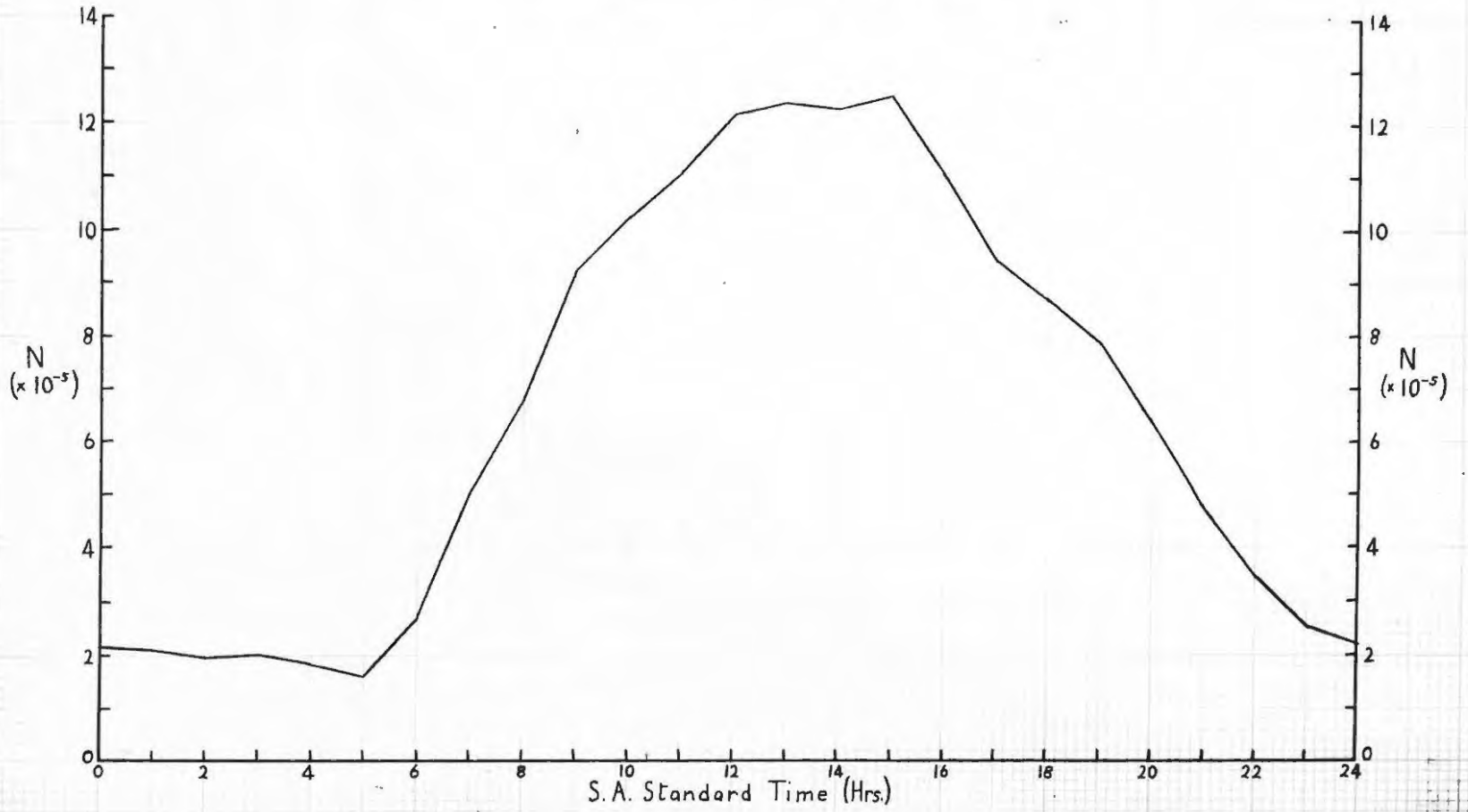

Time (hours)	November		December		January		February	
	h_M	r	h_M	r	h_M	r	h_M	r
6	131	8.9	118	11	130	-	143	17
7	117	4.8	115	3.3	113	4.1	121	5.6
8	121	2.0	118	2.6	114	3.0	113	2.8
9	119	2.2	119	1.5	114	3.2	115	2.6
10	121	3.5	116	2.1	115	3.6	116	2.5
11	118	2.7	115	2.7	112	3.4	117	8.4
12	122	5.2	109	3.6	111	3.4	113	2.9
13	119	4.0	114	3.4	110	3.8	113	2.3
14	119	4.8	113	2.6	112	3.6	115	2.2
15	118	3.5	116	2.0	115	2.4	116	3.8
16	125	4.3	114	3.4	115	4.2	115	4.4
17	119	5.5	115	3.8	114	5.1	115	3.8
18	127	8.0	114	5.6	114	3.8	113	5.0

Table 1:18(a) - Adjusted mean values of h_M (km.) for the E layer.

Time (hours)	November		December		January		February	
	h_M	r	h_M	r	h_M	r	h_M	r
7	238	22	227	11	224	11	237	5.9
8	225	14	225	14	215	9.7	219	11
9	213	13	200	14	203	13	219	9.0
10	199	20	180	10	179	11	205	21
11	197	26	185	11	182	18	189	14
12	195	19	166	20	179	12	200	24
13	200	15	180	11	162	13	192	18
14	200	13	194	16	198	21	202	13
15	206	18	215	14	199	16	204	12
16	221	8.7	220	11	198	20	214	10
17	214	7.6	228	19	209	7.8	214	18
18	-	-	244	8.6	220	12	232	3.9

Table 1:18(b) - Adjusted mean values of h_M (km.) for the F_1 layer.

Time (hours)	November		December		January		February	
	h_M	r	h_M	r	h_M	r	h_M	r
0	357	14	354	16	328	21	339	10
1	342	14	354	24	337	15	348	20
2	325	14	351	29	320	19	337	13
3	339	14	320	35	306	14	335	14
4	335	14	326	30	323	17	334	14
5	326	12	315	18	311	11	336	18
6	295	14	309	16	287	9.7	306	16
7	309	18	301	14	283	10	294	12
8	331	15	335	25	306	12	307	16
9	332	12	335	17	319	17	318	18
10	339	18	325	16	328	17	319	14
11	347	19	352	35	321	18	334	21
12	348	19	338	15	332	14	343	22
13	348	14	333	12	326	21	337	12
14	344	10	341	14	323	17	330	10
15	333	13	334	10	314	15	330	12
16	323	11	324	11	296	14	322	11
17	320	13	319	12	292	11	311	11
18	311	12	313	15	290	9.1	303	7.4
19	305	8.5	301	8.2	292	9.1	297	11
20	302	12	307	7.4	299	7.8	291	7.5
21	308	9.4	314	14	306	12	299	8.1
22	330	11	312	16	312	12	317	17
23	344	14	338	15	335	16	322	17
24	360	15	344	11	333	15	340	21

Table 1:18(c) - Adjusted mean values of h_M (km.) for the F_2 layer.

Time (hours)	November		December		January		February	
	h_m	r	h_m	r	h_m	r	h_m	r
6	109	24	98	22	116	-	122	18
7	99	10	95	8.8	90	9.2	89	9.7
8	104	5.0	106	6.4	98	7.2	94	9.2
9	108	7.9	109	5.9	101	3.3	103	5.1
10	102	7.2	101	3.1	98	8.0	103	6.6
11	101	6.9	105	6.5	100	4.8	93	15
12	101	7.8	90	12	99	7.3	99	2.9
13	109	9.0	105	9.5	95	5.0	94	11
14	100	9.4	106	7.0	98	4.3	90	5.6
15	103	7.6	106	5.6	101	4.7	93	9.4
16	108	5.1	102	8.0	98	7.1	93	5.4
17	94	14	87	14	96	11	93	9.4
18	95	23	103	9.3	93	7.0	90	11

Table 1:19(a) - Adjusted mean values of h_m (km.) for the E layer.

Time (hours)	November		December		January		February	
	h_m	r	h_m	r	h_m	r	h_m	r
7	177	32	165	13	147	18	182	13
8	163	17	150	29	122	20	144	26
9	128	24	90	29	119	35	149	16
10	75	80	60	38	78	22	132	47
11	70	58	65	51	82	51	87	21
12	82	70	35	54	97	41	109	52
13	95	25	66	34	54	50	60	46
14	95	35	63	47	92	61	89	40
15	125	29	125	35	88	59	126	20
16	156	21	116	21	82	50	136	24
17	153	18	152	32	132	21	156	30
18	-	-	215	14	176	16	191	13

Table 1:19(b) - Adjusted mean values of h_m (km.) for the F_1 layer.

Time (hours)	November		December		January		February	
	h_m	r	h_m	r	h_m	r	h_m	r
0	257	7.3	260	17	239	19	231	16
1	241	13	250	19	244	17	238	11
2	237	17	250	12	232	17	231	15
3	235	12	246	28	228	21	224	12
4	234	14	231	21	225	27	227	18
5	231	14	223	13	239	16	236	29
6	204	13	195	18	206	14	222	12
7	217	27	192	30	151	34	201	18
8	217	23	143	37	167	30	196	16
9	219	23	206	40	185	40	207	14
10	206	43	197	27	232	35	204	21
11	228	42	238	56	203	38	214	16
12	233	57	221	18	222	36	235	37
13	240	18	217	30	205	30	215	26
14	233	26	212	23	212	28	220	15
15	237	18	219	27	210	28	217	16
16	239	17	221	21	199	22	225	14
17	236	15	215	8.5	192	16	215	11
18	234	13	219	7.7	212	12	216	9.1
19	220	13	203	15	206	12	210	8.4
20	208	11	207	13	197	11	200	10
21	214	20	212	11	203	11	203	8.9
22	225	12	218	14	220	12	219	14
23	252	14	229	16	230	18	224	17
24	265	10	246	13	238	10	237	27

Table 1:19(c) - Adjusted mean values of h_m (km.) for the F_2 layer.

FIG. 1·40

True Heights of Layers.

Means for November, 1945 (Adjusted).

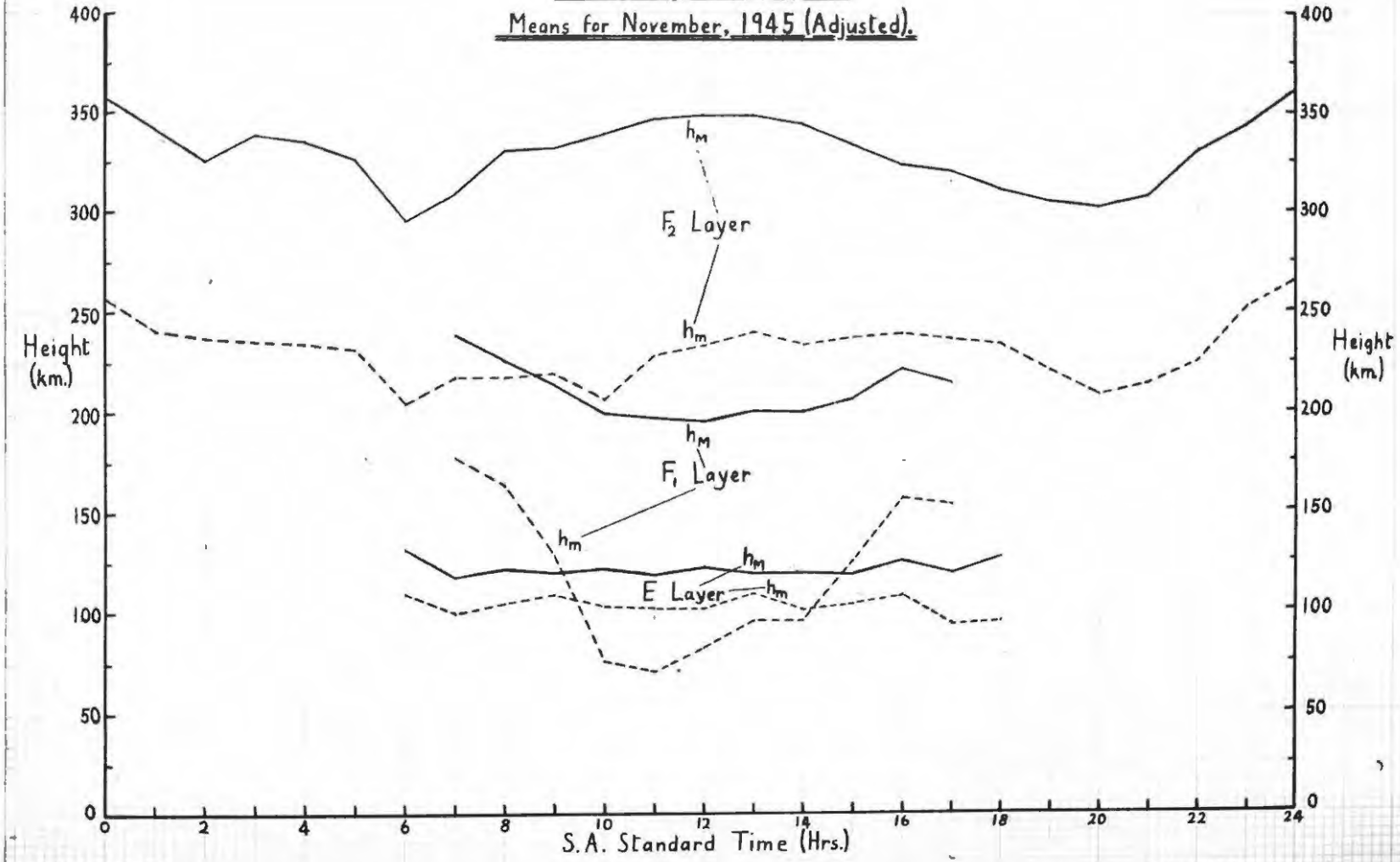

FIG. 1·41

True Heights of Layers.

Means for December, 1945 (Adjusted.)

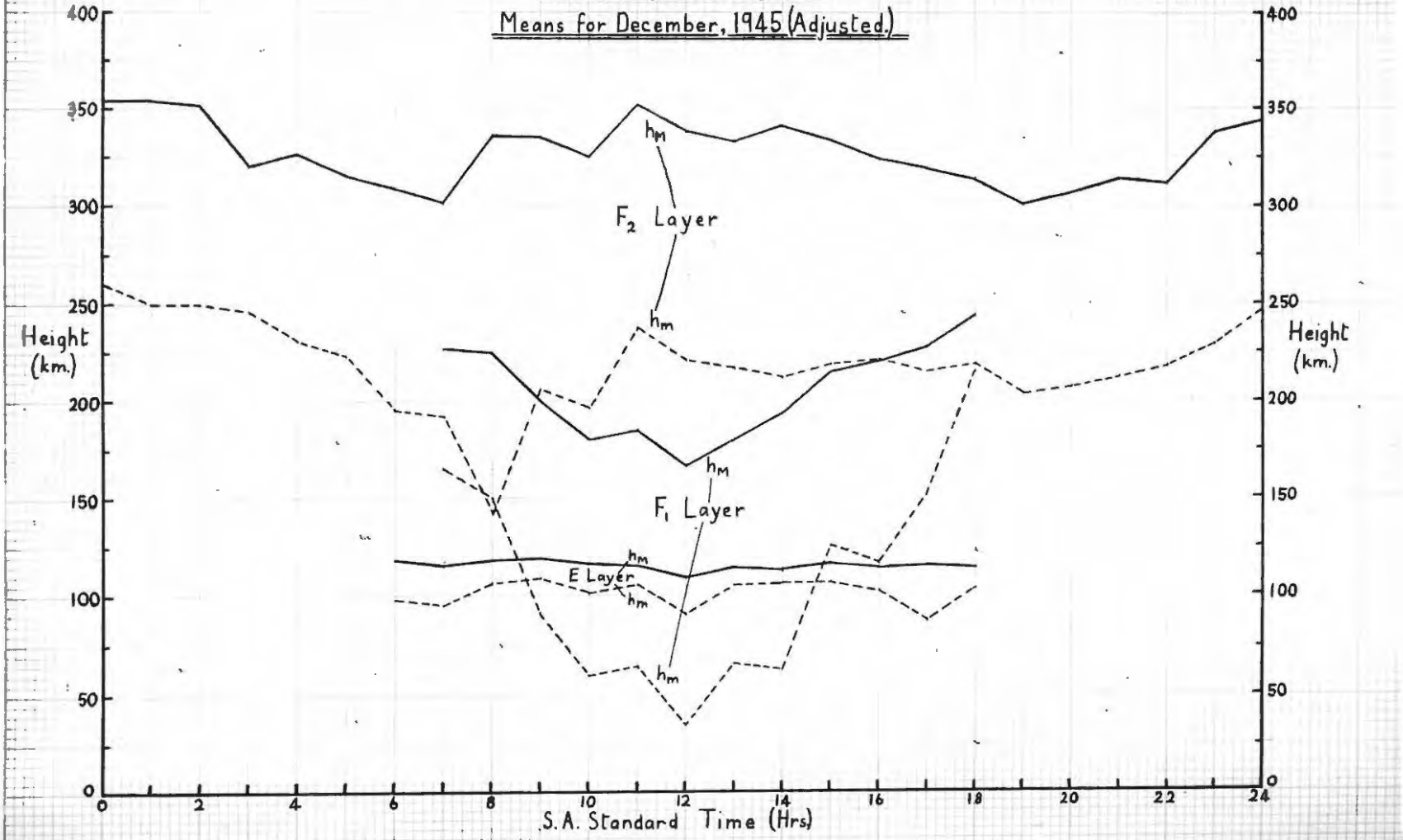

FIG. 1·43

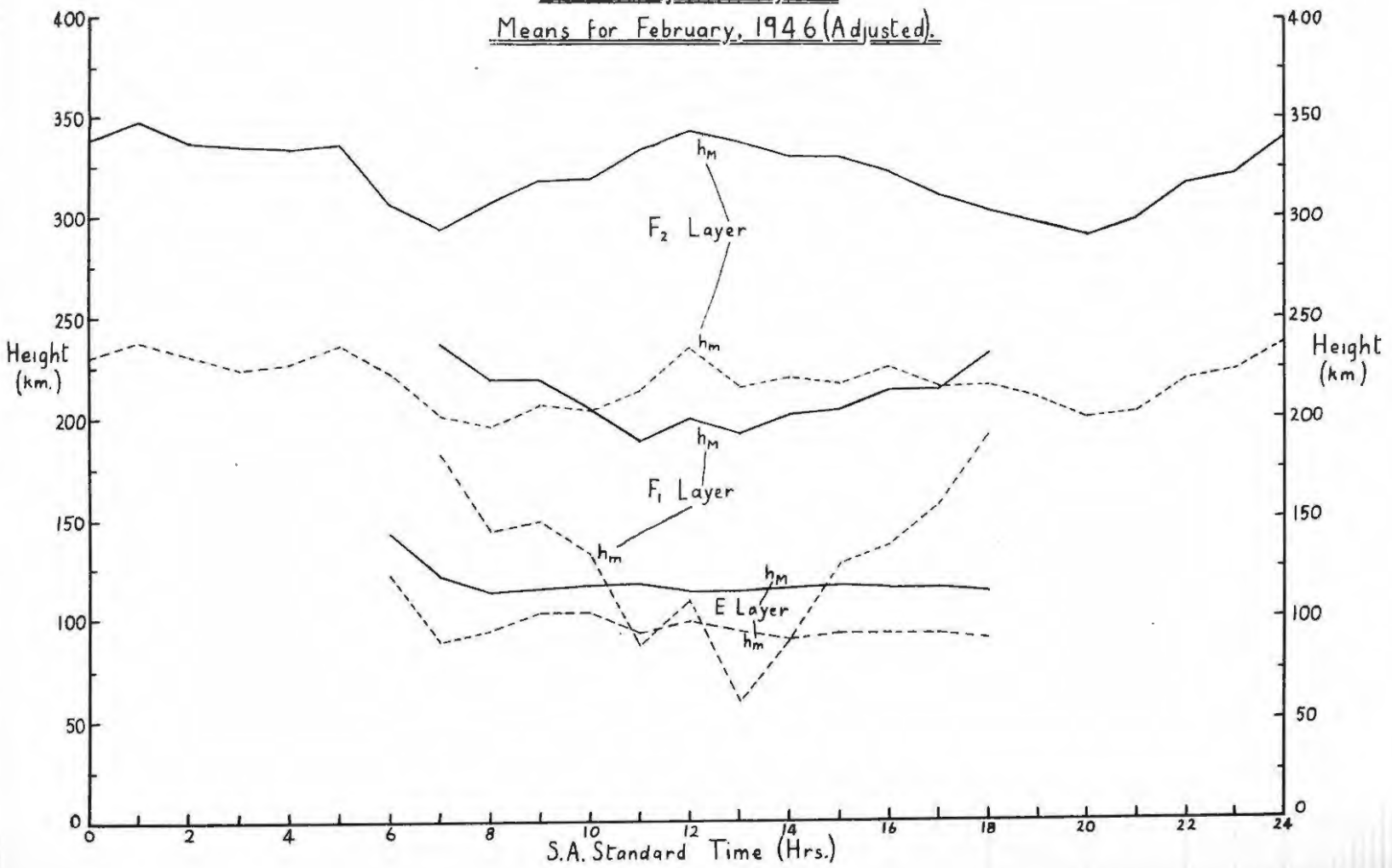
True Heights of Layers.
Means for February, 1946 (Adjusted).
Height (km.)
Height (km)
400
350
300
250
200
150
100
50
0
h_M
F_2 Layer
h_m
h_M
F_1 Layer
h_m
h_M
E Layer
h_m
0
2
4
6
8
10
12
14
16
18
20
22
24
S.A. Standard Time (Hrs.)

Since graphs of the type of figs. 1.40 - 1.43 have not previously been published, it seems of interest to comment on their general features.

E layer.

Electron densities for this layer could be observed only during the daytime, as during the night the f^0 fell below the lower limit of the transmitter. The values of these quantities rise to a maximum about local noon (12h 14m S.A. Standard Time) and fall off evenly on either side of it, showing no marked seasonal effect.

The h_M's for the layer are remarkably constant at about 115-120 km. during the daylight hours, with a semithickness of something less than 20 km.; there seems to be some indication of a fall in height of the layer between 6 and 8 hours.

F_1 layer.

In this layer seasonal effects are more marked. As for the E layer, the electron densities rise to a maximum in the middle of the day and fall off fairly evenly on each side. The maxima in November and February (approx. 3.3×10^5 electrons per $cm.^3$) are considerably higher than those of 2.85×10^5 electrons per $cm.^3$ found in December and January. This is a surprising result in view of the fact that the sun is more nearly overhead, and would therefore be expected to produce more ionisation during the two midsummer months. This may reasonably be attributed to expansion due to heating: a similar explanation has been put forward to explain the same phenomenon in the F_2 region.

The graphs/

The graphs of the true heights give a vivid illustration of the manner in which this layer is differentiated from the F_2 layer only during the daylight hours: it will be seen that near sunrise and sunset its h_M rises into the F_2 region; during the night, of course, it combines with the F_2 layer to form what is usually termed the "F region".

The F_1 layer appears to acquire amazing thicknesses during the midday period, overlapping completely the E layer in some places; semithicknesses of 120 km. and more are not uncommon. The literal interpretation is obviously erroneous, and must be attributed to the fact that the layer is not parabolic - agreement for the τ's during the scaling was usually very poor. An alternative explanation is that the layer is parabolic only near the maximum over the region where heights are scaled, and falls off more quickly below this.

F_2 region.

The taking of averages of individual days, differing widely from each other and showing most irregular graphs, yields satisfactory curves, not very dissimilar in their general nature from those of the E and F_1 layers.

The expansion occuring round the summer solstice is much more marked than for those layers, however. Compare for instance, the noon value for February of 12.4×10^5 electrons per cm^3 with that for January which is only 7.2×10^5.

In general the thickness of the layer is about 120 km., falling to a minimum of 100 km. or just less

around/

around sunrise and sunset, and increasing to a maximum of nearly 150 km. between 8 and 10 hours. There are two maxima in h_M, one in the middle of the day and the other at midnight or shortly afterwards, and two minima near sunrise and sunset. The first minimum may be attributed to the ionisation of the lower layers in the atmosphere by the rising sun, the previous day's ionisation having recombined during the night. The increase in height during the middle of the day (which is contrary to any theory of layer formation in an isothermal atmosphere) coupled with the flattening of the curve for N over the corresponding period (particularly noticeable in December and January) lends support to the view that bodily upward expansion of the atmosphere due to heating by the sun's rays takes place. The ions are carried upward more rapidly than they can be replaced by new ones by photoionisation and this prevents the expected rise in N, while the height of the layer is raised. This rise, however, is much less than that of virtual height naively assumed by previous investigators who, using virtual heights uncorrected for the retardation produced by the F_1 layer instead of true ones, have assumed h_M to rise to 400 or 500 km. at this time.

Electron Density Maps.

With the usual method of presentation of results in the form of graphs as in figs. 1.31 - 1.43, it is necessary to refer to three graphs simultaneously in order to gain a composite picture of ionospheric conditions.

With values of the maximum electron density N, its true height h_M and the semithickness of the layer τ, the/

the electron density n at any height h is determined for that layer. Assuming that ionisation from the E layer upwards is due only ~~to~~ and entirely to the presence of the E, F_1 and F_2 layers, having each a parabolic distribution, it is possible with the data of tables 1:17, 1:18 and 1:19 to calculate the electron density at any height.

In order to reduce the number of mean graphs and represent the three variables with which we are concerned (i.e., electron density n, height h and time of day T) in two dimensions, recourse must be had to a graphical plot in which two of the variables are used as co-ordinates and lines are plotted for constant values of the third. To make such a contour map a more vivid illustration of average conditions, it becomes obvious that the height must be plotted along the vertical axis and, to conform with usual procedure, the time along the horizontal axis. The map therefore takes the form of lines of equal electron density, and will be referred to, from now on, as an"electron density map".

Referring to fig. 1.25, it will be seen that the electron density n is related to the height h in a parabolic layer by the expression

$$N - n = \frac{N}{\tau^2}(h - h_M)^2 \quad . \quad . \quad . \quad . \quad . \quad (1.8)$$

From this the heights at which the electron density has the value n are:

$$h = h_M \pm \tau\left(1 - \frac{n}{N}\right)^{\frac{1}{2}} \quad . \quad . \quad . \quad . \quad . \quad . \quad (1.9)$$

Points calculated by this equation may be plotted directly on the electron density map, but in practice the layers frequently overlap, and it is difficult to decide which

of/

of the three layers should be regarded as responsible for the electron density at a given height. The construction of the map is greatly aided by a graphical representation of electron density as a function of height for each hour, as an example of which that for February, 12 hours, is shown in fig. 1.44. These graphs were constructed by using the alternative form of eqn. (1.8),

$$n = N\left\{1 - \left(\frac{h_M - h}{\tau}\right)^2\right\} \quad . \quad . \quad . \quad . \quad . \quad (1.10)$$

The parabolic distribution of n above the maximum has no experimental confirmation, but seems to be the most reasonable assumption under the circumstances. Whenever two layers overlapped at a given height the one with the higher electron density was taken. As values were only available for each hour, difficulties arose, such as the estimation of the time and height at which the maximum electron density reached a given value or at which a given electron density passed from one layer to another. These were in all cases solved by linear interpolation, in the first case by reference to the graphs of N and h_M vs. T, and in the second by calculation as follows:

For a given n,

at time t_1, let layer A have height $(h_A)_1$
and layer B " " $(h_B)_1$

at time t_2, let " A " " $(h_A)_2$
and " B " " $(h_B)_2$

To find the time t at which $h_A = h_B = h$, we have:

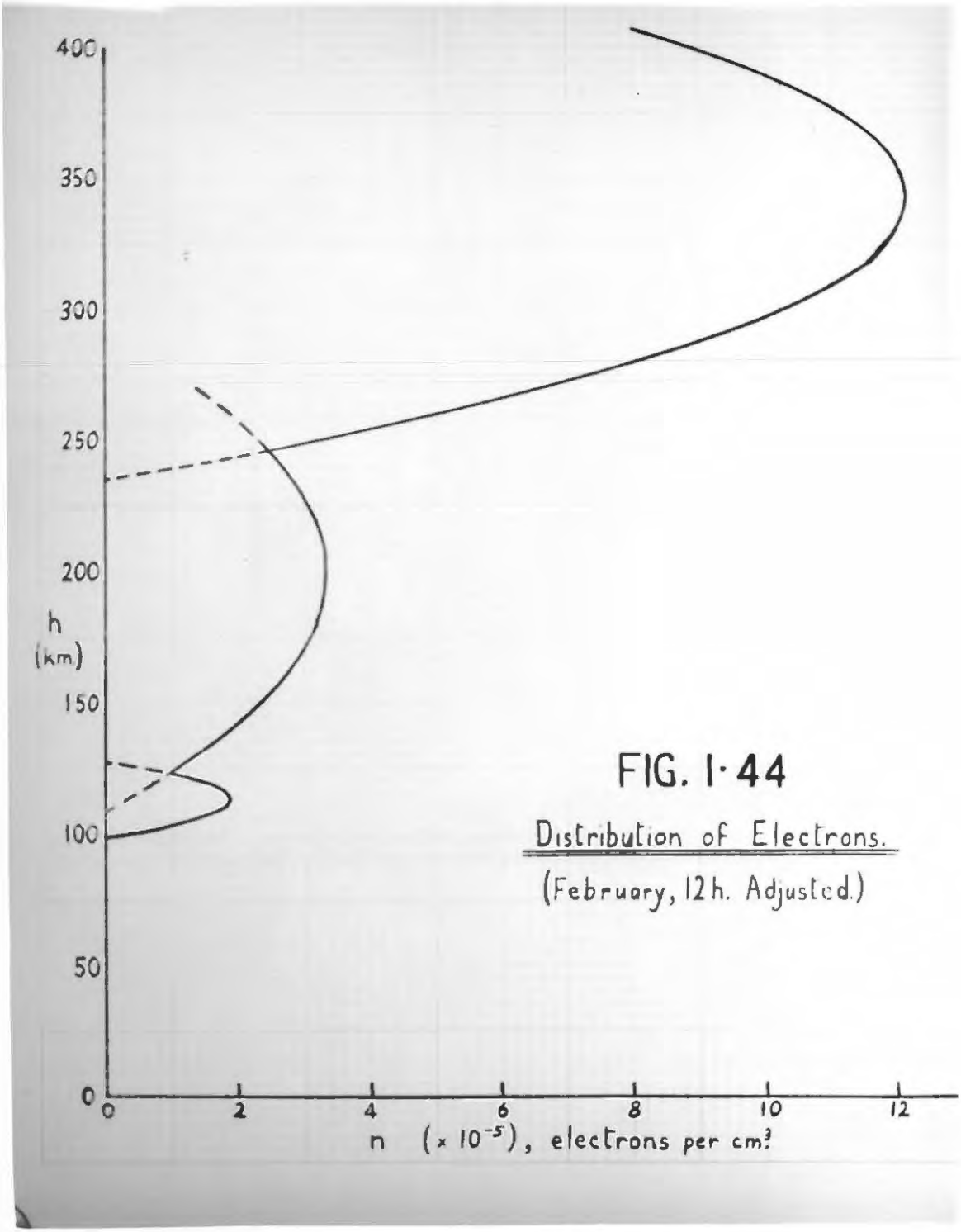

FIG. 1·44

Distribution of Electrons.

(February, 12 h. Adjusted.)

$$h = (h_A)_1 + \frac{(h_A)_2 - (h_A)_1}{t_2 - t_1}(t - t_1)$$

and $$h = (h_B)_1 + \frac{(h_B)_2 - (h_B)_1}{t_2 - t_1}(t - t_1) \quad ;$$

solving, we find:

$$t - t_1 = \frac{t_2 - t_1}{1 + \frac{(h_B)_2 - (h_A)_2}{(h_A)_1 - (h_B)_1}} \quad . \quad . \quad . \quad . \quad . \quad (1.11)$$

and $$h = (h_A)_1 + \left\{(h_A)_2 - (h_A)_1\right\}\left\{t - t_1\right) \quad . \quad . \quad (1.12)$$

In this manner the electron density maps shown in figs. 1.45 - 1.48 were drawn. Each of these contains all the information, for one month, which may have been obtained from the corresponding three graphs of figs. 1.31 - 1.43.

Points to note are:

(1) The now well-established D layer, lying around 60 km., is not, of course, included in these maps, as the apparatus is not suitable for measuring its characteristics.

(2) The E layer is very thin compared with the other two; it is represented at night by dotted lines, since it exists then, but is below the range of the transmitter and therefore cannot be measured.

(3) During the daytime there is continuous ionisation from the E layer upwards; the F_1 layer has only a broad maximum and is not associated with steep ionisation gradients, as are the E and F_2 layers.

(4) Between 240 and 300 km. the electron density is remarkably constant during the daytime, particularly during/

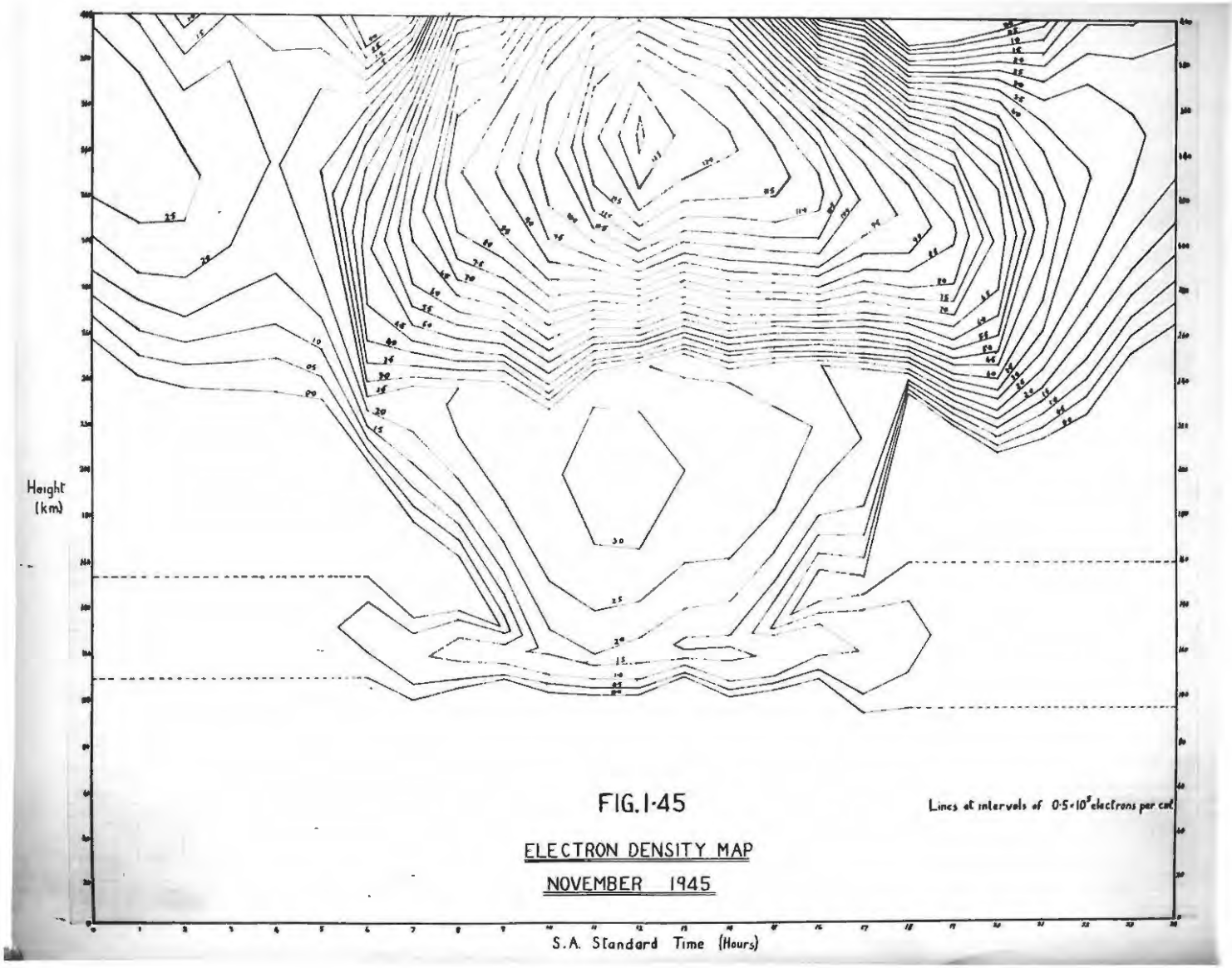

FIG. 1·45

Lines at intervals of $0{\cdot}5 \times 10^5$ electrons per cm³

ELECTRON DENSITY MAP

NOVEMBER 1945

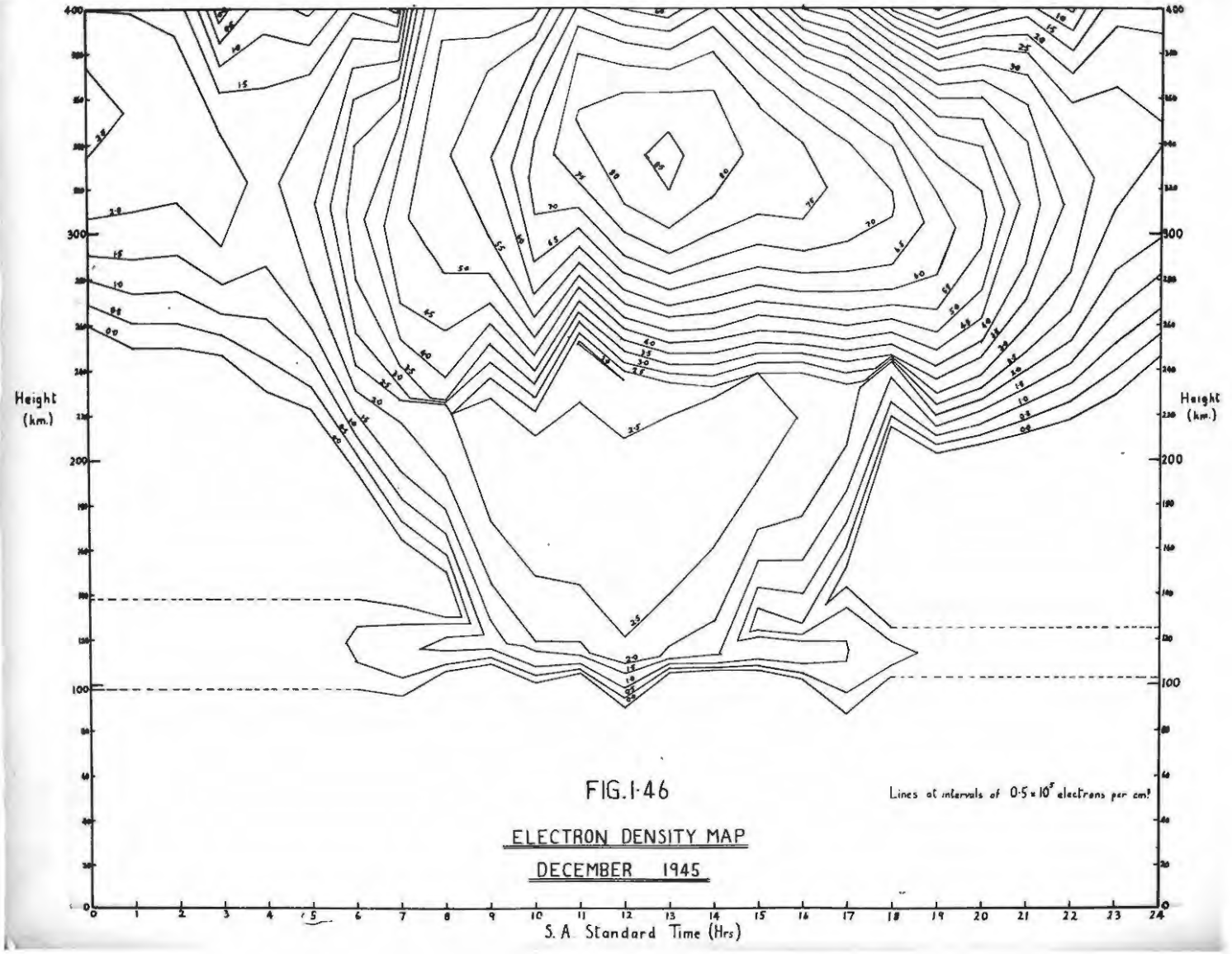

FIG. 1·46

Lines at intervals of 0.5×10^5 electrons per cm³

ELECTRON DENSITY MAP

DECEMBER 1945

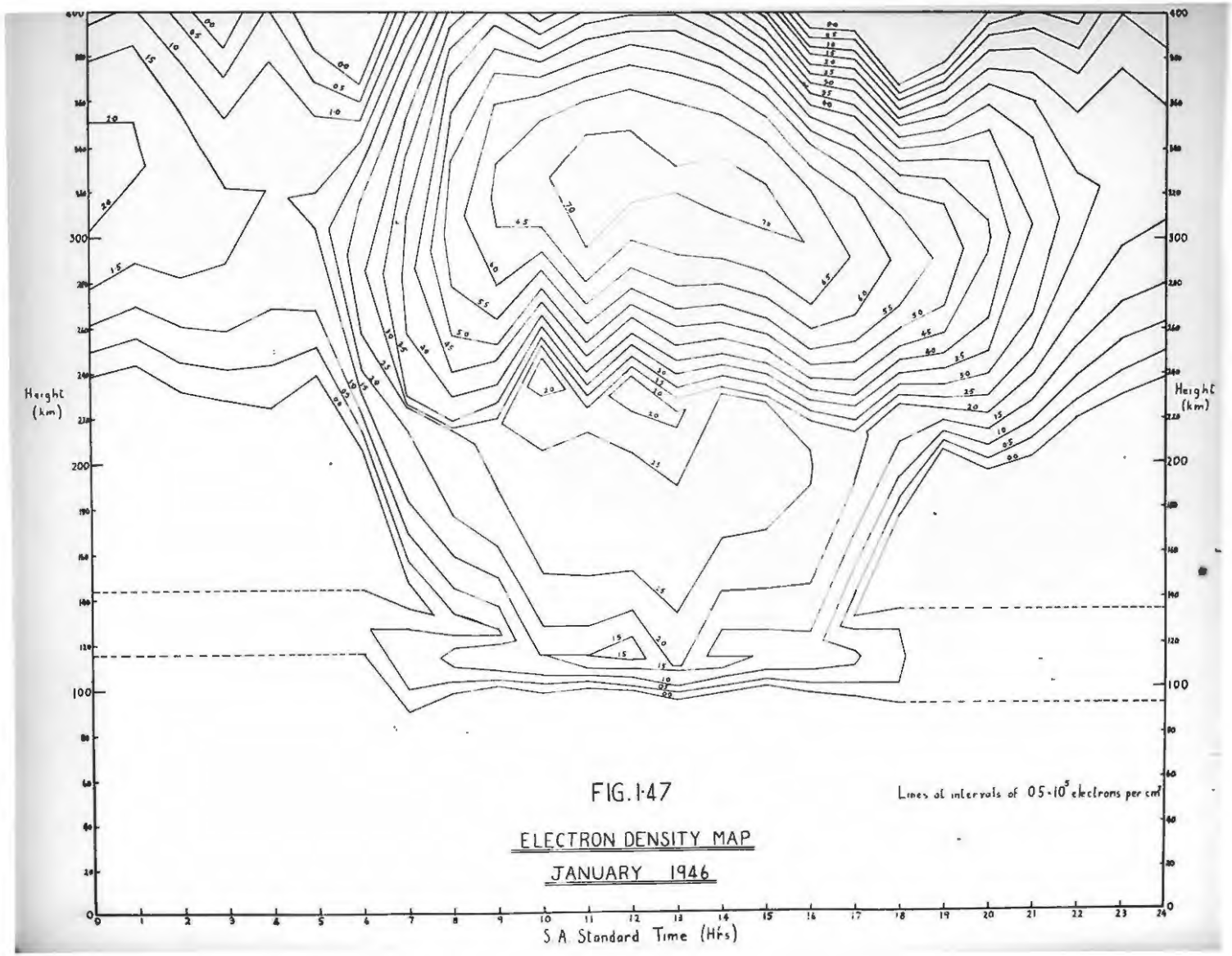

FIG. 1·47

Lines at intervals of $0.5 \cdot 10^5$ electrons per cm^3

ELECTRON DENSITY MAP

JANUARY 1946

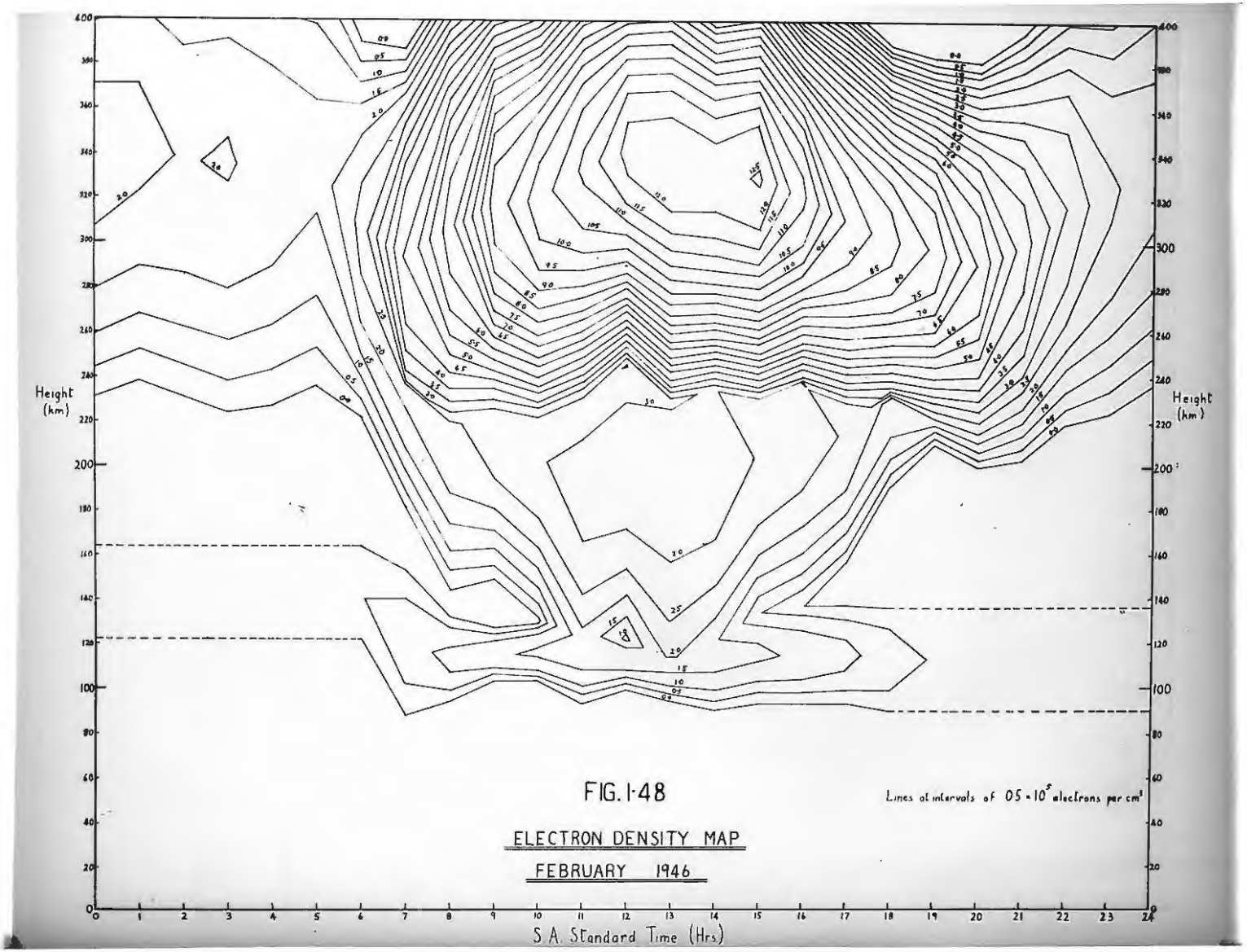

FIG. 1·48

Lines at intervals of 0.5×10^5 electrons per cm^3

ELECTRON DENSITY MAP

FEBRUARY 1946

during the afternoon.

(5) Although drawn in for completeness, the portions of these maps lying above the maximum of the F_2 region are not likely to reflect existing conditions, since the continuation of a parabolic distribution above the maximum is entirely hypothetical and unconfirmed by experimental evidence.

The construction of these maps concludes the experimental part of this work. Following the design and construction of all the apparatus required, photographic records of reasonably good standard have been produced over a four-month period, a programme of very complete scaling has been carried out, and after rejecting disturbed days, the average results have been presented in a new and concise form. These will be used and compared with theory in the following sections.

Part 1 (b)

Theory of the Production of an Ionised Layer in a Non-Isothermal Atmosphere and its Application to Experimental Results.

Theory of Layer Formation in a Non-Isothermal Atmosphere.

Introduction.

The theory of the propagation of an electromagnetic wave in an ionised medium in the presence of an external magnetic field is in a satisfactory state of development, due mainly to the work of Appleton and co-workers (1:28), (1:39) and others (1:40), (1:41); on it rests much of the deductions of section 1 (a). On the other hand, no reasonably complete theory has been proposed to account for the production of the layers, and still less for their variations. This is not due to a lack of attempts, but the problem is much more complex; we are not here dealing with a laboratory-controlled experiment, but with a natural phenomenon for which even the number of contributory causes is not known.

Even a cursory glance at any of the mean graphs of part 1 (a) shows beyond doubt a daily variation, and hence we must attribute to the sun a dominant role in the formation of these layers. Other causes are, however, not excluded: cosmic rays, α and β rays from various sources, stellar radiation, lunar radiation, meteors and cosmic dust, and charged particles from thunderclouds have all been suggested as possible ionising agents. The effects of these must, however, be small compared with that of the sun's radiation, and in any case, owing to the irregular nature of most of them, they are intractable to theoretical treatment at present. Their effects are most likely to be detected

at/

at night, but even then they are probably masked by bodily movements of the earth's atmosphere.

Most prominent among the theories put forward to account for the formation of these layers is that of Chapman (1:8), which attributes their production to the ionising action of solar ultraviolet radiation on the earth's atmosphere. A large number of simplifying assumptions is necessarily made:

(i) The radiation is monochromatic, and

(ii) is incident on an atmosphere, the density of which varies exponentially with height.

(iii) The atmosphere is at rest and uniform in composition.

(iv) The temperature is the same at all points in the atmosphere at all times.

(v) The force of gravitation is constant with height.

(vi) All the absorbed energy causes ionisation.

Working on these assumptions, Chapman obtains curves of rate of ion-production vs. height, without resorting to the use of little known constants. The problem is treated in a very general way, and families of curves are drawn for various latitudes and seasons, but no serious attempt is made at applying the electron density charts to experimental data then available.

Charts showing the ionisation of the upper atmosphere have been constructed by Millington (1:42) using Chapman's theory, but do not seem to have had much use.

Various approximate theories have been put forward by Hulburt (1:43), (1:44), in which the best

available/

available values of the constants are estimated and the general expression for the ionisation in any ionospheric region under equilibrium conditions is deduced. From these a family of curves of virtual heights vs. frequency are calculated, and one is chosen to fit an experimental record. In a later paper (1:45) an attempt was made to fit this theory to the observed daily curve of monthly mean values of maximum electron density of the E layer. The values of the constants are so uncertain that eventually they were chosen so as to give the best fit; this was fairly satisfactory over the daytime part of the curve.

Comparison shows that Chapman's and Hulburt's theories are the same in fundamental content, being based on the same initial assumptions. Their application to the E region has met with considerable success, but no attempts have been made to apply them to the higher more irregular regions.

With the true heights and thicknesses of figs. 1.40 - 1.43 and the maximum electrons densities of figs. 1.31 - 1.39 available, we are in a much better position to test Chapman's theory in its application to the higher layers than previous investigators have been, with only the maximum electron densities and virtual heights.

That the detailed application of Chapman's theory to the F_2 region would not meet with any degree of success, can be seen from the facts that:

(i) The maximum electron densities of this region for December and January during the middle part of the day are much lower than the corresponding values in November and February: this is contrary

to/

to Chapman's theory, which would require a higher maximum electron density during the solsticial period, because of the smaller zenith distance.

(ii) During all four months the height of maximum electron density in this region rises in the middle part of the day: Chapman's theory would require it to fall to a minimum about noon.

The most obvious defect in Chapman's theory, which gives rise to these discrepancies, is the fundamental assumption that the temperature is constant at all times and heights. It has been suggested (1:46) that the F_2 region becomes heated during summer days and expands upwards. This would account, qualitatively at least for the two discrepancies from Chapman's theory mentioned above, for:

(i) During December and January the greater loss of electrons by expansion more than compensates for the slight increase in production due to the smaller solar zenith distance.

(ii) The layer is shifted bodily upwards by expansion, and so the height of maximum electron density also rises in the middle of the day.

A quantitative theory taking account of expansion has not previously been given, to the writers' knowledge. The best way of developing this theory seems to be to reject Chapman's assumption of an isothermal atmosphere and instead to allow the temperature to vary with height in a known way. The distribution of molecules with height in such an atmosphere will not be exponential, and will first be derived.

Distribution of molecules with height in a non-isothermal atmosphere.

At height h let the pressure be p and the absolute temperature T, and at height h + dh let the corresponding values be p + dp and T + dT.

Dealing with a vertical column of the atmosphere of unit cross section,

nett upward force on a section of height dh = - dp

nett downward force on this section = $g\rho dh$

where ρ is the density of the atmosphere at height h and g is the acceleration due to gravity at height h.

If there is no vertical movement, i.e., the atmosphere is in equilibrium:

$$- dp = g\rho dh \quad . \quad . \quad . \quad . \quad . \quad . \quad . \quad . \quad (1.13)$$

From the simple gas laws, writing k for Boltzmann's constant and m for the mean molecular mass,

$$\rho = \frac{m}{k} \cdot \frac{p}{T} \quad . \quad . \quad . \quad . \quad . \quad . \quad . \quad . \quad (1.14)$$

Substituting this in (1.13) and integrating between limits p and p_o corresponding to heights h and h_o, we find:

$$\log_e \frac{p}{p_o} = - \frac{mg}{k} \int_{h_o}^{h} \frac{dh}{T} \quad . \quad . \quad . \quad . \quad . \quad . \quad (1.15)$$

Again from the gas laws, putting n' for the number of molecules per $cm.^3$ at height h and n'_o for the corresponding value at a reference level h_o, the temperature at this height being T_o, we have on substitution in (1.15):

$$n' = n'_o \frac{T_o}{T} \exp\left\{ - \frac{mg}{k} \int_{h_o}^{h} \frac{dh}{T} \right\} \quad . \quad . \quad . \quad . \quad . \quad . \quad (1.16)$$

The integral cannot be evaluated unless some assumption is made as to the form of the function $T = f(h)$. Two special cases will be considered:

(a) when T is a constant;
(b) when T is a linear function of h.

Case (a): - when $T = T_o$, eqn. (1.16) becomes:

$$n' = n'_o \exp\left\{ - \frac{mg}{kT_o}(h - h_o) \right\} \quad . \quad . \quad . \quad (1.17)$$

This is the exponential distribution of molecules with height assumed by Chapman and Hulburt.

Case (b):- when $T = T_o + \gamma(h - h_o)$ . . . (1.18) in which γ is the temperature gradient, eqn. (1.16) becomes:

$$n' = n'_o \frac{T_o}{T_o + \gamma(h - h_o)} \exp\left\{ - \frac{mg}{k} \int_{h_o}^{h} \frac{dh}{T_o + \gamma(h - h_o)} \right\} \quad (1.$$

$$= n'_o \frac{T_o}{T_o + \gamma(h - h_o)} \exp\left\{ - \frac{mg}{k} \log_e \frac{T_o + \gamma(h - h_o)}{T_o} \right\}$$

$$= n'_o \left\{ 1 + \gamma \frac{h - h_o}{T_o} \right\}^{-(1 + \frac{mg}{k\gamma})} \quad . \quad . \quad . \quad . \quad . \quad . \quad (1.19)$$

With $\gamma = 0$ eqn. (1.19) becomes indeterminate, but on expanding by the binomial theorem, which is valid for small values of γ, and proceeding to the limit $\gamma \longrightarrow 0$, it may be shown to reduce to eqn. (1.17).

The effect of a temperature gradient on the molecular density may be seen from table 1;20, which

has/

h (km.)	n'/n'_o			
	$\gamma = 0.00$ (deg/km.)	$\gamma = 2.02$ (deg/km.)	$\gamma = 4.05$ (deg/km.)	$\gamma = 8.10$ (deg/km.)
200	1.00	1.00	1.00	1.00
225	3.64×10^{-1}	3.44×10^{-1}	3.25×10^{-1}	2.92×10^{-1}
250	1.33×10^{-1}	1.32×10^{-1}	1.30×10^{-1}	1.22×10^{-1}
275	4.78×10^{-2}	5.54×10^{-2}	5.98×10^{-2}	6.25×10^{-1}
300	1.74×10^{-2}	2.53×10^{-2}	3.05×10^{-2}	3.64×10^{-2}
325	6.28×10^{-3}	1.22×10^{-2}	1.69×10^{-2}	2.27×10^{-2}
350	2.29×10^{-3}	6.24×10^{-3}	9.93×10^{-3}	1.52×10^{-2}

Table 1:20 - Values of n'/n'_o for various γ's.

has been worked out assuming the values $h_o = 200$ km., $T_o = 400^0$K, $m = 15 \times 1.66 \times 10^{-24}$ gm., $g = 900$ cm.sec.$^{-2}$ and $k = 1.38 \times 10^{-16}$ erg x deg.$^{-1}$.

Intensity of incident radiation at height h.

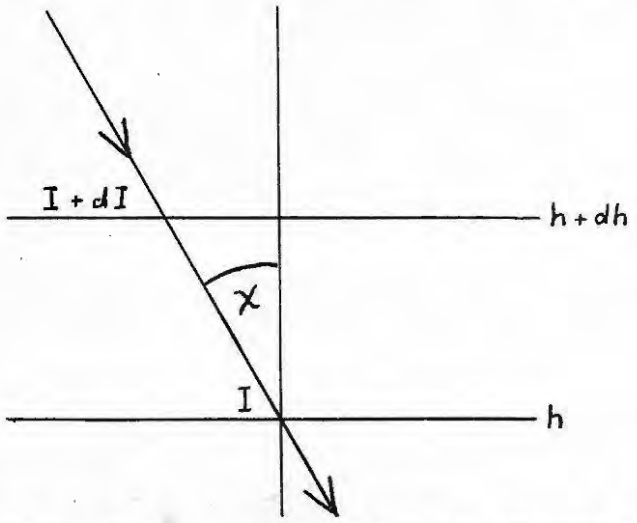

Fig. 1.49 - Intensity at height h.

We follow Chapman in assuming that the radiation responsible/

responsible for the formation of a layer is monochromatic and ultraviolet in character. The wave will be absorbed in passing through the atmosphere, and at height h let its intensity be I, and at height h + dh , I + dI, as in fig. 1.49. If the solar zenith distance is χ, then the fraction of I absorbed in passing through height dh is

$$dI = \beta n' I \sec\chi . dh \quad . \quad . \quad . \quad . \quad . \quad . \quad (1.20)$$

where β is the atomic absorption coeffient (in cm^2).

For an atmosphere in which T varies with height, using eqns. (1.16) and (1.20), we have:

$$\int_{I_\infty}^{I} \frac{dI}{I} = \int_{\infty}^{h} \left\{ \beta n'_o \frac{T_o}{T} \sec\chi \exp\left(-\frac{mg}{k}\int_{h_o}^{h} \frac{dh}{T}\right)\right\} dh$$

i.e.,

$$I = I_\infty \exp\left\{ n'_o T_o \beta \sec\chi \int_{\infty}^{h} \frac{1}{T} \exp\left(-\frac{mg}{k}\int_{h_o}^{h} \frac{dh}{T}\right) dh \right\} \quad (1.21)$$

in which I_∞ is the intensity of the beam at $h = \infty$, i.e.effectively before is has reached the earth's atmosphere.

Rate of ion production at height h.

Suppose q is the number of ion pairs produced per cm^3 per sec. at height h. Then if w is the energy absorbed in ionising one molecule, and assuming that all the energy absorbed produces ionisation,

$$q = \frac{\beta n' I}{w}$$

and/

and on substitution for I from eqn. (1.21), writing also

$$C = \frac{mg}{k} \quad . \quad . \quad . \quad . \quad . \quad . \quad . \quad . \quad (1.22)$$

we have:

$$q = \frac{\beta n_o' I_\infty}{w} \cdot \frac{T_o}{T} \exp\left\{ - C \int_{h_o}^{h} \frac{dh}{T} + \right.$$

$$\left. + n_o' T_o \beta \sec\chi \int_{\infty}^{h} \frac{1}{T} \exp\left(- C \int_{h_o}^{h} \frac{dh}{T}\right) dh \right\} \quad . \quad . \quad (1.23)$$

Again considering the two cases:

Case (a):- $T = T_o$

$$q = q_a$$

$$= \frac{\beta n_o' I_\infty}{w} \exp\left\{ - \frac{C}{T_o}(h - h_o) + \right.$$

$$\left. + n_o' \beta \sec\chi \int_{\infty}^{h} \exp\left(- \frac{C}{T_o}(h - h_o)\right) dh \right\} \quad . \quad . \quad .$$

$$= \frac{\beta n_o' I_\infty}{w} \exp\left\{ - \frac{C}{T_o}(h - h_o) - \right.$$

$$\left. - \frac{n_o' \beta T_o}{C} \sec\chi \exp\left[- \frac{C}{T_o}(h - h_o) \right] \right\} \quad . \quad . \quad . \quad (1.24)$$

which, in our notation, agrees with Hulburt and with Chapman.

Case (b):- $T = T_o + \gamma(h - h_o)$

Here/

Here:

$$q = q_b$$

$$= \frac{\beta n_o' I_\infty}{w} \cdot \frac{T_o}{T_o + \gamma(h - h_o)} \exp\left\{ - C \int_{h_o}^{h} \frac{dh}{T_o + \gamma(h - h_o)} + \right.$$

$$+ n_o' T_o \beta \sec\chi \int_{\infty}^{h} \frac{1}{T_o + \gamma(h - h_o)} \cdot$$

$$\left. \cdot \exp\left(- C \int_{h_o}^{h} \frac{dh}{T_o + \gamma(h - h_o)} \right) dh \right\}$$

$$= \frac{\beta n_o' I_\infty}{w} \left(1 + \gamma \frac{H - h_o}{T_o} \right)^{-1} \exp\left\{ \log_e \left(1 + \gamma \frac{h - h_o}{T_o} \right)^{-C/\gamma} + \right.$$

$$+ n_o' \beta \sec\chi \int_{\infty}^{h} \left(1 + \gamma \frac{h - h_o}{T_o} \right)^{-1} \cdot$$

$$\left. \cdot \exp\left[\log_e \left(1 + \gamma \frac{h - h_o}{T_o} \right)^{-C/\gamma} \right] dh \right\}$$

$$= \frac{\beta n_o' I_\infty}{w} \left(1 + \gamma \frac{h - h_o}{T_o} \right)^{-(1 + C/\gamma)} \cdot$$

$$\cdot \exp\left\{ n_o' \beta \sec\chi \int_{\infty}^{h} \left(1 + \gamma \frac{h - h_o}{T_o} \right)^{-(1 + C/\gamma)} dh \right\}$$

$$= \frac{\beta n_o' I_\infty}{w} \left(1 + \gamma \frac{h - h_o}{T_o} \right)^{-(1 + C/\gamma)} \cdot$$

$$\cdot \exp\left\{ - \frac{n_o' \beta T_o}{C} \sec\chi \left(1 + \gamma \frac{h - h_o}{T_o} \right)^{-C/\gamma} \right\} . \quad . \quad (1.25)$$

On substituting $\gamma = 0$ and proceeding to the limit, as before, eqn. (1.25) reduces to equation (1.24).

Layer formation.

If ions are produced according to eqns. (1.24) or (1.25), there will be an equal number n of positive and negative ions per cm^3. In such an ionised gas the rate of recombination is generally assumed to be proportional to n^2, the proportionality constant α, being known as the recombination coefficient.

The rate of increase of ion density is then given by

$$\frac{dn}{dt} = q - \alpha n^2 \quad . \quad . \quad . \quad . \quad . \quad . \quad (1.26)$$

Case (a):- $T = T_o$.

On substitution from eqn. (1.24), eqn. (1.26) becomes:

$$\frac{dn}{dt} + \alpha n^2 = \frac{\beta n_o' I_\infty}{w} \exp\left\{-\frac{G}{T_o}(h - h_o) - \right.$$

$$\left. - \frac{n_o' \beta T_o}{G} \sec\chi \exp\left(-\frac{G}{T_o}(h - h_o)\right)\right\} \quad . \quad (1.27)$$

According to Chapman this equation cannot be solved explicitly. We therefore impose the condition that during the middle part of the day $\frac{dn}{dt} = 0$. This will be seen from the electron density maps to be confirmed for the F_2 layer at points below the maximum. Eqn. (1.27) then reduces to:

$$n_a^2 = B \exp\left\{-\frac{G}{T_o}(h - h_o) - \frac{1}{F} \exp\left(-\frac{G}{T_o}(h - h_o)\right)\right\} \quad (1.28)$$

where we have written

$$B = \frac{\beta n_o' I_\infty}{\alpha w} \quad . \quad . \quad . \quad . \quad . \quad . \quad . \quad (1.29)$$

and

$$F = \frac{C \cos \chi}{n_o' \beta T_o} \quad . \quad . \quad . \quad . \quad . \quad . \quad . \quad (1.30)$$

Eqn. (1.28) may be derived from Hulburt's equations with suitable changes in notation, but the above approximation was not made by Chapman.

Case (b):- $T = T_o + \gamma(h - h_o)$.

Since the differential equation obtained by substituting from eqn. (1.25) in eqn. (1.26) does not appear to have an explicit solution, we proceed at once to make the approximation $\frac{dn}{dt} = 0$, obtaining:

$$n_b^2 = B\left(1 + \gamma\frac{h - h_o}{T_o}\right)^{-(1 + C/\gamma)} \cdot \exp\left\{-\frac{1}{F}\left(1 + \gamma\frac{h - h_o}{T_o}\right)^{-C/\gamma}\right\} \quad . \quad . \quad . \quad . \quad (1.31)$$

Maximum value of n.

Eqns. (1.28) and (1.31) give the value of the electron density at any point in the layer. The maximum value N is important for comparison with experiment and can be found by equating $\frac{dn}{dh}$ to zero.

Case (a):- $T = T_o$.

$$\frac{dn}{dh} = \frac{n}{2}\frac{C}{T_o}\left[\frac{1}{F}\exp\left\{-\frac{C}{T_o}(h - h_o)\right\} - 1\right]$$

$= 0$ for a maximum or a minimum.

Either (i) $\frac{n}{2} = 0$, which obviously gives a minimum,

or (ii) $$\frac{1}{F}\exp\left\{-\frac{C}{T_o}(h - h_o)\right\} = 1 \quad . \quad . \quad . \quad (1.32)$$

Putting this in eqn. (1.28) we get for the maximum value of n,

$$N_a^2 = BF\exp(-1) \quad . \quad . \quad . \quad . \quad . \quad . \quad (1.33)$$

which is also obtained by Hulburt.

Case (b):- $T = T_o + \gamma(h - h_o)$.

Differentiating (1.31) and simplifying:

$$\frac{dn}{dh} = \frac{n}{2T_o}\left(1 + \gamma\frac{h - h_o}{T_o}\right)^{-1}\left\{\frac{C}{F}\left(1 + \gamma\frac{h - h_o}{T_o}\right)^{-C/\gamma} - \gamma\left(1 + \frac{C}{\gamma}\right)\right\}$$

$= 0$ for a maximum or a minimum.

Again,

(i) $\frac{n}{2T_o} = 0$ gives a minimum.

(ii) $1 + \gamma\frac{h - h_o}{T_o} = \infty$ gives again $n = 0$ for $h = \infty$

(iii) $$\frac{C}{F}\left(1 + \gamma\frac{h - h_o}{T_o}\right)^{-C/\gamma} = \gamma\left(1 + \frac{C}{\gamma}\right)$$

i.e., $$\frac{1}{F}\left(1 + \gamma\frac{H - h_o}{T_o}\right)^{-C/\gamma} = 1 + \frac{\gamma}{C} \quad . \quad . \quad . \quad (1.34)$$

Substituting back in (1.31), we obtain the maximum value of n,

$$N_b^2 = B\left\{F\left(1 + \frac{\gamma}{C}\right)\right\}^{(1 + \gamma/C)}\exp\left\{-\left(1 + \frac{\gamma}{C}\right)\right\} \quad . \quad . \quad (1.35)$$

which reduces to eqn. (1.33) on putting $\gamma = 0$.

Height of maximum electron density, h_M.

Case (a):- $T = T_o$

The height $(h_M)_a$ is given by equation (1.32), writing $h = (h_M)_a$, and is:

$$(h_M)_a = h_o - \frac{T_o}{C} \log_e F \quad . \quad . \quad . \quad . \quad . \quad (1.36)$$

With constant temperature T_o throughout the day and substituting for F from eqn. (1.30), the variation of $(h_M)_a - h_o$ with χ may be seen by putting (1.36) in the form:

$$(h_M)_a - h_o = \text{constant} - \log_e \cos \chi$$

$\log_e \cos \chi$ is always negative, and is numerically smallest in the middle of the day. Thus according to the theory of an isothermal atmosphere, the height of maximum electron density should fall to a minimum at local noon. This is contrary to observation for the F_2 region.

Case (b):- $T = T_o + \gamma(h - h_o)$.

The height of maximum electron density obtained by putting $h = (h_M)_b$ in eqn. (1.34) is:

$$(h_M)_b = h_o + \frac{T_o}{\gamma}\left[\left\{F\left(1 + \frac{\gamma}{C}\right)\right\}^{-\gamma/C} - 1\right] \quad . \quad (1.37)$$

Again it may be shown by expanding into a series that in the limit $\gamma \longrightarrow 0$, eqn. (1.37) reduces to (1.36).

Comparison of the two cases.

The changes in behaviour brought about by the assumption of a linear temperature gradient with height

may/

may be illustrated by means of the ratios, $\frac{N_b}{N_a}$ and $\frac{(h_M)_b - h_o}{(h_M)_a - h_o}$. By this method the use of a number of questionable constants may be eliminated, and, for purposes of this comparison only, values of the remaining constants have been chosen from the following considerations;

h_o. The composition of the atmosphere at this reference height should be the same as that throughout the layer. There is reason to believe that the atmospheric gases exist mainly in the atomic form from 200 km. upwards (1:47). h_o has therefore been chosen as 200 km. because the value of T_o becomes less certain as the height increases.

$C = \frac{mg}{k}$. From the considerations just mentioned the value of m was taken as 15 atomic weight units; the value of g corrected for a mean F_2 height of 300 km is approx. 900 cm.sec.$^{-2}$; while Boltzmann's constant, k, is well established as 1.38×10^{-16} erg deg.$^{-1}$. The value of C is thus 16.2 deg.km.$^{-1}$.

T_o. The value of T_o is very doubtful, but after consideration of various estimates the tentative value of 360°K was chosen for this purpose.

$F = \frac{C \cos \chi}{n'_o \beta T_o}$. The estimates of n'_o and β are very numerous and diverse. Eventually β was taken as 2×10^{-18} cm.^{2} and n'_o as 5×10^{12} cm.$^{-3}$ on very debatable grounds. Putting $\chi = 0$ for simplicity, we find $F = 4.4 \times 10^{-2}$.

Dividing eqn. (1.35) by eqn. (1.33), we obtain:

γ (deg.km.$^{-1}$)	$\frac{N_b}{N_a}$	$\frac{(h_M)_b - h_o}{(h_M)_a - h_o}$	$(h_M)_b - (h_M)_a$ (km.)
- 8.10	2.36	0.545	- 29.5
- 6.49	1.95	0.614	- 27.0
- 4.86	1.64	0.690	- 21.6
- 3.24	1.38	0.781	- 15.5
- 1.62	1.17	0.885	- 8.3
0.00	1.00	1.00	0.0
1.62	0.858	1.12	8.3
3.24	0.738	1.28	19.4
4.86	0.640	1.44	30.6
6.49	0.555	1.63	43.6
8.10	0.483	1.85	58.3
9.7	0.423	2.08	75.3
11.3	0.372	2.34	93.7
13.0	0.326	2.63	112
14.6	0.288	2.94	135
16.2	0.255	3.30	160

Table 1:21 - Effect of γ on the layer.

$$\left(\frac{N_b}{N_a}\right)^2 = F^{\gamma/c}.\left(1 + \frac{\gamma}{c}\right)^{1 + \gamma/c}.\exp(-\gamma/c) \quad . \quad (1.38)$$

and from eqns. (1.36) and (1.37),

$$\frac{(h_M)_b - h_o}{(h_M)_a - h_o} = -\frac{c}{\gamma}\,\frac{\left\{F\left(1 + \frac{\gamma}{c}\right)\right\}^{-\gamma/c} - 1}{\log_e F} \quad . \quad . \quad . \quad (1.39$$

To obtain some idea of the absolute difference in height of the maxima, we use:

$$(h_M)_b - (h_M)_a = T_o\left[\frac{1}{\gamma}\left\{\left[F(1+\frac{\gamma}{C})\right]^{-\gamma/C} - 1\right\} + \frac{1}{C}\log_e F\right] \quad \ldots\ldots\ldots (1.40)$$

obtained by ~~substituting~~ subtracting eqn. (1.36) from eqn. (1.37).

The values obtained are shown in table 1:21, and, graphically, in figs. 1.50 and 1.51. The graphs show that a positive value of γ produces a lowering of the maximum electron density in the layer and raises its height.

By drawing on figs. 1.40 - 1.43 approximate curves for the variation of h_M during the day according to Chapman's theory, the difference in height caused by expansion may be estimated as about 80 km. From fig. 1.51 it appears that this difference would correspond to a γ of 10 deg.km.$^{-1}$.

Effect of variables on the shape of the layer.

The general theory, as summarised in eqns. (1.31) (1.35) and (1.37), does not lend itself to easy physical interpretation, and in order to clarify its meaning, it has been thought advisable to represent graphically the variations in shape of the layer brought about by changes in the variables. The number of little-known constants included under the symbols B and F is considerable, and, in order to eliminate as far as possible numerical errors arising from the use of uncertain values, eqns. (1.31) and (1.35) may be divided, giving:

$$\left(\frac{n_b}{N_b}\right)^2 = \left(1+\gamma\frac{h_b - h_o}{T_o}\right)^{-(1+C/\gamma)} \cdot \left\{F(1+\frac{\gamma}{C})\right\}^{-(1+\gamma/C)} \cdot$$

$$\cdot \exp\left\{(1+\frac{\gamma}{C}) - \frac{1}{F}\left(1+\gamma\frac{h_b - h_o}{T_o}\right)^{-C/\gamma}\right\} \quad \ldots (1.41)$$

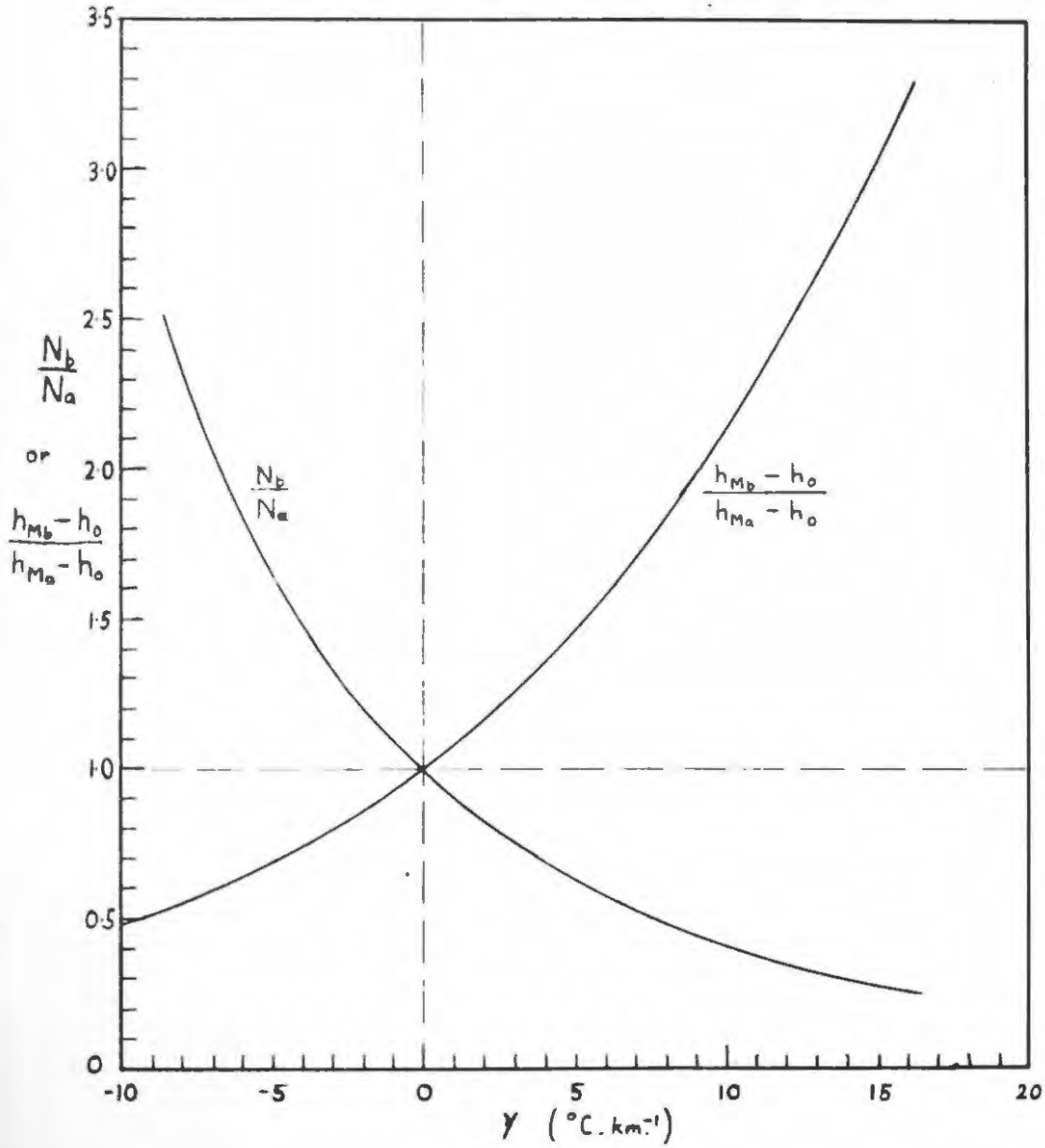

FIG. 1·50

Effect of γ on the Layer.

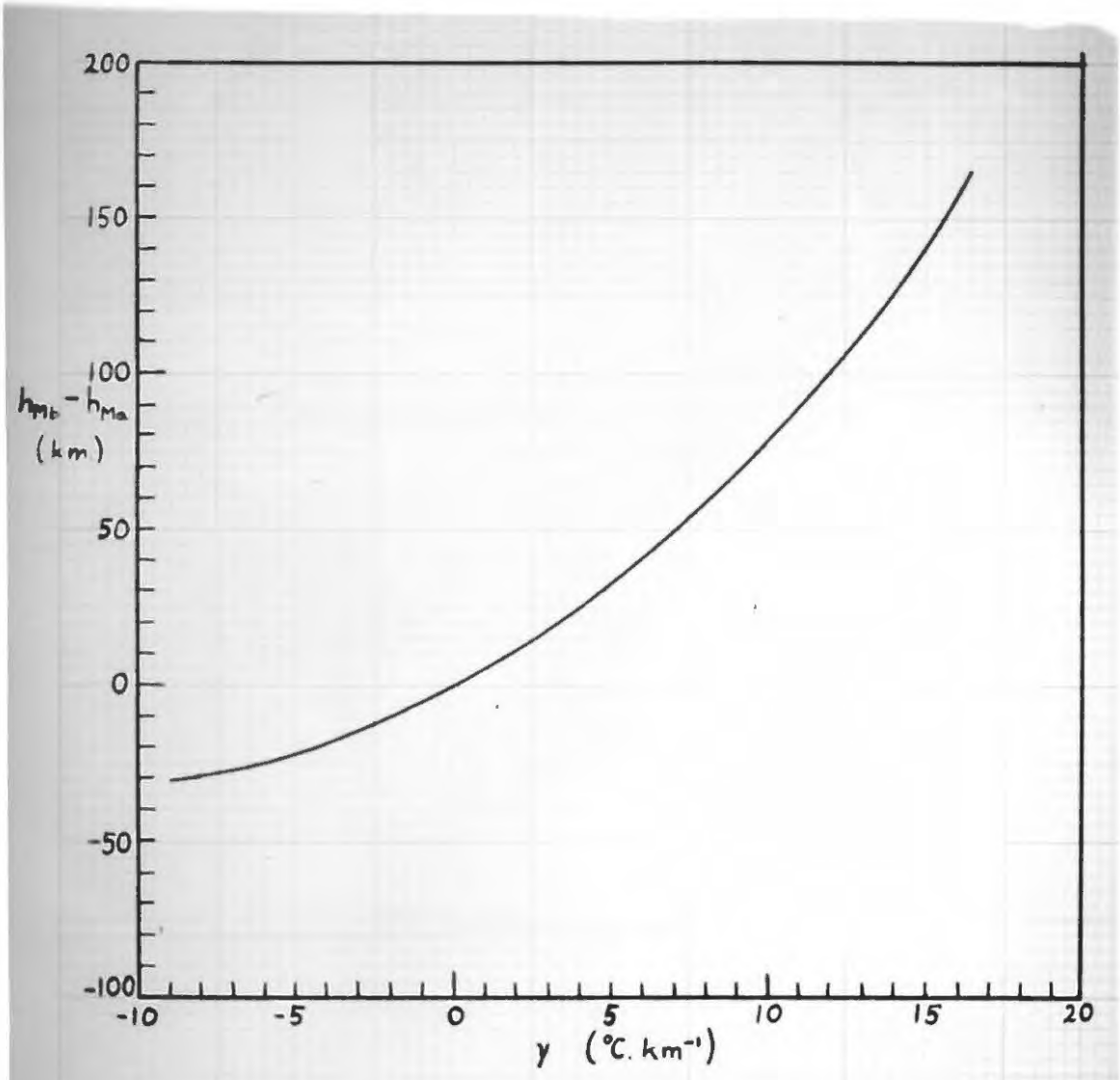

FIG. 1·51

Effect of γ on h_M for a Layer.

in which B does not appear.

The constant C appears to have been evaluated with as much certainty as possible on page 81 and its value is kept at 16.2 deg.km.$^{-1}$ throughout the remainder of this work. For similar reasons h_o is left at 200 km.

In the R.H.S. of eqn. (1.41) we are thus left with four parameters, the height h_b, the temperature T_o at 200 km., the temperature gradient γ, and F. We shall now show the actual shape of the layer by plotting $\frac{n_b}{N_b}$ against h_b for various values of γ, T_o and F, using eqn. (1.41).

h_b (km.)	n_b/N_b			
	$\gamma = 0.0$ deg/km.	$\gamma = 4.0$ deg/km.	$\gamma = 6.0$ deg/km	$\gamma = 8.0$ deg/km.
220	0.0285	0.0297	0.0312	0.0318
240	0.251	0.205	0.189	0.174
260	0.662	0.507	0.450	0.402
280	0.953	0.790	0.705	0.631
300	0.988	0.951	0.875	0.805
320	0.861	1.000	0.970	0.916
340	0.686	0.985	0.998	0.968
360	0.521	0.925	0.982	0.988
380	0.386	0.851	0.946	0.980
400	0.284	0.767	0.897	0.960

Table 1:22 - Values of $\frac{n_b}{N_b}$ vs. h_b for various values of γ.
$T_o = 500^oK$ $F = 5.0 \times 10^{-2}$.

The curve for $\gamma = 0$ (fig. 1.52) is, of course, derived/

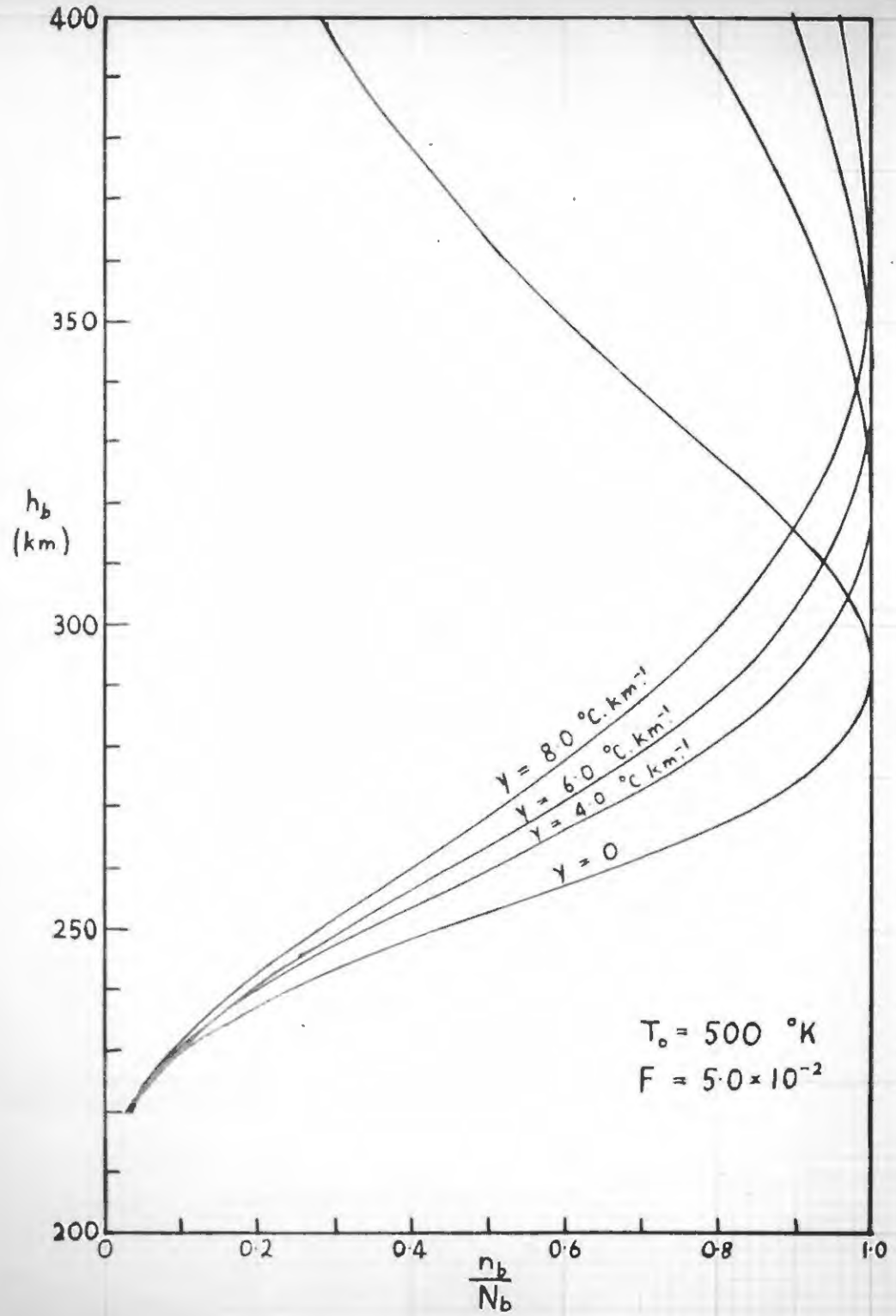

FIG. 1·52

Effect of γ on Shape of Layer.

derived from eqns. (1.28) and (1.33), and represents the distribution of electrons at constant temperature, i.e., on Chapman's theory. We note again the effect of a positive γ in raising the height h_M. In addition it is seen to increase the thickness of the layer, and the electron density above the maximum decreases more slowly than in an isothermal atmosphere. The importance of a knowledge of layer thickness in any attempt to estimate γ is thus clearly brought out.

h_b (km)	n_b/N_b		
	$T_o = 400^oK$	$T_o = 500^oK$	$T_o = 600^oK$
220	0.0553	0.0312	0.0188
240	0.313	0.189	0.116
260	0.649	0.450	0.316
280	0.880	0.705	0.541
300	0.981	0.875	0.745
320	0.992	0.970	0.881
340	0.954	0.998	0.954
360	0.893	0.982	0.996
380	0.823	0.946	0.993
400	0.731	0.897	0.971

Table 1:23 - Values of n_b/N_b vs h_b for three values of T_o. $\gamma = 6.0$ deg.km^{-1}; $F = 5.0 \times 10^{-2}$.

From fig. 1.53 it will be seen that an increase in T_o produces an increase in the height of maximum electron density, but the thickness of the layer is not altered to any great extent.

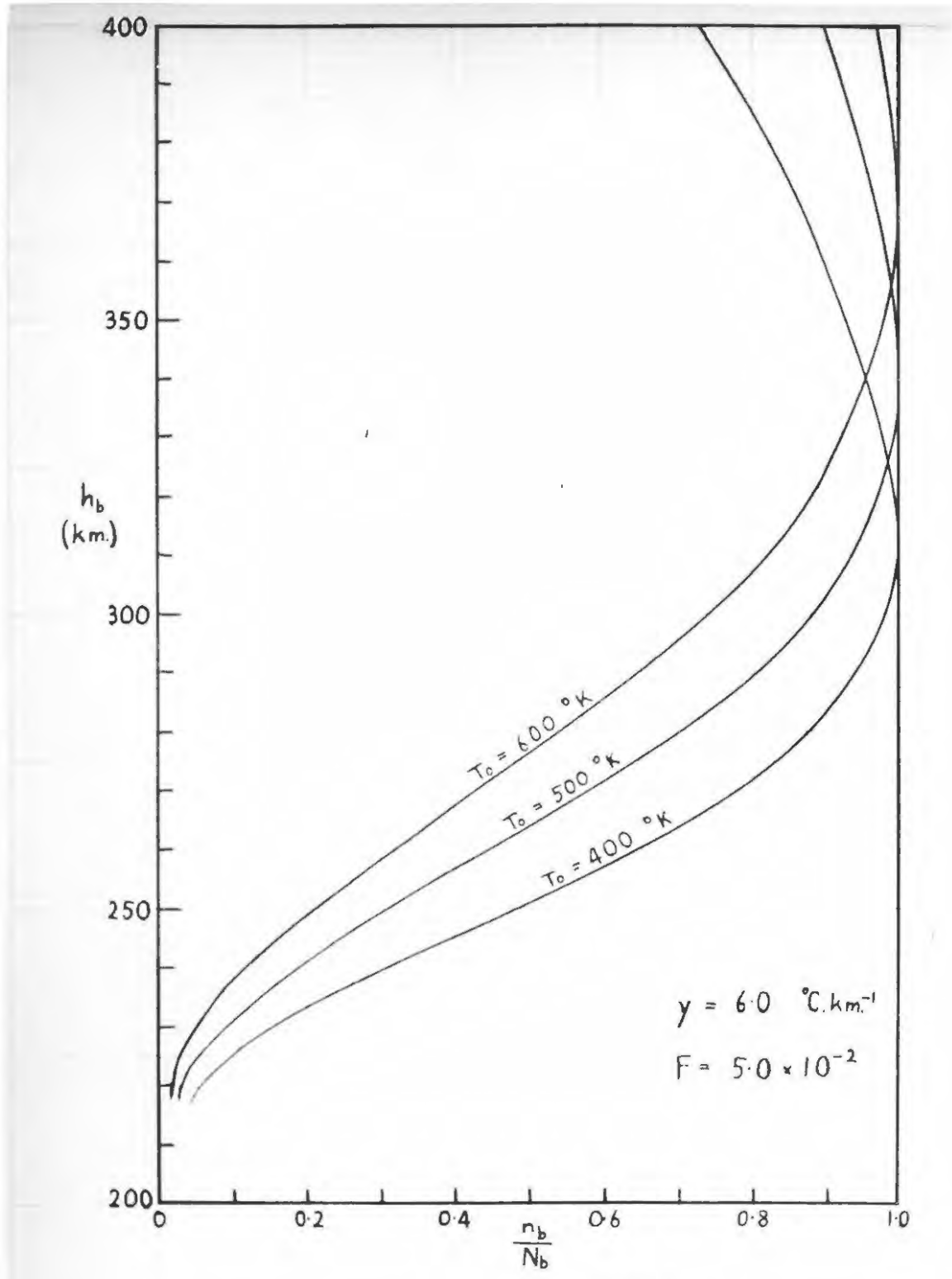

FIG.1·53

Effect of T_o on Shape of Layer.

h_b (km)	n_b/N_b		
	F = 0.040	F = 0.050	F = 0.060
220	0.0089	0.0312	0.0681
240	0.0915	0.189	0.293
260	0.294	0.450	0.584
280	0.550	0.705	0.815
300	0.763	0.875	0.949
320	0.907	0.970	1.000
340	0.981	0.998	0.991
360	0.998	0.982	0.955
380	0.987	0.946	0.902
400	0.956	0.897	0.841

Table 1:24 - Values of n_b/N_b vs h_b for three values of F. $\gamma = 6.0$ deg.km^{-1}; $T_o = 500^oK$.

The thickness of the layer is again practically unchanged by F, but the height h_M decreases with increasing F (fig. 1.54). Remembering that for a given T_o (and therefore n_o') F is proportional to $\cos\chi$ from eqn. (1.30), these curves show a result analogous to the theory for an isothermal atmosphere, i.e., the height of maximum electron density decreases to a minimum at local noon, all the other parameters remaining constant. However, since the theory of expansion demands atmospheric heating during the middle part of the day, T_o and γ cannot be taken as constant. If the increase in T_o is greater than that of $\cos\chi$, it alone would account for a rise in h_M, even if γ were constant.

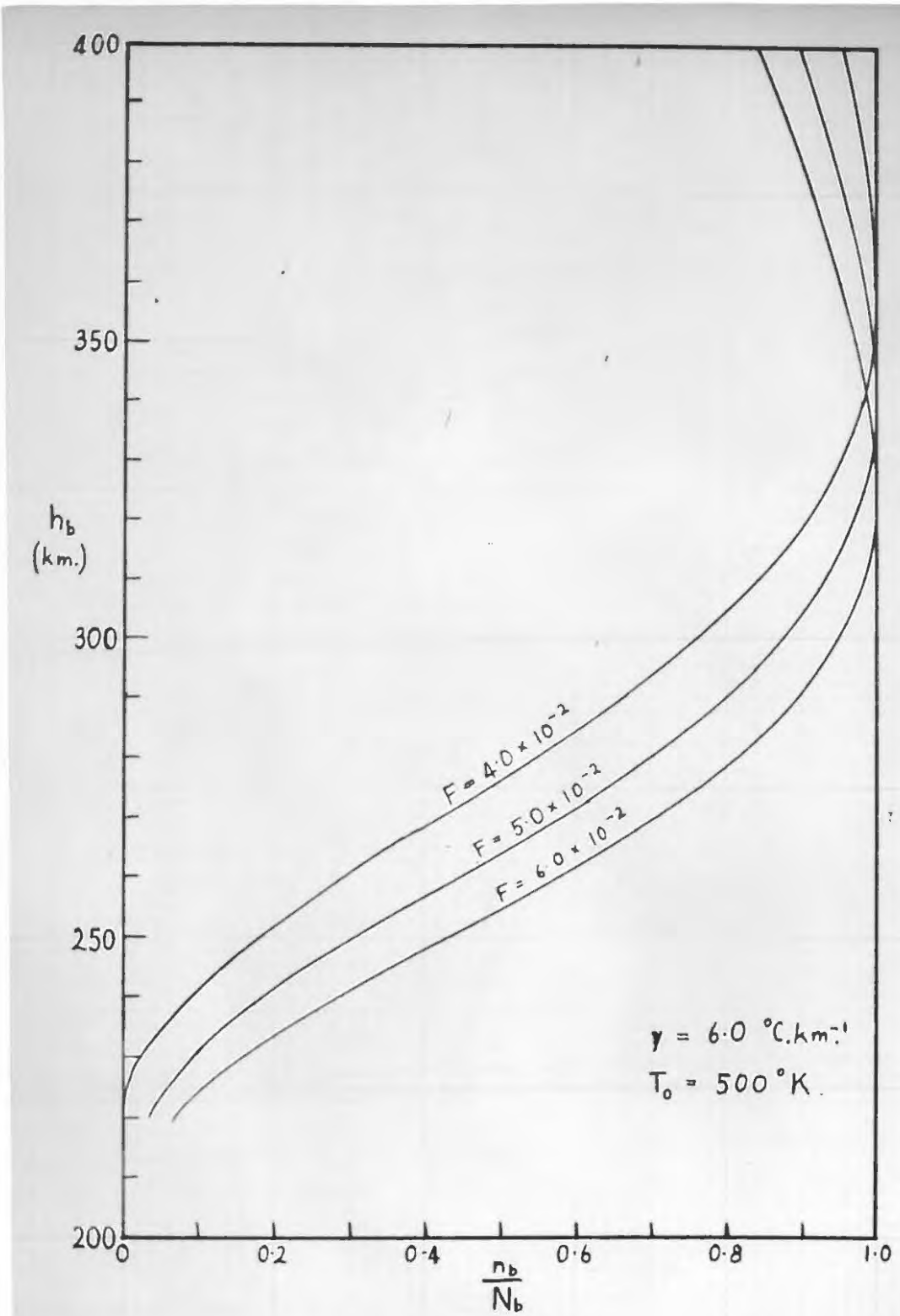

FIG. 1·54

Effect of F on Shape of Layer.

Application of the foregoing theory to experimental results.

The application to experimental results of a theory with equations as complex as those derived in this treatment is a problem which must present some difficulty. The experimental data are in the form of parabolas from each of which the three quantities h_M, τ and N may be read off. From the theory there emerge three useful equations, which for convenience are here repeated, dropping the subscripts:

$$n^2 = B\left(1 + \gamma\frac{h - h_o}{T_o}\right)^{-(1 + C/\gamma)} \cdot \exp\left\{-\frac{1}{F}\left(1 + \gamma\frac{H - h_o}{T_o}\right)^{-C/\gamma}\right\} \quad . \quad . \quad . \quad . \quad (1.31)$$

$$N^2 = B\left\{F\left(1 + \frac{\gamma}{C}\right)\right\}^{(1 + \gamma/C)} \exp\left\{-\left(1 + \frac{\gamma}{C}\right)\right\} \quad . \quad . \quad (1.35)$$

$$h_M = h_o + \frac{T_o}{\gamma}\left[\left\{F\left(1 + \frac{\gamma}{C}\right)\right\}^{-\gamma/C} - 1\right] \quad . \quad . \quad . \quad . \quad (1.37)$$

Considering C as known, we see that these equations still contain no less than four unknowns: B, γ, T_o and F. B may be eliminated as before by dividing eqn. (1.31) by (1.35):

$$\left(\frac{n}{N}\right)^2 = \left(1 + \gamma\frac{h - h_o}{T_o}\right)^{-(1 + C/\gamma)} \left\{F\left(1 + \frac{\gamma}{C}\right)\right\}^{-(1 + \gamma/C)} \cdot \exp\left\{\left(1 + \frac{\gamma}{C}\right) - \frac{1}{F}\left(1 + \gamma\frac{h - h_o}{T_o}\right)^{-C/\gamma}\right\} \quad . \quad (1.41)$$

but this leaves only two equations with the three unknowns γ, T_o and F.

At first sight it may seem that by taking two values of h and the corresponding two values of n, we could obtain two numerical equivalents of (1.41) which, together with (1.37) would allow solution for all three unknowns. This is a fallacy, however, because, by dividing eqns. (1.31) and(1.35) the absolute value of N has been eliminated, and the parabola now yields only two quantities.

It is therefore necessary to assume a numerical value for one of the three remaining unknowns, the one chosen being that which is the best known. The temperature gradient γ is out of the question, as the only available estimates are wild guesses (1:48), (1:49). F contains the absorption coefficient β, for which estimates range from 10^{-17} to 10^{-20} cm.^{2} (1:47), while T_o is most unlikely to range below 350°K or above 700°K (1:47), i.e., through no more than a factor of 2. T_o is therefore the obvious choice. We shall, however, not assume a fixed value of T_o, but apply the theory for a number of values of T_o between these limits, deferring discussion of its actual value until later.

Algebraic solution of the eqns. (1.41) and (1.37) is impracticable as a routine method, and resort is therefore made to a graphical method, which can be applied quickly to most conditions met with in the F_2 region. It should be remembered that the final equations are only true if $\frac{dn}{dt} = 0$, a condition which is well fulfilled

for/

for the F_2 region below its maximum from 8 h to 16h S.A.S.T., as previously pointed out.

Graphical solution for F and γ.

The value of n for substitution in eqn. (1.41) may be read at any height below h_M, where the electron density is greater than 0.3N. These limits are those beyond which the curve differs appreciably from parabolic form, and between which all the virtual heights are originally scaled.

In order to construct a family of curves of n/N vs. γ for various values of F from eqn. (1.41) the value of $\frac{h - h_o}{T_o}$ must be settled. A value of h which gives an n agreeing with the conditions outlined in the previous paragraph is 280 km., as may be verified by an examination of the electron density maps. Assuming that T_o will be of the order of 400^0K, we find

$$\frac{h - h_o}{T_o} = \frac{280 - 200}{400} = \frac{1}{5} \quad . \quad . \quad . \quad . \quad (1.42)$$

Recalling that C = 16.2 ^{0}C/km., and substituting in (1.41), this simplifies to:

$$\left(\frac{n}{N}\right)^2 = \left(1 + \frac{\gamma}{5}\right)^{-\left(1 + \frac{16.2}{\gamma}\right)} \left\{F\left(1 + \frac{\gamma}{16.2}\right)\right\}^{-\left(1 + \frac{\gamma}{16.2}\right)} \cdot$$

$$\cdot \exp\left\{\left(1 + \frac{\gamma}{16.2}\right) - \frac{1}{F}\left(1 + \frac{\gamma}{5}\right)^{-\frac{16.2}{\gamma}}\right\} \quad . \quad . \quad (1.43)$$

Choosing values of γ which give simple numerical values to the indices (γ = 1.62; 3.24; 4.86; 6.49; 8.10; 9.7), and using eqns. (1.28) and (1.33) for γ = 0, various values of F may be substituted to give

n/N

$\frac{n}{N}$ greater than 0.3. In this way the family of curves shown in fig. 1.55 was drawn.

Eqn. (1.37) may be written, with the usual value of C:

$$\frac{h_M - h_o}{T_o} = \frac{1}{\gamma}\left[\left\{F\left(1 + \frac{\gamma}{16.2}\right)\right\}^{-\frac{\gamma}{16.2}} - 1\right] \quad . \quad . \quad (1.44)$$

With the values of γ used before a similar family of curves may be drawn, and is shown in fig. 1.56.

These curves exhibit a number of interesting points:

(i) The occurence of maxima in the curves of $\frac{n}{N}$ for $F = 5 \times 10^{-2}$ and $F = 10^{-1}$ for values of γ equal to 1.2 and 8 deg.km.$^{-1}$ respectively indicate that under these conditions n becomes equal to N, i.e., the maximum electron density passes through the height h for which $\frac{h - 200}{T_o} = \frac{1}{5}$.

As was illustrated by fig. 1.54, an increase in F corresponds to a lowering of the height and the curves for values of F greater than 10^{-1} refer entirely to values of n above h_M, and therefore cannot be used for practical purposes.

(ii) In fig. 1.56 the curves below $\frac{h_M - 200}{T_o} = 0.2$ again refer to conditions when the maximum is below the selected height h, and therefore have no practical value.

The simultaneous graphical solution of eqns. (1.43) and (1.44) may now be accomplished, if values taken both from fig. 1.55 and from fig. 1.56 are plotted on the same diagram, using as coordinates the variables F and γ or, preferably, $\log_{10}F$ and γ. This has been

done/

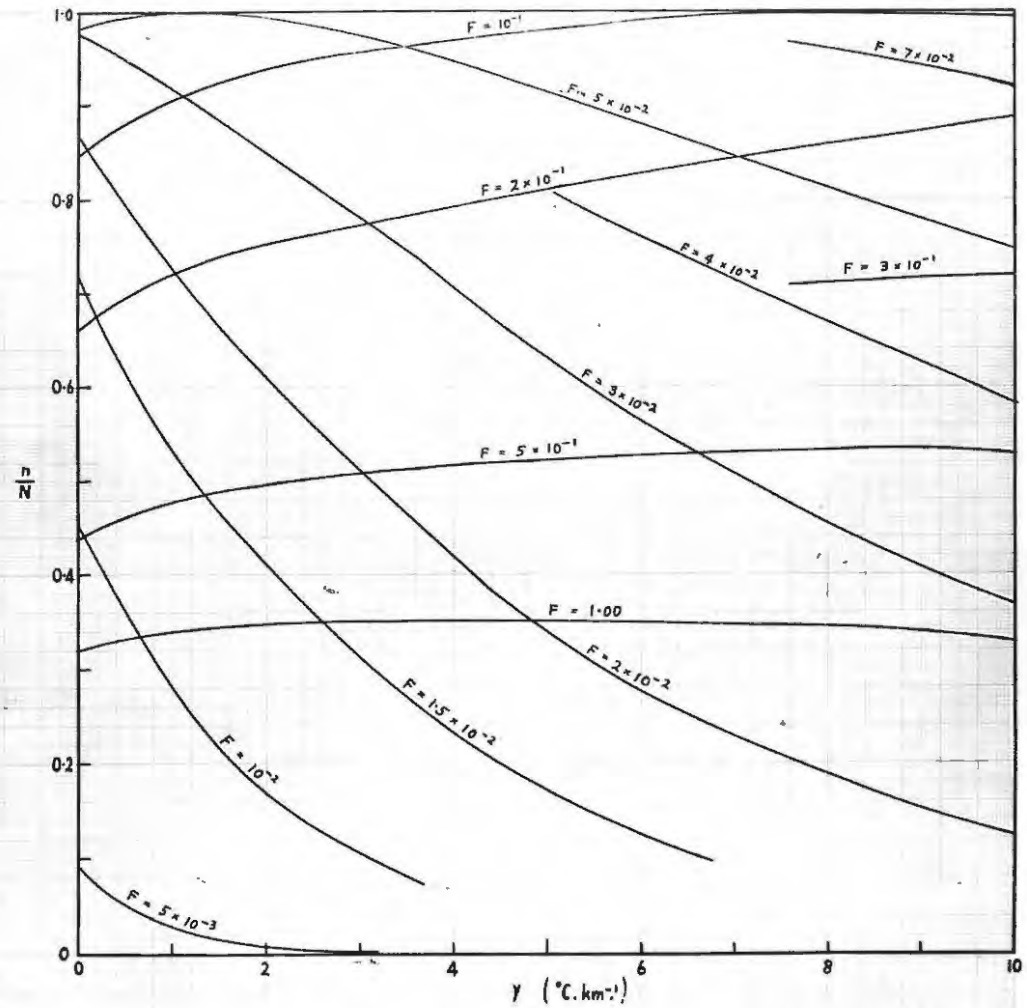

FIG.1·55

Curves of $\frac{n}{N}$ vs. γ for $\frac{h-h_0}{l_0} = \frac{1}{5}$, From Equation (1·43).

done in fig. 1.57, where lines of constant $\frac{n}{N}$ from fig. 1.55 are drawn in full and those of constant $\frac{h_M - 200}{T_o}$ from fig. 1.56 are shown dotted.

The process of evaluating γ and F for a given experimental parabola now resolves itself into the following series of simple operations:

(i) Select a reasonable value of T_o.

(ii) Estimate the value of h by substituting this value of T_o in the equation $\frac{h - 200}{T_o} = \frac{1}{5}$.

(iii) From the parabola, find n at this value of h, and also N.

(iv) Hence calculate $\frac{n}{N}$.

(v) From the parabola read off h_M.

(vi) Evaluate $\frac{h_M - 200}{T_o}$, using the value of T_o chosen in (i).

(vii) On fig. 1.57 locate the point which satisfies simultaneously ~~(x)~~ (iv) and (vi), and read off the values of γ and $\log_{10}F$.

The whole procedure is repeated for each value of T_o selected.

The curve $\frac{n}{N} = 1.0$ represents the maximum electron density, and thus the part of the graph above this is not shown, as it has no use. It coincides with the line $\frac{h_M - 200}{T_o} = 0.2$, which also represents the electron density/

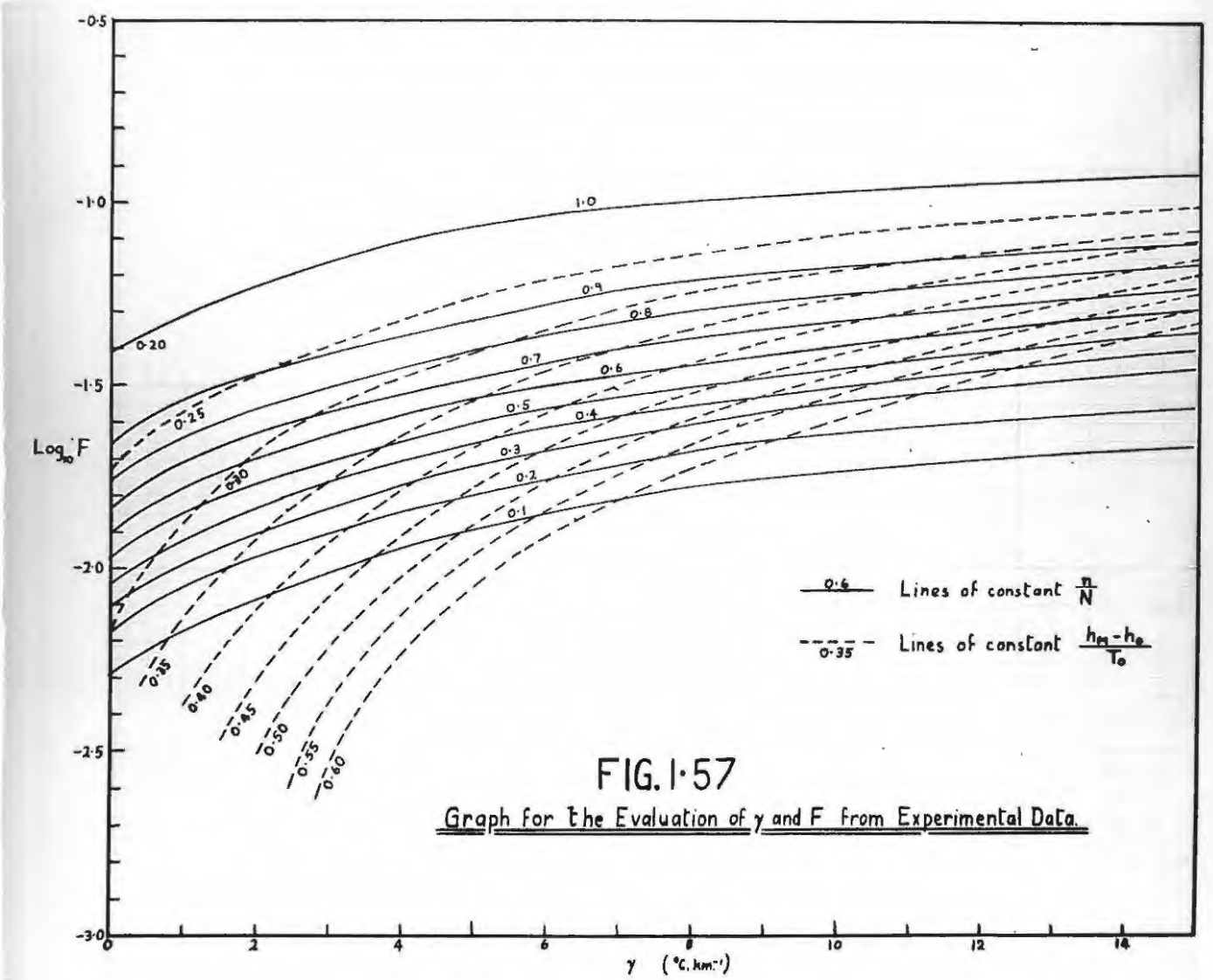

FIG. 1·57

Graph for the Evaluation of γ and F from Experimental Data.

density maximum.

The angle between the two families of curves increases as we estimate n further below the maximum, and therefore values of γ and F estimated from values of n scaled near the maximum are not very accurate. This could be avoided by choosing the fraction $\frac{h - 200}{T_o} + \frac{1}{5}$, but this would introduce other difficulties by putting n below 0.3 N in the normal applications.

The two families of curves tend to run parallel for values of γ greater than 15 deg.km.$^{-1}$, and this introduces uncertainty in values estimated in this region. Since for γ = 15 deg.km.$^{-1}$ and T_o = 250°K (a very low estimate), the temperature at 350 km. would be 2500°K, which is more than anyone has hitherto dared to suggest, this is no disadvantage. Godfrey and Price (1:53) have shown by considerations of radiation equilibrium that this temperature cannot rise above 3300°K.

Treatment of the results of Part 1 (a).

The process just developed was applied to the experimental results for November 1945 - February 1946. The value of T_o being unknown, the estimation of and F was repeated for each parabola for a series of values of T_o, varying in steps of 50°K from 250 to 600°K. In many cases the higher values of T_o gave values of lying well off the graph, and these, in accordance with the discussion on the previous page, have not been taken into account.

The results are tabulated below in the first two lines of each section.

S.A.S. Time	T_o (°K)	250	300	350	400	450	500	550	600
8 h	γ	11.7	10.7	9.2	8.5	8.0	9.5	11	-
	100F	3.94	4.34	4.68	5.25	5.85	7.50	9.33	-
cosχ =	$\beta \times 10^{18}$	6.54	3.74	2.23	1.49	1.13	0.72	0.48	-
= 0.529	B/n'_o	306	170	89.2	55.8	41.8	32.8	24.6	-
9 h	γ	11.4	9.9	8.9	7.9	7.9	6.5	10	-
	100F	3.71	4.02	4.49	4.87	5.70	5.89	8.71	-
cosχ =	$\beta \times 10^{18}$	9.21	5.35	3.09	2.14	1.54	1.22	0.68	-
= 0.701	B/n'_o	373	193	103	67.1	50.5	35.0	28.6	-
10 h	γ	13.5	12.7	11.6	10.7	9.2	11.5	13.0	-
	100F	4.36	5.01	5.46	5.92	6.03	7.76	9.12	-
cosχ =	$\beta \times 10^{18}$	11.2	5.11	3.02	2.10	1.73	1.10	0.78	-
= 0.836	B/n'_o	506	263	147	96.4	71.9	58.3	47.9	-
11 h	γ	11.3	9.65	8.3	7.6	7.1	7.0	5.5	-
	100F	3.21	3.36	3.61	4.01	4.52	5.21	5.25	-
cosχ =	$\beta \times 10^{18}$	14.1	8.45	5.08	3.43	2.55	1.82	1.50	-
= 0.927	B/n'_o	812	420	220	142	105	76.0	55.2	-
12 h	γ	10.2	9.3	8.0	7.2	6.6	6.7	5.5	9.8
	100F	2.69	3.14	3.36	3.76	4.20	4.98	5.07	8.32
cosχ =	$\beta \times 10^{18}$	17.5	9.45	5.69	3.82	2.87	1.99	1.62	0.84
= 0.966	B/n'_o	1070	525	280	177	131	93.8	68.8	57.0
13 h	γ	8.5	8.2	7.1	6.0	6.0	5.5	4.0	9
	100F	2.11	2.67	2.92	3.19	3.82	4.22	4.17	7.94
cosχ =	$\beta \times 10^{18}$	22.0	10.9	6.44	4.43	3.10	2.31	1.93	0.87
= 0.952	B/n'_o	970	500	261	161	119	86.4	61.5	50.3
14 h	γ	9.8	8.9	7.5	6.8	6.1	5.4	3.6	8.6
	100F	2.69	3.10	3.29	3.73	4.13	4.44	4.09	8.03
cosχ =	$\beta \times 10^{18}$	16.0	8.75	5.30	3.52	2.67	2.04	1.83	0.80
= 0.884	B/n'_o	826	433	228	144	105	75.0	55.4	44.6
15 h	γ	7.8	7.4	6.3	5.6	4.8	3.8	8	-
	100F	2.25	2.79	3.09	3.55	3.86	4.05	7.59	-
cosχ =	$\beta \times 10^{18}$	16.7	8.45	4.92	3.21	2.48	1.94	0.86	-
= 0.769	B/n'_o	693	357	186	118	85.2	59.5	45.0	-
16 h	γ	6.5	6.1	5.2	4.8	3.6	5	12	-
	100F	2.01	2.57	2.98	3.52	3.69	5.62	10	-
cosχ =	$\beta \times 10^{18}$	14.9	7.31	4.07	2.52	2.07	1.12	0.52	-
= 0.613	B/n'_o	559	280	143	89.6	64.1	44.4	42.6	-

Table 1:25 - Experimental values of γ and F and derived values of β and B/n'_o - November 1945.

S.A.S. Time	T_o (°K)	250	300	350	400	450	500	550	600
8 h	γ	20	20	17	16	17	20	–	–
	100F	7.08	7.41	7.94	8.32	8.91	10.0	–	–
cos χ =	$\beta \times 10^{18}$	3.85	2.30	1.39	1.00	0.784	0.57	–	–
= 0.559	B/n'_o	124	86.2	40.3	28.1	25.6	24.4	–	–
9 h	γ	13.5	12.3	11.6	10.9	10.1	10.0	13	–
	100F	4.57	4.98	5.58	6.27	6.58	7.59	10.0	–
cos χ =	$\beta \times 10^{18}$	7.75	4.46	2.57	1.73	1.38	0.98	0.61	–
= 0.726	B/n'_o	150	82.0	44.7	29.0	22.6	16.4	13.1	–
10 h	γ	15	14	11.9	11.0	13	16	–	–
	100F	5.37	6.03	6.31	6.68	8.32	10.0	–	–
cos χ =	$\beta \times 10^{18}$	7.79	4.35	2.67	1.91	1.29	0.87	–	–
= 0.857	B/n'_o	210	108	56.4	39.6	32.2	29.1	–	–
11 h	γ	9.2	8.6	7.5	7.1	6.2	5.5	4.5	8.3
	100F	2.24	2.77	3.00	3.44	3.76	4.05	4.21	7.24
cos χ =	$\beta \times 10^{18}$	20.6	10.4	6.24	4.09	3.14	2.38	1.90	0.94
= 0.945	B/n'_o	450	213	114	75.8	52.8	38.7	28.0	22.1
12 h	γ	11.5	10.2	9.0	8.1	7.3	6.1	10	14
	100F	3.59	3.85	4.27	4.74	5.13	5.22	8.32	10.0
cos χ =	$\beta \times 10^{18}$	13.4	7.81	4.54	3.09	2.39	1.92	1.00	0.71
= 0.983	B/n'_o	346	184	97.0	60.7	44.9	33.8	26.0	27.5
13 h	γ	11.7	10.8	9.2	8.4	7.9	9.0	15	–
	100F	3.85	4.30	4.59	5.09	5.71	7.16	10.0	–
cos χ =	$\beta \times 10^{18}$	12.2	6.89	4.15	2.84	2.12	1.38	0.82	–
= 0.969	B/n'_o	330	183	95.0	61.0	44.7	33.4	35.0	–
14 h	γ	12.7	12.0	11.1	9.9	8.8	9.0	10.5	12.5
	100F	4.07	4.62	5.05	5.41	5.75	6.53	8.32	10.0
cos χ =	$\beta \times 10^{18}$	10.8	5.98	3.52	2.49	1.97	1.41	0.92	0.56
= 0.904	B/n'_o	326	178	97.6	64.5	46.7	35.1	29.0	23.0
15 h	γ	11.5	10.2	9.2	8.4	7.6	9.0	10.8	–
	100F	3.73	4.05	4.47	5.07	5.52	7.24	8.91	–
cos χ =	$\beta \times 10^{18}$	10.4	6.00	3.49	2.33	1.79	1.12	0.75	–
= 0.792	B/n'_o	283	153	82.6	51.2	37.5	27.4	22.6	–
16 h	γ	10.1	9.2	7.8	7.6	6.2	11	–	–
	100F	3.52	4.07	4.33	5.18	5.31	8.71	–	–
cos χ =	$\beta \times 10^{18}$	8.89	4.82	2.92	1.85	1.51	0.75	–	–
= 0.641	B/n'_o	236	123	65.7	42.3	30.3	25.8	–	–

Table 1:26 - Experimental values of γ and F and derived values of β and B/n'_o - December 1945.

S.A.S. Time	T_o (°K)	250	300	350	400	450	500	550	600
8 h	γ	22	15	16	22	-	-	-	-
	100F	6.61	7.24	8.71	11.0	-	-	-	-
cos χ =	$\beta \times 10^{18}$	4.03	2.31	1.23	0.74	-	-	-	-
= 0.546	B/n'_o	209	57.0	33.6	30.6	-	-	-	-
9 h	γ	16	14	12.7	13.5	-	-	-	-
	100F	5.89	6.61	7.08	7.94	-	-	-	-
cos χ =	$\beta \times 10^{18}$	5.92	3.31	1.99	1.34	-	-	-	-
= 0.715	B/n'_o	171	78.0	44.6	34.0	-	-	-	-
10 h	γ	8.7	7.3	6.5	5.7	5.5	5	12	-
	100F	2.75	3.01	3.45	3.87	4.52	5.25	9.77	-
cos χ =	$\beta \times 10^{18}$	15.0	8.62	4.84	3.26	2.34	1.65	0.74	-
= 0.848	B/n'_o	218	108	57.9	36.4	27.1	18.7	17.1	-
11 h	γ	13.5	12.1	11.3	9.8	10.8	13.5	-	-
	100F	5.13	5.60	6.28	6.41	8.13	9.55	-	-
cos χ =	$\beta \times 10^{18}$	8.92	5.11	2.94	2.18	1.44	1.00	-	-
= 0.937	B/n'_o	191	102	56.4	37.1	27.8	25.8	-	-
12 h	γ	11.0	9.5	8.6	8.5	7.5	8.5	10.3	-
	100F	3.55	3.78	4.31	5.10	5.47	7.08	8.91	-
cos χ =	$\beta \times 10^{18}$	13.4	7.91	4.46	2.85	2.23	1.41	0.93	-
= 0.976	B/n'_o	239	126	65.5	42.1	31.1	22.0	18.0	-
13 h	γ	14	11.8	10.9	10.0	9.8	13	-	-
	100F	4.90	5.16	5.82	6.25	7.08	9.12	-	-
cos χ =	$\beta \times 10^{18}$	9.59	5.70	3.26	2.30	1.70	1.08	-	-
= 0.962	B/n'_o	208	104	55.6	37.8	28.4	24.6	-	-
14 h	γ	11.8	10.4	9.2	8.5	9.2	13.5	-	-
	100F	4.28	4.64	5.13	5.73	7.08	9.55	-	-
cos χ =	$\beta \times 10^{18}$	10.2	5.91	3.44	2.33	1.58	0.96	-	-
= 0.896	B/n'_o	192	100	54.2	35.3	26.5	24.0	-	-
15 h	γ	11.7	10.3	9.7	8.1	12	-	-	-
	100F	4.61	5.10	5.83	6.03	8.91	-	-	-
cos χ =	$\beta \times 10^{18}$	8.26	4.70	2.64	1.93	1.10	-	-	-
= 0.782	B/n'_o	165	86.2	47.3	30.5	25.5	-	-	-
16 h	γ	13	10.8	12.5	-	-	-	-	-
	100F	6.17	6.48	8.32	-	-	-	-	-
cos χ =	$\beta \times 10^{18}$	4.96	2.96	1.49	-	-	-	-	-
= 0.629	B/n'_o	116	60.5	36.5	-	-	-	-	-

Table 1:27 - Experimental values of γ and F and derived values of β and B/n'_o - January 1946.

S.A.S. Time	T_o (°K)	250	300	350	400	450	500	550	600
8 h cos χ = = 0.487	γ	14	12.2	11.2	13	–	–	–	–
	100F	6.03	6.52	6.92	8.71	–	–	–	–
	$\beta \times 10^{18}$	3.94	2.28	1.39	0.83	–	–	–	–
	B/n'_o	130	67.0	39.8	28.4	–	–	–	–
9 h cos χ = = 0.664	γ	12.4	11.4	10.5	9.2	10.3	–	–	–
	100F	4.76	5.37	6.03	6.27	8.03	–	–	–
	$\beta \times 10^{18}$	6.81	3.78	2.17	1.58	1.03	–	–	–
	B/n'_o	300	155	85.3	57.1	41.2	–	–	–
10 h cos χ = = 0.803	γ	13	12.1	11.2	9.6	10.8	–	–	–
	100F	5.01	5.73	6.31	6.43	8.13	–	–	–
	$\beta \times 10^{18}$	7.83	4.29	2.51	1.86	1.23	–	–	–
	B/n'_o	365	193	106	71.1	54.3	–	–	–
11 h cos χ = = 0.896	γ	12.1	11.3	10.2	9.4	9.0	9.0	12	–
	100F	4.02	4.55	4.95	5.57	6.09	7.16	9.33	–
	$\beta \times 10^{18}$	10.9	6.03	3.57	2.40	1.84	1.28	0.81	–
	B/n'_o	557	296	162	103	80.5	56.1	47.8	–
12 h cos χ = = 0.937	γ	8.9	8.4	7.2	6.5	5.8	5.3	4.5	7.5
	100F	2.40	2.95	3.19	3.60	4.01	4.38	4.79	7.76
	$\beta \times 10^{18}$	19.0	9.73	5.79	3.88	2.92	2.18	1.66	0.87
	B/n'_o	864	430	224	145	105	77.6	54.9	41.1
13 h cos χ = = 0.922	γ	12.1	11.4	9.8	9.2	8.0	8.3	11.0	–
	100F	3.91	4.45	4.71	5.32	5.62	6.53	8.71	–
	$\beta \times 10^{18}$	11.5	6.34	3.85	2.58	2.05	1.44	0.90	–
	B/n'_o	727	386	203	134	96.0	73.2	60.4	–
14 h cos χ = = 0.853	γ	10.8	9.6	8.3	7.9	7.3	8.8	12	–
	100F	3.61	3.92	4.34	4.97	5.67	7.24	9.55	–
	$\beta \times 10^{18}$	11.5	6.66	3.87	2.56	1.88	1.20	0.76	–
	B/n'_o	656	348	179	119	84.0	65.8	56.4	–
15 h cos χ = = 0.734	γ	11.5	10.7	9.1	8.0	7.7	10.0	12	–
	100F	3.89	4.41	4.74	5.06	5.75	7.85	9.77	–
	$\beta \times 10^{18}$	9.21	5.09	3.05	2.16	1.59	0.95	0.64	–
	B/n'_o	671	358	186	121	89.5	70.7	56.2	–
16 h cos χ = = 0.574	γ	9.4	7.7	7.1	6.3	5.0	9.9	–	–
	100F	3.29	3.48	4.05	4.60	4.67	8.51	–	–
	$\beta \times 10^{18}$	8.51	5.05	2.80	1.86	1.53	0.69	–	–
	B/n'_o	475	239	132	82.5	61.4	47.5	–	–

Table 1:28 - Experimental values of γ and F and derived values of β and B/n'_o - February 1946.

The values of γ obtained are practically all above 5 $^{o}C.km.^{-1}$, which points straight away to temperatures of the order of 1000^{o}K in the F_2 layer. Further discussion on this point is, however, premature, because we have no means of selecting any particular value of T_o as yet.

Some indication of the correct values of T_o and γ may be obtained by performing two tests.

Test I.

Since by eqn. (1.30)

$$F = \frac{C \cos \chi}{n_o' \beta T_o},$$

$$\beta = \frac{C \cos \chi}{n_o' T_o F} \quad . \quad . \quad . \quad . \quad . \quad . \quad (1.45)$$

As the maintenance of the layer is presumably due to ionisation of a particular species of molecules or atoms, β should be constant. Cos χ may be calculated from the Nautical Almanac, we have a value of F for each T_o from the preceding tables, while n_o' will be a function of T_o which may be estimated on the assumption of a linear gradient between 100 and 200 km.

From eqn. (1.19), with the same notation, but with subscripts referring to the height in km., we have:

$$n'_{200} = n'_{100}\left(1 + \gamma \frac{200 - 100}{T_{100}}\right)^{-(1 + C/\gamma)} . \quad (1.46)$$

The reason for this choice of 100 km. as the reference level in evaluating n'_{200} is that values of n'_{100} and T_{100} appear to be reasonably concordant when estimated by different workers; also the temperature T_{100} is likely to change less, being closer to the earth's surface,

than/

than that at 200 km. Finally, Hulburt (1:47) and Vassy and Vassy (1:49) agree in supposing that above 100 km. oxygen and nitrogen exist in the atomic form; thus we are justified in retaining the value 16.2 $^{o}C.km.^{-1}$ for C which we have used so far. We have estimated from the values given by these workers that the most suitable value for n'_{100} is 2×10^{14} atoms $cm.^{-3}$ and for T_{100} is $360^{o}K$. With these values,

$$= \frac{T_{200} - 360}{100} \ ^{o}C.km^{-1}$$

and therefore, substituting in eqn. (1.46),

$$n'_{200} = 2 \times 10^{14} \left(\frac{T_{200}}{360}\right)^{-\left(1 + \frac{1620}{T_{200} - 360}\right)} . \quad (1.47)$$

From this equation values of n'_{200} (i.e., n'_{o} in eqn.(1.45)), may be calculated for various values of T_{200} (i.e., T_{o} in eqn. (1.45)). This has been done in table 1:29.

T_o (^{o}K)	250	300	350	400	450	500	550	600
$n'_o \times 10^{-12}$ $cm.^{-3}$	1.33	1.76	2.34	2.72	2.88	3.16	3.48	3.74

Table 1:29 - Values of n'_o for various T_o.

We may now calculate values of β from (1.45) for each of the T_o's assumed, at every hour for each month. These are shown in the third line of each section of tables 1:25 - 1:28.

Test II.

The second test depends on the evaluation of the constant B, previously eliminated by division of eqns. (1.31) and (1.35) on page 87.

B is/

B is defined by eqn. (1.29)

$$B = \frac{\beta n_o' I_\infty}{\alpha W} \quad . \quad . \quad . \quad . \quad . \quad . \quad . \quad . \quad (1.29)$$

and from (1.35) is also given by

$$B = N^2 \left\{ F\left(1 + \frac{\gamma}{C}\right) \right\}^{-(1 + \gamma/C)} \exp\left(1 + \frac{\gamma}{C}\right) \quad . \quad . \quad . \quad (1.48)$$

From (1.29) it is seen that B is not a constant, since it contains n_o' which is a function of T_o. In addition, the variation of α with temperature is of the form

$$\alpha \propto T^{-\frac{1}{2}}$$

according to kinetic theory; this may be simply deduced from e.g. (1:50). The temperature in the F_2 layer is not likely to vary by more than a factor of 4, e.g. from $300^\circ K$ to $1200^\circ K$, i.e., α changes by a factor of 2. Therefore the recombination coefficient α will be considered here as a constant, and we may write:

$$\frac{B}{n_o'} = \frac{\beta I_\infty}{\alpha W} \qquad \text{from eqn. (1.29)}$$

$$= \frac{N^2 \exp(1 + \gamma/C)}{n_o' \left\{ F\left(1 + \frac{\gamma}{C}\right) \right\}^{(1 + \gamma/C)}} \quad . \quad \text{from eqn. (1.48)}$$

$$= \text{constant}$$

The quantity B/n_o', calculated from eqn. (1.48) with the values of F, γ and T_o obtained from tables 1:25 - 1:28, should be constant at all times and for all months. Its values are shown in the fourth row of each section of tables 1:25 - 1:28.

Discussion of the tests.

The correct value of β as remarked on page 88, is very doubtful. Since the tables 1:25 - 1:28 have been drawn up to cover temperatures T_o from 250°K to 600°K, which range includes all estimates seen in the literature, it seems very unlikely that the temperature will fall outside these limits. On these grounds the correct value of β should appear in the third row of each section, and values in the neighbourhood of $\beta = 2 \times 10^{-18}$ cm.^{2} are seen to fulfil this condition. Choosing $\beta = 2 \times 10^{-18}$ cm.^{2}, values of T_o have been interpolated to the nearest 10°K, and are given in table 1:30.

S.A.S. Time (hours)	T_o (°K)			
	November	December	January	February
8	370	320	320	320
9	410	380	350	360
10	410	410	470	390
11	480	540	410	430
12	500	490	470	520
13	540	460	430	450
14	500	450	420	440
15	490	430	390	410
16	450	390	330	390

Table 1:30 - Values of T_o corresponding to $\beta = 2 \times 10^{-18}$.

Theoretically, if a value of B/n_o' is chosen to give the same value of T_o as the value $\beta = 2 \times 10^{-18}$ at a certain time, this value of B/n_o' should give the identical set of values of T_o shown in table 1:30.

However/

Month	T_o corresponding to $\beta = 2 \times 10^{-18}$, at 12 h from table 1:29	Corresponding value of B/n'_o (cm^{-3})
November	500	93.8
December	490	35.5
Jan uary	470	27.5
February	520	68.5
	Mean:	56.4 $cm.^{-3}$

Table 1:31 - Values of B/n'_o corresponding to $\beta = 2 \times 10^{-18}$.

However, B contains α and I_∞, both of which may vary with temperature, and with season, sunspot activity, etc, respectively. Hence we shall not expect exact agreement in practice. To find the best value of B/n'_o corresponding to $\beta = 2 \times 10^{-18}$ $cm.^2$, B/n'_o data corresponding to the T_o's of table 1:30 at 12 hours are tabulated in table 1:31. The largest deviation from the mean is about 50% which may be considered satisfactory judged by ~~is~~ ionospheric standards.

S.A.S. Time (hours)	T_o (°K)			
	November	December	January	February
8	400	330	300	320
9	430	330	330	400
10	510	350	350	450
11	550	440	350	500
12	600	410	370	550
13	570	410	350	560
14	550	420	350	550
15	510	390	340	550
16	470	370	310	460

Table 1:32 - Values of T_o corresponding to $B/n'_o = 56.4$ $cm.^{-3}$

Taking this mean value of B/n_o', a table similar to table 1:30 may be constructed, interpolating from the last row of each section of tables 1:25 - 1:28. This is shown in table 1:32.

The agreement between the two tests is very pleasing, as they rest on independent grounds, and therefore it does not seem out of place to take t he mean values from these two tables as the best representative values for further discussion. These are given in table 1:33.

S.A.S. Time (hours)	T_o (°K)			
	November	December	January	February
8	385	325	310	320
9	420	355	340	380
10	460	380	410	420
11	515	490	380	465
12	550	450	420	535
13	555	435	390	505
14	525	435	385	495
15	500	410	365	480
16	460	380	320	425

Table 1:33 - Mean values of T_o.

The absolute values of these T_o's depend, of course, on the arbitrary choice of β as 2×10^{-18}. The effect of changing β is shown in table 1:34, which is limited to the month of November. In each case the value of B/n_o' was so chosen as to make the values of T_o equal at 12 hours. The choice of β thus affects the absolute value of T_o, but not its variation with time of day.

Previous/

S.A.S. Time (hours)	$\beta = 10^{-18}$ $B/n'_o = 60$		$\beta = 2 \times 10^{-18}$ $B/n'_o = 94$		$\beta = 5 \times 10^{-18}$ $B/n'_o = 250$	
	Test I	Test II	Test I	Test II	Test I	Test II
8	470	390	370	340	280	270
9	520	420	410	360	310	280
10	510	490	410	400	310	310
11	600	540	480	460	350	340
12	590	590	500	500	370	370
13	590	550	540	490	390	350
14	590	540	500	470	360	340
15	540	500	490	430	350	330
16	510	460	450	400	330	310

Table 1:34 - Effect of the choice of β on T_o - November.

Previous estimates have been made of the mean temperature at 200 km., but they vary widely in order of magnitude. Martyn and Pulley (1:48), from considerations of electron collision frequencies and of auroral spectra, have tentatively adopted the value of 1000°K at 200 km. in the daytime; Hulburt (1:47) has assumed the value 360°K above 100 km. for lack of better evidence; while Vassy and Vassy (1:49), assuming complete dissociation of both oxygen and nitrogen, obtained a temperature gradient which gives T_o at 200 km. as 600°K in summer. The values in table 1:33, having a mean of about 430°K, are well in accord with these estimates. It may be seen from table 1:34 that a β much larger than 10^{-18} would give values of T_o which are much lower, and such values as $\beta > 3 \times 10^{-17}$, suggested by Bradbury for the F_2 region (1:51) would

give/

give T_o well below 200°K. This is difficult to justify as a daytime value, since even measurements made at night on aurorae in the polar regions (1:52) gave the temperature as 240°K.

It may be seen that T_o rises towards the middle of the day and falls off with some delay in the afternoon. This is true no matter what β is chosen to be. It shows that heating of the atmosphere does take place even at a height of 200 km., the temperature rising by about 30% of its value at 8 hours.

Estimates have been made by various methods of the "temperature of the F_2 region". We shall calculate the temperature at 300 km., T_{300}, from the values of T_o and the corresponding γ's for comparison with these estimates.

The results at 300 km., shown in table 1:35, are so scattered that little significance can be attached to individual variations. They do show in general that the temperature in summer 300 km. above Grahamstown is of the order of 1200°K. This is in agreement with the rough estimates for the daytime summer temperature in the F_2 layer:

(i) Appleton and Naismith, (1:54), from considerations of the variation in N between summer and winter noon, estimate that the temperature cannot be less than 1200°K in summer.

(ii) Fuchs (1:55) has concluded from estimated scale heights that the temperature of the F_2 region may rise as high as 1900°K.

(iii) Martyn and Pulley (1:48) confirm Appleton's result/

S.A.S. Time (hours)	November			December		
	T_o (°K)	γ (°C/km)	T_{300} (°K)	T_o (°K)	γ (°C/km)	T_{300} (°K)
8	385	8.7	1255	325	18.5	2175
9	420	7.9	1210	355	11.5	1505
10	460	9.7	1430	380	11.4	1520
11	515	6.5	1165	490	5.6	1050
12	550	5.5	1100	450	7.3	1180
13	555	4.5	1005	435	8.0	1235
14	525	4.5	975	435	9.1	1345
15	500	3.8	880	410	8.2	1230
16	460	3.9	850	380	7.7	1150
Mean	485	6.1	1097	408	9.7	1376

S.A.S. Time (hours)	January			February		
	T_o (°K)	γ (°C/km)	T_{300} (°K)	T_o (°K)	γ (°C/km)	T_{300} (°K)
8	310	15.2	1830	320	11.8	1500
9	340	13.0	1640	380	9.7	1350
10	410	5.7	980	420	10.1	1430
11	380	10.4	1420	465	9.0	1365
12	420	8.1	1230	535	4.7	1005
13	390	10.2	1410	505	8.6	1365
14	385	8.7	1255	495	8.6	1355
15	365	9.2	1285	480	9.1	1390
16	320	11.6	1480	425	5.6	985
Mean	369	10.2	1392	447	8.6	1305

Table 1:35 - Temperatures at 300 km.

result of a temperature of 1200°K.

(iv) Vassy and Vassy, assuming complete dissociation of O_2 and N_2, obtain a summer temperature of 1080°K, from the estimated scale height of 70 km. given by Appleton.

(v) Godfrey and Price (1:53), by a consideration of the equilibrium between absorption and secondary radiation, conclude that the temperature is of the order of 1000°K, and cannot exceed 3300°K.

It will be observed that the mean values for T_o are smaller for the midsummer months December and January than for November and February, while the reverse holds for the temperatures at 300 km. This gives valuable support to the expansion theory, for, near the solstice, when heating is greatest, the atmosphere at 200 km. becomes heated in the middle part of the day, and is forced upwards by expansion, leaving cooler gas to take its place. The heated mass of gas would produce greater absorption of the solar radiation, thus preventing it from reaching the 200 km. level, where it would normally cause more heating.

As a last interesting point, we may make an estimation of the intensity of active incident radiation I_∞ above the earth's atmosphere. From eqn. (1.29)

$$I_\infty = \left(\frac{B}{n_o'}\right)\frac{\alpha w}{\beta} \quad \ldots\ldots\ldots\ldots (1.49)$$

We have assigned to B/n_o' the value 56.4 $cm.^{-3}$ from the results of test I. The value of α is open to discussion, and seems to vary with ion density and height, according to Wells and Shapley (1:56); a reasonable mean seems to

be/

be 5×10^{-10} c.g.s. units. β has been fixed at $2 \times 10^{-18} cm.^2$; and the value of the ionisation potential w is given by Bacher and Goudsmit (1:57) as 13.55 e.v. for O and 14.48 e.v. for N. As a mean 14 e.v. has been used. Hence we find

$$w = 14 \times 1.59 \times 10^{-12} = 2.23 \times 10^{-11} \text{ erg.}$$

Hence from (1.49)

$$I_\infty = 0.313 \text{ erg } cm.^{-2} \text{ sec.}^{-1}$$

Hulburt (1:47) has calculated that the total black body radiation of energy per quantum greater than 13.7 e.v. received from the sun is 8×10^{-3} erg $cm^{-2} sec^{-1}$, which is much lower than the above estimate.

Substituting back the v alue 8×10^{-3} in eqn. (1.49), we find $B/n'_o = 1.44$, and from tables 1:25 - 1:28 this would give T_o at least as high as $2000^\circ K$. This is ridiculous, and we can only conclude that the sun does not behave as a black body in this spectral region. A similar conclusion has been drawn by other workers (1:51), (1:58), (1:59), (1:60).

Conclusions.

The introduction of a linear temperature gradient into the theory of layer formation yields equations which may be applied with success for data for the F_2 layer, presented in the form of parabolas representing the distribution of ion density with height. The values of the temperatures at 200 and 300 km. obtained are in accordance with previous estimates, and are of a more quantitative nature.

The main weakness seems to lie in the assumptions regarding/

regarding the absorption coefficient β. In the first place its value is not fixed by the theory, and in the second place it varies with the frequency of the radiation absorbed, and an assumption of a mean value is not necessarily justified. Again, the manner in which the recombination coeffient α varies with the temperature and pressure is not well established. Finally the theory is limited in its application by the assumption that $\frac{dn}{dt} = 0$ and by its neglect of the earth's curvature. Re-examination of these points seems to be the next step in its development.

It should be pointed out that the assumption of complete dissociation of oxygen and nitrogen above 100 km. is not a weakness, since a numerical recalculation is all that is required to apply the theory to an atmosphere containing constituents of known molecular weight.

References to Parts 1(a) and 1(b).

(1:1) MacDonald, H.M.; Proc.Roy.Soc., 71, 251 (1903) and A90, 50 (1914).

(1:2) Sommerfeld, A.; Ann. der Physik, 28, 665 (1909).

(1:3) Van der Pohl, B.; Phil. Mag., 38, 365 (1919).

(1:4) Appleton, E.V. and Barnett; Proc. Roy. Soc., A109, 621 (1925)

(1:5) Breit, G. and Tuve, M.A.; Phys. Rev., 28, 554 (1926).

(1:6) Appleton, E.V. and Ratcliffe, J.A.; Proc. Roy. Soc. A115, 291 (1927).

(1:7) Berkner, L.V., Wells, H.W. and Seaton, S.L.; Trans. Edin. Meeting Ass. Terr. Mag. and Elec., 340 (1936).

(1:8) Chapman, S.; Proc. Phys. Soc., 43, 26 and 483 (1931).

(1:9) White, F.W.G.; Electromagnetic Waves, Ch.V, (Methuens Series Monographs), London, 1942, 2nd Ed.

(1:10) Tonks, L.; Nature, 132, 101 and 710 (1933).

(1:11) Norton, K.A.; ibid., 132, 676 (1933).

(1:12) Hartree, D.R.; ibid., 132, 929 (1933).

(1:13) Darwin, C.G.; Proc. Roy. Soc., A146, 17 (1934) and A182, 152 (1943).

(1:14) Ratcliffe, J.A.; Proc. Phys. Soc., 51, 747 (1939).

(1:15) Fleming, J.A.; Trans. Wash. Meeting Ass. Terr. Mag. and Elec., 527 (1939).

(1:16) Halliday, E.C., Proc. Phys. Soc., 48, 421 (1936).

(1:17) Higgs, A.J.; Mon. Roy. Not. Astron. Soc., 102, 24, (1942).

(1:18) Walker, G.D.; Trans. S.A. Inst. Elec. Eng., 34, 60 (1943).

(1:19) Gledhill, J.A. and Szendrei, M.E.; Trans. Roy. Soc. S.A.; 31, 315 (1947).
(1:20) Pulley, O.O.; Proc. Phys. Soc., 46, 853 (1934).
(1:21) Ratcliffe, J.A. and White, F.W.G.; ibid., 45, 399 (1933).
(1:22) Colwell and Friend; Phys. Rev., 50, 632, (1936).
(1:23) Goubau; Phys. Z., 31, 333 (1930).
(1:24) Puckle, O.S.; Time Bases, p. 30, Chapman and Hall, London (1945).
(1:25) Best and Ratcliffe, J.A.; Proc. Phys. Soc., 50, 233 (1938).
(1:26) Berkner, L.V.; Trans, Wash. Meeting Ass. Terr. Mag. and Elec., fig.6, p. 428 (1939).
(1:27) Appleton, E.V.; Proc. Phys. Soc., 42, 321 (1930).
(1:28) Appleton, E.V.; Proc. Roy. Soc., A162, 451 (1937).
(1:29) Murray and Hoag; Phys. Rev., 51, 333 (1937).
(1:30) Booker and Seaton; ibid., 57, 87 (1940).
(1:31) Bannon, J. and Wood, F.W.; Terr. Mag. and Atmos. Elec., 51, 89 (1946).
(1:32) Berkner, L.V.; Trans. Wash. Meeting Ass. Terr. Mag. and Elec., 502 (1939).
(1:33) Shapley, A.H.; Terr. Mag. and Atmos. Elec., 51, 247 (1946).
(1:34) Bartels, J., Heck, N.H. and Johnston, H.F.; Terr. Mag. and Atmos. Elec., 44, 411 (1939).
(1:35) Fisher, R.A.; "Statistical Methods for Research Workers", 9th ed., p. 204, Oliver and Boyd, Edinburgh, 1944.
(1:36) Fisher, R.A.; ibid., Ch. VI.
(1:37) Waldmeier, M.; Terr. Mag. and Atmos. Elec., 51, 274 (1946).

(1:38) Terman, F.E.; "Measurements in Radio Engineering", 1st ed., p. 292, McGraw Hill, New York, 1935.

(1:39) Appleton, E.V.; Union. Internat. Radiotél. Sci. Mem. Sci., 1, 23 (1938).

(1:40) Larmor; Phil. Mag., 48, 1025 (1924).

(1:41) Hartree, D.R.; Proc. Camb. Phil. Soc., 25, 97 (1929) and 27, 143 (1931); also Proc. Roy. Soc., A131, 428 (1931).

(1:42) Millington, G.; Proc. Phys. Soc., 44, 580 (1932) and 47, 263 (1935).

(1:43) Hulburt, E.O.; Phys. Rev.; 31, 1018 (1928).

(1:44) Hulburt, E.O.; ibid., 53, 344 (1938).

(1:45) Hulburt, E.O.; ibid., 55, 639 (1939).

(1:46) Hulburt, E.O.; ibid., 46, 822 (1934).

(1:47) Hulburt, E.O.; "Physics of the Earth", Ch.X, p. 492, ed. J.A. Fleming, 1939.

(1:48) Martyn, D.F. and Pulley, O.O.; Proc. Roy. Soc., A154, 455, (1936).

(1:49) Vassy, A. and Vassy, M.E.; J. de Phys. et Rad., Ser. 8, 3, 8 (1942).

(1:50) Kennard, E.H.; "Kinetic Theory of Gases", 1st ed., Ch. II and III, McGraw Hill, New York, 1938.

(1:51) Bradbury, N.E.; Terr. Mag. and Atmos. Elec., 43, 55 (1938).

(1:52) Vegard; Geofys. Publik., 9, No.11.
Vegard and Tonsberg, ibid., 11, No.2; 12, No.3.

(1:53) Godfrey and Price; Proc. Roy. Soc., A163, 228 (1937).

(1:54) Appleton, E.V. and Naismith, R.; Proc. Roy. Soc., A150, 685 (1935).

(1:55) Fuchs; Beitr. Geophys., 47, 1 (1936).
(1:56) Wells, H.W. and Shapley, A.H.; Terr. Mag. and Atmos. Elec., 51, 401 (1946).
(1:57) Bacher and Goudsmit; "Atomic Energy States", McGraw Hill, New York, 1932.
(1:58) Saha; Proc. Roy. Soc., A160, 155 (1937).
(1:59) Mc Nish; J.Appl. Phys., 8, 718 (1937).
(1:60) Hunter, A.; Rep. on Prog. Phys., 9, 5 (1943).